Numerical and experimental analysis of mechanical characterization of sacroiliac joint in physiology and pathology

生理病理状態における仙腸関節の力学的役割に関する
数値的および実験的解析

Doctoral dissertation

Ryota TOYOHARA

Division of Human Mechanical Systems and Design
Graduate School of Engineering, Hokkaido University

2023

Abstract

Sacroiliac joints (SIJs) are synovial joints located between sacrum and ilium of human pelvis. Surrounding ligaments strongly support SIJs, making the joint relatively less mobile. Although SIJs are considered to act as a damper, receiving impact between the upper and the lower body. Unexpected forces or repeated impacts can cause SIJ dysfunction, leading to pain. To relieve pain, fixing and stabilizing SIJs have been performed as treatments, however, biomechanical approaches on SIJs are poorly performed to date. In this dissertation, mechanical characterization of SIJs in physiology and pathology is introduced, in particular focusing on stress environment on SIJs as well as mechanical contribution of the surrounding ligaments.

In Chapter 1, as the background of this study, fundamental aspects of SIJs and their dysfunction as well as treatments are introduced, referring to previous studies. The purpose and the outline of this study are then described.

In Chapter 2, finite element analysis on movements and functions of SIJs during walking is demonstrated. It is hypothesized that SIJs may work as shock-absorbing systems. A 3D finite element model of a pelvis with detailed SIJ structure and ligament arrangement are used to perform stress analysis under walking conditions. It is indicated that walking load concentrates on SIJs due to morphology of pelvic ring, however, slight mobility of SIJs relieve the high stress.

In Chapter 3, the relationship between SIJ surface morphology and joint motion resistance is investigated. SIJ surface has fine irregularities and is considered to restrict SIJ motion in a particular direction. SIJ surface models are fabricated based on X-ray CT data and used to measure shear resistance by using an in-house experimental setup. SIJ surface morphology is characterized by bone-to-bone contact at medial and inferior parts and wide gaps at anterior and posterior regions. The results indicate that there are differences in resistance depending on the direction of joint movement and alignments.

In Chapter 4, considering pathological conditions, finite element models of acetabular dysplasia pelves are created to determine stress distributions on SIJs in standing. Numerical analyses are performed in pre- and post-operative pelves. From comparisons of the two types of pelves, it is demonstrated that a lack of posterior coverage of acetabula may interrupt proper transmission of load from femurs, resulting in an unnecessary stress increase on SIJs.

In Chapter 5, effectiveness of a treatment with pelvic belts for SIJ dysfunction is elucidated. Although this treatment is often used clinically, few studies have investigated the mechanism of their effectiveness. Lumbar pressure distribution caused by pelvic belts is experimentally measured and stress environment of pelves is numerically analyzed using a finite element model. It is demonstrated that pelvic belts may rotate pelves externally and compress SIJs, reducing excessive movements of SIJs and ligaments loading.

In Chapter 6, this study is summarized and prospects for future research is provided.

Table of Contents

Abstract ..... **I**

Table of Contents ..... **III**

List of Figures ..... **VIII**

List of Tables ..... **XVII**

Chapter 1 Introduction **1**

1.1 BACKGROUND 2

1.2 JOINT STRUCTURE 2

1.3 PELVES 6

1.3.1 Pelvic bony structure 7

1.3.2 Pelvic ligaments 11

1.4 SACROILIAC JOINTS (SIJS) 13

1.4.1 Articular surface morphology 14

1.4.2 Joint motion 15

1.4.3 Sacroiliac joint dysfunction 17

1.5 TREATMENTS FOR SACROILIAC JOINT DYSFUNCTION 19

1.5.1 Strategy of treatments 19

1.5.2 Treatment options 19

1.6 PREVIOUS RESEARCH ON SACROILIAC JOINTS 24

1.6.1 Sacroiliac joint motion 24

1.6.2 Articular surface structure 25

1.6.3 Sacroiliac joint dysfunction and treatments 27

1.7 RESEARCH PURPOSES 30

1.8 THESIS OUTLINE 31

Chapter 2 Finite element analysis of mechanical environment of sacroiliac joints during bipedal walking 33

2.1 INTRODUCTION 34

2.2 METHODS 35

2.2.1 Finite element model of pelves 35

2.2.2 Material properties 37

2.2.3 Mesh generation 38

2.2.4 Walking Loads 38

2.2.5 Boundary conditions 38

2.2.6 Analytical parameters 41

2.3 RESULTS 42

2.3.1 Displacement of pelves 42

2.3.2 Rotational motion of sacroiliac joints 44

2.3.3 Displacement of sacroiliac joints 45

2.3.4 Equivalent stress on sacroiliac joints 46

2.3.5 Loads of pelvic ligaments 47

2.4 DISCUSSION 49

2.4.1 Motion of sacroiliac joints during bipedal walking 49

2.4.2 Load transition of sacroiliac joints 50

2.5 CONCLUSIONS 52

Chapter 3 Experimented analysis of relation between articular surface and motion resistance on sacroiliac joints 53

3.1 INTRODUCTION 54

3.2 MATERIALS AND METHODS 55

3.2.1 Pelvic surface model with sacroiliac joints 55

3.2.2 Extraction of articular surface 56

3.2.3 Joint sliding test 58

3.3 RESULTS 62
3.3.1 Articular gap height distribution 62
3.3.2 Joint motion resistance 63
3.3.3 Joint repositioning 65
3.4 DISCUSSION 67
3.5 CONCLUSIONS 70

Chapter 4 Finite element analysis of effect of pelvic morphology on stress environment of sacroiliac joint: acetabular dysplasia pelvis 71

4.1 INTRODUCTION 72
4.2 METHODS 74
4.2.1 Finite element model of acetabular dysplasia pelves 74
4.2.2 Material properties 76
4.2.3 Mesh generation 77
4.2.4 Loading and boundary conditions 77
4.2.5 Analytical parameters 78
4.3 RESULTS 79
4.3.1 Acetabular head indices 79
4.3.2 Displacement of pelves 80
4.3.3 Rotational motion of sacroiliac joints 82
4.3.4 Equivalent stress on sacroiliac joints 83
4.3.5 Compressive stress on sacroiliac joints 85
4.3.6 Loads on pelvic ligaments 87
4.4 DISCUSSION 92
4.5 CONCLUSIONS 95

Chapter 5 Numerical and experimental validation of effectiveness of pelvic belts as a treatment for sacroiliac joint dysfunction 96

5.1 INTRODUCTION 97

5.2 METHODS 98

5.2.1 Finite element model of pelves with surrounding soft tissues 98

5.2.2 Material properties 99

5.2.3 Mesh generation 100

5.2.4 Loading and boundary conditions 101

5.2.5 Analytical parameters 104

5.2.6 Model validation 104

5.3 RESULTS 105

5.3.1 Horizontal displacement of innominate bones 105

5.3.2 Minimum principal stress on sacroiliac joints 107

5.3.3 Displacement of sacroiliac joints 108

5.3.4 Loads on pelvic ligaments 110

5.3.5 Minimum principal strain on soft tissues and pelves 111

5.3.6 Comparison with previous studies 112

5.4 DISCUSSION 113

5.5 CONCLUSIONS 115

Chapter 6 Conclusions and prospects 116

6.1 CONCLUSIONS 117

6.2 PROSPECTS 120

Acknowledgements 123

References 125

Publications 139

Conferences **140**

Award **142**

List of Figures

Fig. 1.1 Structure of synovial joints (modified from Schünke et al., 2017). 4
Fig. 1.2 Structure of pelves (modified from “BioDigital Human”)..... 6
Fig. 1.3 Differences between male (left) and female (right) pelves. The central circles and lines are arcuate lines and pubic arches, respectively (modified from Anatomy of the Human Body). 7
Fig. 1.4 Loads on pelves 8
Fig. 1.5 Pelves on the sagittal view (modified from “BioDigital Human”). 8
Fig. 1.6 Position of sacra on spines (modified from “BioDigital Human”). 9
Fig. 1.7 Structure of sacra (“BoneAndSpine”). 10
Fig. 1.8 Ligament positions with the anterior view (modified from Kapandji, 1974). 12
Fig. 1.9 Ligament positions with the posterior view (modified from Kapandji, 1974). 12
Fig. 1.10 Structure of sacroiliac joints on the transverse plane (Murakami, 2018a). 13
Fig. 1.11 Ligaments and fat in the posterior sacroiliac joint area (Poilliot et al., 2019a). 14
Fig. 1.12 Shape of sacroiliac joints (modified from “BioDigital Human”). 14
Fig. 1.13 Surface contours of the sacral articular facet (Kapandji, 1974). 15
Fig. 1.14 (a) Nutation motion and (b) counter-nutation motion of sacroiliac joints (Kapandji, 1974). 16
Fig. 1.15 Motion of pelves under loadings (Kapandji, 1974)..... 16
Fig. 1.16 Ligaments restricting nutation motion. 17
Fig. 1.17 Histogram between ages and patients with sacroiliac joint dysfunction (data from Murakami, 2018a)..... 18
Fig. 1.18 One finger test (Murakami, 2017). 19

Fig. 1.19 Anesthesia injection on a patient (left) and on a skeletal specimen (right) (Murakami et al., 2007b). 20
Fig. 1.20 Pelvic belts (Soisson et al., 2015). 21
Fig. 1.21 Manual therapy (Katada, 2019). 21
Fig. 1.22 Anterior fixation. (Left) Model. (Center) X-ray image. (Right) CT scan (Murakami et al., 2007a). 23
Fig. 1.23 Posterior fixation. 23
Fig. 1.24 iFuse implant system (Miller et al., 2013). 23
Fig. 1.25 Scheme of experimental setup for physiological load application (Hammer et al., 2019c). 24
Fig. 1.26 A partial removal of the right complex of sacrospinous and sacrotuberous ligaments on a finite element model (left) and on a cadaver (right) (Hammer et al., 2019a). 25
Fig. 1.27 (Left) An android model. (Right top) An air cylinder and (right bottom) an attachment position for psoas major muscles (Sanaka et al., 2022). 26
Fig. 1.28 (A) A sacral auricular surface densitogram with the Hounsfield unite (HU) scale. (B) The same densitogram divided into the three regions: superior, anterior and inferior region (Poilliot et al., 2021). 27
Fig. 1.29 Finite element models of (left) posterior and (right) anterior fixations (Venayre et al., 2021). 28
Fig. 1.30 A pressure measuring system (A) without and (B) with a pelvic belt. (C) A finite element model with resultant force vectors for pelvic compression (Sichting et al., 2014). 29
Fig. 2.1 Anterior view (left) and left lateral view (right) of the pelvic model used for finite elements simulations (Toyohara et al., 2020). 35
Fig. 2.2 Positions and names of ligaments in the pelvic model with anterior (left) and posterior (right) views (Toyohara et al., 2020). 36

Fig. 2.3 (a) The yellow arrows indicate where the joint moments are applied, the red arrows indicate where the surface loads are applied, and (b) the blue point indicates where the pelvis is fixed (Toyohara et al., 2020). 40
Fig. 2.4 Resultant displacement distribution of pelvis excluding femora (top 2 lines) and pelvis surrounding sacroiliac joints (bottom 2 lines) on a representative example (Toyohara et al., 2020). 43
Fig. 2.5 Change of mean values of maximum resultant displacement in pelvis excluding femora (Toyohara et al., 2020). 43
Fig. 2.6 Resultant displacement vector diagrams of sacroiliac joints (SIJs) with the cartilage model on a representative example (Toyohara et al., 2020). 44
Fig. 2.7 Change of mean values of maximum resultant displacement of right and left SIJs (Toyohara et al., 2020). 45
Fig. 2.8 Equivalent stress distribution of right sacroiliac joints (SIJs) on a representative example viewed from sacral sides (Toyohara et al., 2020). 46
Fig. 2.9 Change of mean values of maximum equivalent stress in right SIJs (Toyohara et al., 2020). 47
Fig. 2.10 Comparison of (a) the mean loads and (b) the mean load rates on ligaments of the right part of the pelvis between the bone and cartilage model. The loads of ligaments are the sum of each ligament, which has 2 to 30 spring components. Here, the loads on pubic ligament PL, anterior longitudinal ligament LLA, and posterior longitudinal ligament LLP were halved due to their location at the center of the spinopelvic complex (Toyohara et al., 2020). 48
Fig. 3.1 The anterior and posterior sides are synovial joints and ligamentous regions, respectively (modified from Schünke et al., 2017). The edges of synovial joint area are shown in red lines. 54

Fig. 3.2 A pelvic model. The blue and red models are the sacrum and ilium models, respectively. The black lines are the cuting lines with intervals of 30 mm. 55
Fig. 3.3 Surface models of a sacrum (blue, left) and ilium (red, right). The dark areas indicate surface regions. 57
Fig. 3.4 Investigation procedure of articular gap height distribution. 57
Fig. 3.5 Surface models with bases of a sacrum (blue, left) and ilium (red, right). 58
Fig. 3.6 Surface models of ABS resin after acetone vapor process. (Left) A sacrum and (right)ilium. 59
Fig. 3.7 Surface models of polyester resin. (Left) A sacrum and (right) ilium. 59
Fig. 3.8 A joint motion resistance test device. 60
Fig. 3.9 Experimental conditions on (left) directions and (right) alignments. 61
Fig. 3.10 Articular gap height distribution on the sacrum. The gap height increases from red to blue. A: anterior, I: inferior, P: posterior, S: superior... 62
Fig. 3.11 A representative shear coefficient on the in-vivo condition. 63
Fig. 3.12 Shear coefficients at four displacement points from initial positions (a) on the in-vivo conditions and (b) on all conditions. Inf.: inferior, Sup.: superior, Ant.: anterior, Post.: posterior. 64
Fig. 3.13 Repositioning on in-vivo (top), nutation (center) and counter-nutation (bottom) conditions. The horizontal axes are maximum pulling force in increments of 2N. The vertical axes are finnal posision returned 0 N on (a) parallel and (b) perpendicular to pulling directions. Inf.: inferior, Sup.: superior, Ant.: anterior, Post.: posterior. 65
Fig. 3.14 Repositioning on the posterior to anterior (1st line), anterior to posterior (2nd line), inferior to superior (3rd line) and superior to inferior (4th line) directions. The horizontal axes are maximum pulling force in increments of 2N. The vertical axes are finnal posision returned 0 N on (a)

parallel and (b) perpendicular to pulling directions. Inf.: inferior, Sup.: superior, Ant.: anterior, Post.: posterior. 66
Fig. 4.1 Radiographs of a (a) preoperative and (b) postoperative acetabular dysplasia pelvis (Iwai et al., 2014). 73
Fig. 4.2 Finite element models of the preoperative (left) and postoperative (right) pelves of patient 1. The right is the surgical side. The insets are enlarged views of the right hip joints. The scale bar: 20 mm. I: inferior, L: left, R: right, S: superior. In the pre model, the acetabulum does not cover the femoral head sufficiently. In the post model, the acetabulum widens by the surgical intervention (Toyohara et al., 2022b). 74
Fig. 4.3 The positions and names of ligaments (red circles) and muscles (blue circles) in a pelvic model of patient 1 with anterior (right) and posterior (left) view. The ligaments modelled are as follows: anterior longitudinal ligament (LLA), anterior sacroiliac ligament (ASL), inguinal ligament (INL), pubic ligament (PL), obturator membrane (MO), posterior longitudinal ligament (LLP), posterior sacroiliac ligament (PSL), iliolumbar ligament (IL), interosseous sacroiliac ligament (ISL), long posterior sacroiliac ligament (LPSL), sacrotuberous ligament (ST) and sacrospinous ligament (SS) (Toyohara et al., 2022b). 75
Fig. 4.4 The upper (left) and posterior (right) acetabular head index (AHI) measurement positions with anterior (upper) and posterior (posterior) views. AHI is a ratio of A to B. A means a coverage of acetabulum on the top (upper) or center (posterior) of the femoral heads, and B means a diameter of the femoral head. The left femur and innominate bone are shown in grey and green, respectively. The scale bar: 20 mm. I: inferior, L: left, R: right, S: superior (Toyohara et al., 2022b)..... 78
Fig. 4.5 Resultant displacement vector diagrams of the pelves on anterior (top 2 lines) and upper (bottom 2 lines) views. ‘Pre’ and ‘post’ reflect pre models

and post models, respectively. The arrows indicate the sides of surgical intervention (Toyohara et al., 2022b). 81
Fig. 4.6 Scheme of pelvic deformation. The red and blue arrows indicate inward rotation (inflare) and outward rotation, respectively (Toyohara et al., 2022b). 82
Fig. 4.7 Degree of rotation at the sacroiliac joints on the sides of surgery in all patients, i.e., is the angle of rotation on the sacrum for ilium. The positive and negative values mean the nutation and counter-nutation, respectively (Toyohara et al., 2022b). 82
Fig. 4.8 The scatter plots of reduction of sacral nutation on the surgical sides vs. improvement of acetabular head index (a) on upper coverage and (b) on posterior coverage (Toyohara et al., 2022b). 83
Fig. 4.9 Equivalent stress distribution of the contact surfaces in sacroiliac joints on surgical sides (Toyohara et al., 2022b). 84
Fig. 4.10 Maximum equivalent stress in sacroiliac joints on surgical sides (Toyohara et al., 2022b). 84
Fig. 4.11 The scatter plots of reduction of maximum equivalent stress in the sacroiliac joint on the surgical sides vs. improvement of acetabular head index (a) on upper coverage and (b) on posterior coverage (Toyohara et al., 2022b). 85
Fig. 4.12 Normal stress distribution on the normal direction of the contact surfaces in sacroiliac joints on surgical sides (Toyohara et al., 2022b)..... 86
Fig. 4.13 Minimum normal stress in sacroiliac joints on surgical sides (Toyohara et al., 2022b). 86
Fig. 4.14 The scatter plots of reduction of minimum normal stress in the sacroiliac joint on the surgical sides vs. improvement of acetabular head index (a) on upper coverage and (b) on posterior coverage (Toyohara et al., 2022b). 87

Fig. 4.15 Sacrotuberous ligament (ST), sacrospinous ligament (SS), interosseous sacroiliac ligament (ISL) and posterior sacroiliac ligament (PSL) loading on the surgical sides of all patients (Toyohara et al., 2022b). 89
Fig. 4.16 The scatter plots of reduction of sacrotuberous ligament (ST) and sacrospinous ligament (SS) loading on the surgical sides vs. improvement of acetabular head index (a) (c) on upper coverage and (b) (d) on posterior coverage (Toyohara et al., 2022b). 90
Fig. 4.17 The scatter plots of increase of interosseous sacroiliac ligament (ISL) and posterior sacroiliac ligament (PSL) loading on the surgical sides vs. improvement of acetabular head index (a) (c) on upper coverage and (b) (d) on posterior coverage (Toyohara et al., 2022b). 91
Fig. 5.1 Finite element model of the pelvis including soft tissue, displayed on whole model (left) and hidden the soft tissue (Right) with anterior views. The scale bar: 100 mm. S: superior, L: left (Toyohara et al., 2022a). 98
Fig. 5.2 The positions and names of the pelvic ligaments modelled in this study, in a meshed pelvis model with anterior (left) and posterior (right) views. The ligaments are the anterior longitudinal ligament (LLA), anterior sacroiliac ligament (ASL), iliolumbar ligament (IL), inguinal ligament (INL), long posterior sacroiliac ligament (LPSL), obturator membrane (MO), posterior longitudinal ligament (LLP), posterior sacroiliac ligament (PSL),pubic ligament (PL), interosseous sacroiliac ligament (ISL), sacrospinous ligament (SS) and sacrotuberous ligament (ST). The scale bar: 60 mm. S: superior, L: left, R: right (Toyohara et al., 2022a). 99
Fig. 5.3 Sample of the (a) pelvic rubber belt and (b) padded pelvic belt used in this study (modified from Toyohara et al., 2022a). 101
Fig. 5.4 Scheme of pressure measurement in this study. (Left) A pressure measuring device was placed on a body and the pelvic belts were wrapped

on the device. Blue: a pressure measuring device. Orange: pelvic belt. (Right top) Pressure distribution on the pelvic belts and (right bottom) straightly opened results (Toyohara et al., 2022a). 102
Fig. 5.5 Pelvic belt types and related pressure measurements in-vivo in a setup on the volunteer (left row), and pressure distribution on the pelvic belts (right row). Black areas indicate the anterior superior iliac spines as reference marks (Toyohara et al., 2022a). 103
Fig. 5.6 (a) The red arrows indicate the places and directions the pressures are applied (trimetric view), and (b) the orange arrows indicate where the loads are applied (anterior view). The scale bar: 60 mm. S: superior, L: left, A: anterior (Toyohara et al., 2022a). 104
Fig. 5.7 Horizontal displacement of the innominate bones shown from an anterior (1st line) and posterior (2nd line) view. The positive directions are the directions that the arrows point to, to right on the models. The scale bar: 100 mm. S: superior, L: left, R: right (Toyohara et al., 2022a). 106
Fig. 5.8 Scheme of pelvic deformation. The innominate bone was rotated outward by using pelvic belts (Toyohara et al., 2022a). 106
Fig. 5.9 Minimum principal stress distribution of right (1st line) and left (2nd line) sacroiliac joint cartilage shown from left and right, respectively. The red area shows the tensile area, and the tensile area decreased by pelvic belts. The scale bar: 40 mm. S: superior, A: anterior, P: posterior (Toyohara et al., 2022a). 107
Fig. 5.10 The comparison of mean minimum principal stress rates for the control condition. Right and left mean right and left sacroiliac joints, respectively (Toyohara et al., 2022a). 108
Fig. 5.11 Resultant displacement distribution of right (1st line) and left (2nd line) sacroiliac joint cartilage shown from left and right, respectively. The

very low displacement area (blue area) increased with pelvic belts. The scale bar: 40 mm (Toyohara et al., 2022a). 109
Fig. 5.12 The comparison of mean resultant displacement rates for the control. Right and left mean right and left sacroiliac joints, respectively (Toyohara et al., 2022a). 109
Fig. 5.13 A comparison of ligament loading rates on anterior sacroiliac joint (ASL), sacrotuberous ligament (ST), sacrospinous ligament (SS), posterior sacroiliac ligament (PSL) and interosseous sacroiliac ligament (ISL) for the control. The left and right graphs are the results on the right and left sides of ligaments, respectively (Toyohara et al., 2022a).....110
Fig. 5.14 Minimum principal strain distribution of soft tissue (1st and 3rd lines) and pelvis (2nd and 4th lines). The top and bottom two lines are shown from posterior and right views, respectively. The gray lines indicate the level of the anterior superior iliac spines. The scale bar: 100 mm. S: superior, R: right, A: anterior (Toyohara et al., 2022a). 111

List of Tables

Table 1.1 Classification of joints. 3

Table 2.1 Names of ligaments. 36

Table 2.2 Material properties. C10, C01 and C11 mean the parameters of Mooney-Rivlin model for hyper-elastic bodies (modified from Toyohara et al., 2020). 37

Table 2.3 Mean values of joint moments, surface loads, and pelvic angles (modified from Toyohara et al., 2020)..... 39

Table 2.4 Walking phases. 40

Table 3.1 Joint states on surface models. 56

Table 3.2 Summary of preliminary study for shear and compressive forces. 69

Table 4.1 Material properties for finite element models. C10, C01 and C11 mean the parameter of Mooney-Rivlin model for hyper-elastic bodies (modified from Toyohara et al., 2022b)..... 76

Table 4.2 Number of nodes and elements and average element quality of each finite element models (modified from Toyohara et al., 2022b). 77

Table 4.3 Measured acetabular head indices (AHI) of upper and posterior coverage on the surgical sides. Improve means an increase of AHI from pre model to post model, respectively (Toyohara et al., 2022b)..... 79

Table 5.1 Material properties for the finite element model. C10, C01 and C11 mean the parameter of Mooney-Rivlin models for hyper-elastic bodies. Material properties for cartilage were used for the cartilage model except for SIJs and symphysis cartilages (modified from Toyohara et al., 2022a). 100

Table 5.2 Summary of comparison. 112

Chapter 1

Introduction

1.1 Background

Sacroiliac joints (SIJs) are regarded as a source of low back pain, which is called SIJ dysfunction. This disease is considered to account for approximately 15 - 30% of the symptoms in patients with low back pain (Bernard and Kirkaldy-Willis, 1987; Schwarzer et al., 1995; Forst et al., 2006). This is because of the fact that SIJs are often considered as a non-movable joint due to a small range of motion. Another reason is that X-ray CT and MRI images provide no specific findings, making diagnosis difficult (Murakami, 2017). Conventional surgical treatments for SIJ dysfunction include fixation of joints with screw implants (Wise and Dall, 2008; Smith et al., 2013), wearing pelvic belts (Mens et al., 2006; Hammer et al., 2015), etc., however, the effectiveness of these treatments have not been scientifically proved.

In fact, for example, it has been pointed out that surgical treatments to fix the joints may lead to the loss of SIJ functions (Sanaka et al., 2020). To date, although biomechanical researches on SIJs have been conducted by several groups, physiological functions of SIJs have not been fully understood. Development of treatment methods for SIJ dysfunction based on biomechanics may greatly contribute to national welfare and medical development.

This chapter introduces joints in general, pelves and SIJs regarding to structures and motion, describes SIJ dysfunction and its treatment methods and summarize previous researches on SIJs. The research purpose and the outline of this study are finally described.

1.2 Joint structure

Joints are points of contact between adjacent bones. Joints are classified into three types based on the anatomical characteristics: fibrous joint, cartilaginous joint and synovial joint (Anatomy, Joints; Tortora and Derrickson, 2012). In addition, they are

Table 1.1 Classification of joints.

Anatomical	Fibrous joints		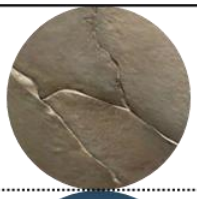
	Cartilaginous joints		
	Synovial joints		
Functional	Synarthroses	(Immovable)	
	Amphiarthroses	(Slightly moveable)	
	Diarthroses	(Freely moveable)	

classified into three types based on the function: synarthrosis (immovable), amphiarthrosis (slightly moveable) and diarthrosis (freely moveable) (Table 1.1).

Fibrous joints are fixed connections composed of collagen-rich tissues and do not have joint cavity. These include sutures in craniums, syndesmosis between tibias and fibulas and gomphoses between teeth and their sockets. In cartilaginous joints, the bones are joined by cartilage without joint cavity. There are joints between sternums and ribs, pubic symphysis and intervertebral joints. Synovial joints have joint capsules and allow

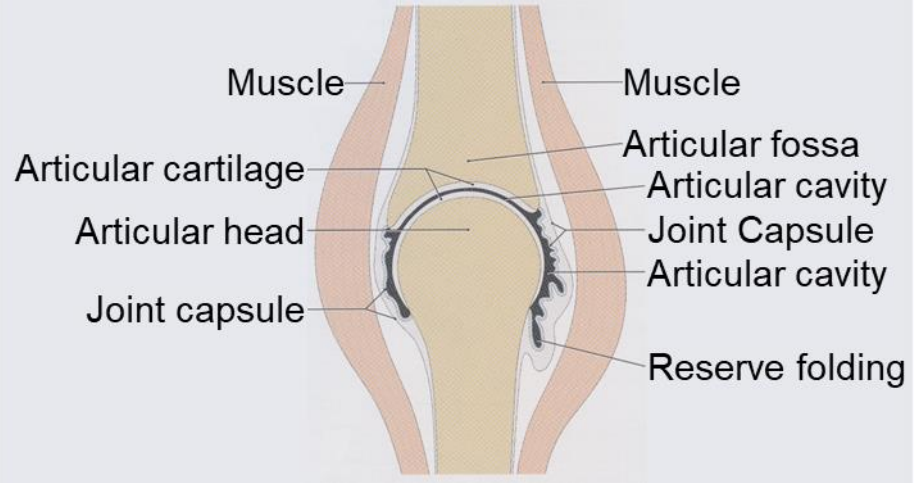

Fig. 1.1 Structure of synovial joints (modified from Schünke et al., 2017).

relatively large joint movements. The surface of bones is covered by hyaline cartilage. Diarthrodial joints are commonly considered as synovial joints.

Figure 1.1 shows a joint structure on a finger as an example of diarthrosis. The joint consists of an articular capsule that is a fibrous connective tissue and encloses two epiphyses, a joint cavity that is the space between the epiphyses and surrounded by the articular capsule and an articular cartilage that covers the epiphyses. In general, the two epiphyses have a convex and concave surface, called an articular head and glenoid fossa, respectively. The joint capsule is covered by a synovial membrane and filled with synovial fluid, which is highly viscous and has functions such as lubrication, shock absorption and oxygen and nutrients supply (Tortora and Derrickson, 2012). Ligaments attach to the outer synovial membrane and strengthen the connection between the two bones.

Cartilages

Cartilage tissues exist in cartilaginous joints and articular cartilage and forms a skeletal system with bones. Cartilages are precursors of bones. Fetal skeletons that are gradually replaced by bone as development progresses are composed of cartilages. However, the epiphyseal cartilages are maintained throughout life as a smooth articular surface (Tortora and Derrickson, 2012). Cartilages are highly functional bearing systems

that maintain a low-friction, low-wear lubricating state in joint movements (Murakami, 2006) and their friction coefficient is smaller than that of ice, which is quite slippery in nature (Hayashi, 2000).

In general, normal cartilage tissues neither contain blood vessels nor nerves within the matrix (Tortora and Derrickson, 2012), however, there are cartilages including SIJs that have nerve fibers (Szadek et al., 2010). Chondrocytes and biopolymers composed cartilage tissues and are intercellular matrix and consists of chondroitin sulfates, collagen fibers and elastic fibers (Suda et al., 2007). They grow and repair slower than other tissues and do not regenerate in adults (Tortora and Derrickson, 2012). The mechanical properties of cartilage are viscoelastic.

Cartilage tissues are classified into three types based on the intercellular matrix and the morphology of cells: hyaline cartilages, fibrocartilages and elastic cartilages (Tortora and Derrickson, 2012). Hyaline cartilages are the most abundant in human body. They contain an elastic gel substance and provide a smooth surface suitable for joint movement. Fibrocartilages have high durability and provide strong connections and chondrocytes are interspersed between bundles of collagen fibers. Elastic cartilages posess strength and elasticity and keep the shape of a specific structure like auricles and chondrocytes exist between meshes of elastic fibers.

Ligaments

Ligaments are bundles of fibers and connect bones to adjacent bones (Murakami, 2006). The stability of joints is related to muscles dynamically while related to morphology of the joint surface and ligaments statically. The attachment of ligaments varies depending on the type of joints. Ligaments are composed of 60 - 80% water and mostly collagen. The main cellular component is fibroblasts and there are almost neither blood vessels nor cells within ligaments.

The collagen fibers of ligaments are arranged parallel to the longitudinal axis and resist tensile loads only. The stress-strain curve of ligaments is nonlinear. With applying

tension to ligaments, the stiffness increases rapidly at first and then increases linearly, indicating an increase is the Young's modulus. In addition, ligaments are a time-dependent viscoelastic material similar to articular cartilages (Murakami, 2006).

1.3 Pelves

Pelves are a deep vase-like structure with a bony ring. They play roles to support body weight and to connect trunks and lower limbs as well as to protect pelvic organs and in birth canals in women (Matsumura, 2013). Figure 1.2 shows a structure of a pelvis.

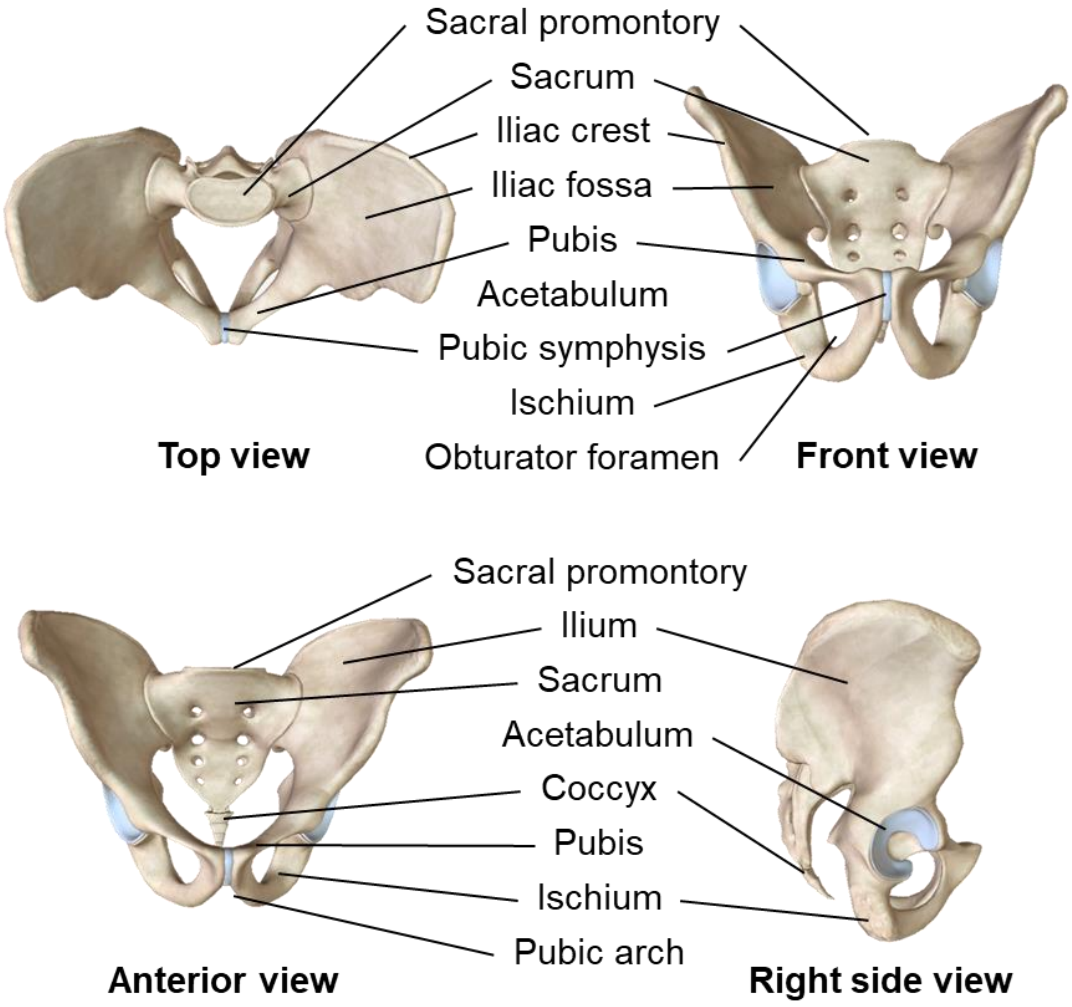

Fig. 1.2 Structure of pelves (modified from “BioDigital Human”).

Pelves exhibit the clearest sex difference in human skeletons. Figure 1.3 shows an overview of male and female pelves. The female pelves are wider and more open for childbirth. On the other hand, the male pelves are narrower. The male pelves are more suitable for bipedal walking, while the female pelves are in a contradictory state called the obstetrical dilemma and obtained a shape that is relatively unsuitable for bipedal walking due to deliveries (Merry, 2010). Therefore, women are more likely to suffer from low back pain.

1.3.1 Pelvic bony structure

Pelves consist of left and right hip bones, sacra and coccyx, which are connected by pubic symphysis and SIJs. Pelves play a major role in transmitting forces from spines to lower limbs. Weight supported by lumbar spines is distributed along sacral alas and through ischial tuberosities towards acetabula (Fig. 1.4). A part of ground reaction forces against body weight are transmitted to acetabula by femoral necks and heads. The other forces are transmitted across pubic branches, balancing forces from the other sides at pubic symphysis. When standing on both feet, weight of the trunk is applied to the both lower limbs via hip joints and pelves are slightly tilted forward. The anterior superior iliac

Fig. 1.3 Differences between male (left) and female (right) pelves. The central circles and lines are arcuate lines and pubic arches, respectively (modified from Anatomy of the Human Body).

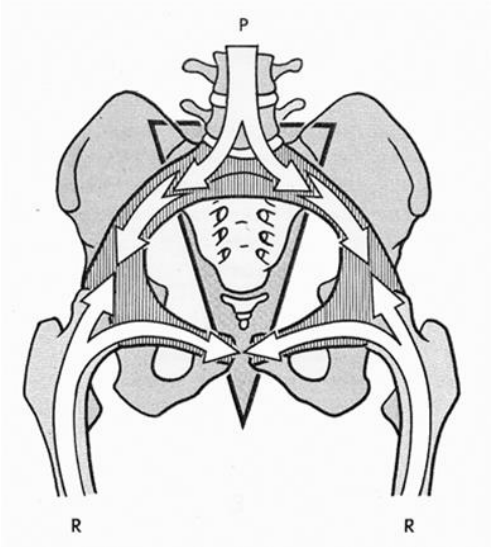

Fig. 1.4 Loads on pelves (Kapandji, 1974).

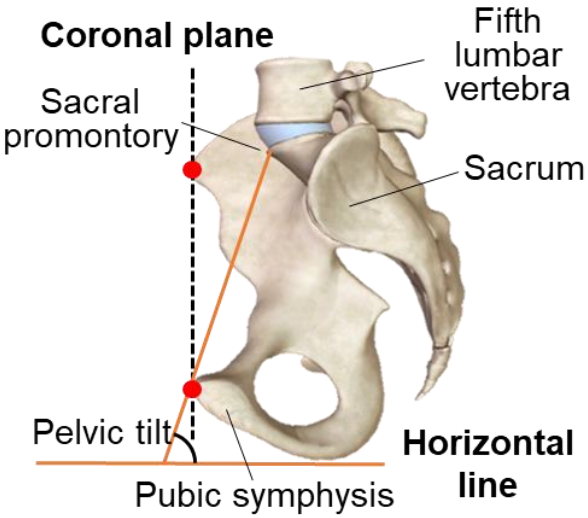

Fig. 1.5 Pelves on the sagittal view (modified from "BioDigital Human").

spines and the upper border of the pubic symphysis are in the same vertical plane (Fig. 1.5) (Matsumura, 2013).

Innominate bones

Innominate bones consist of ilia, ischia and pubes. They are connected posteriorly to sacra via SIJs and anterioirly to the other innominate bones via pubic symphysis to form pelvic rings. Large holes surrounded by ischia and pubes are called obturator foramens and closed by ligamentous membranes. Ilia, ischia and pubes are separated by Y cartilage until childhoods and fuse into one bone in adults (Takai, 2010).

Sacra

Sacra are parts of spines: cervical spines, thoracic spines, lumbar spines, sacra and coccyx, from the top to the bottom (Fig. 1.6). Sacra are divided into five sacral spines at birth, however, in adults, they become one sacrum by osseointegration. Figure 1.7 shows the structure of a sacrum. Sacra can be viewed as inverted triangles between the two iliac bones (Tortora and Derrickson, 2012). There are four transverse lines on the anterior and

posterior surfaces that indicate the fused sacral vertebrae and four pairs of spinal nerve entrances exist at each end of lines. The smooth outer parts of upper surfaces on sacra are sacral alas and the central wide parts are bases of sacra. The angles between bases of the sacra and the horizontal lines are sacral slopes (SS) and are widely used as an index of inclinations of the sacra. In addition, the forward edges of the bases of sacra are sacral promontories that are also one of the points for pelvic measurements. Bilateral sides of the sacra have large auricular surfaces, which form SIJs between the ilia and the sacra (Tortora and Derrickson, 2012).

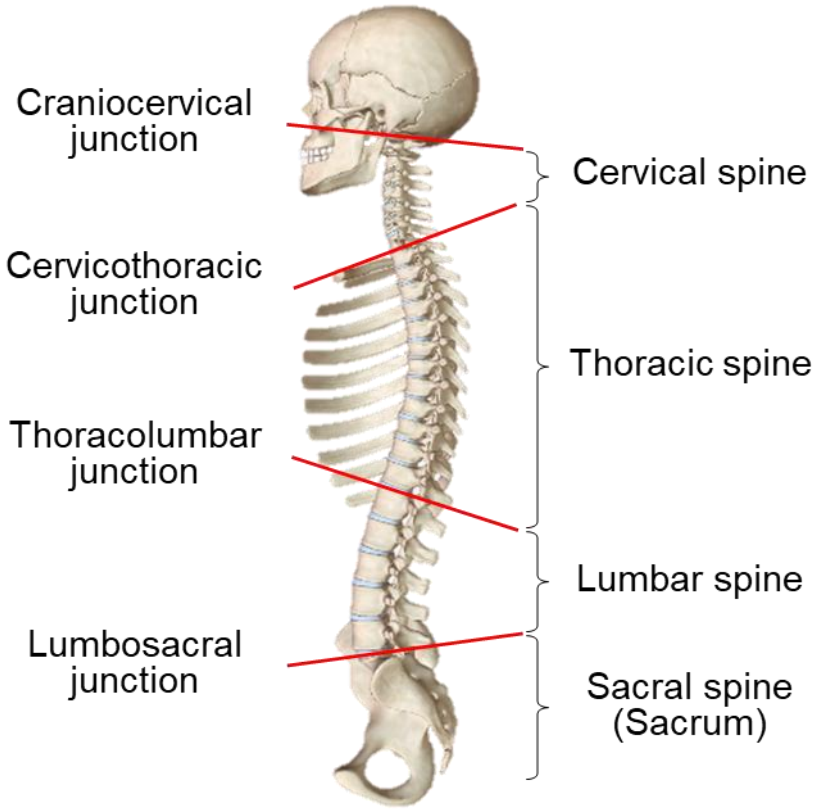

Fig. 1.6 Position of sacra on spines (modified from “BioDigital Human”).

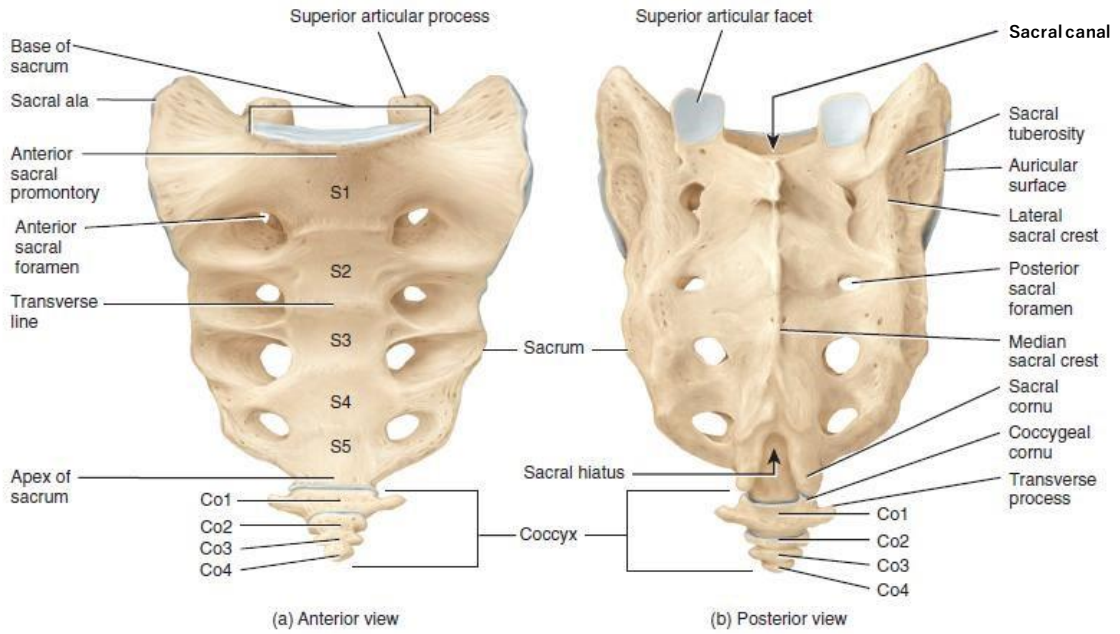

Fig. 1.7 Structure of sacra ("BoneAndSpine").

Pubic symphysis

Pubic symphyses are cartilaginous joints that connect bilateral pubes on the front of pelves and have little mobility. They play an important role in the mechanical balance of the pelves with SIJs (Fig. 1.4). When pubic symphyses are dislocated, innominate bones and the sacrum can not maintain their correct positions, which causes pelvic structures collapse.

Sacroiliac joints (SIJs)

SIJs are located at junctions of spines and pelves and forms pelvic rings with pubic symphyses. Although the joints have little mobility, they are important weight bearing joints, transferring loads from the spines to the lower limbs (Katada, 2019). The periarticular regions are composed of many ligaments and strong against external force.

1.3.2 Pelvic ligaments

Major ligaments around pelves are iliolumbar ligaments that connect the 5th lumbar vertebrae and ilium, anterior sacroiliac ligaments that connect the ilium and the sacrum in front, sacrospinous ligaments that connect the sacrum and the ischial spine, sacrotuberous ligaments that connect the sacrum and the ischial tuberosity, interosseous sacroiliac ligaments that connect the ilium and the sacrum posteriorly, iliofemoral ligaments that connects the femur and the ilium, ischiofemoral ligaments that connect the femur and the ischium and pubofemoral ligaments that connect the femur and the pubic bone (Figs. 1.8, 1.9).

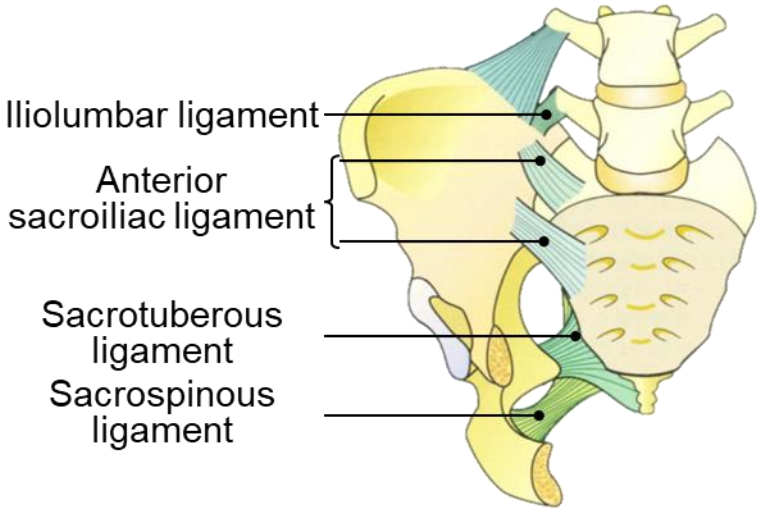

Fig. 1.8 Ligament positions with the anterior view (modified from Kapandji, 1974).

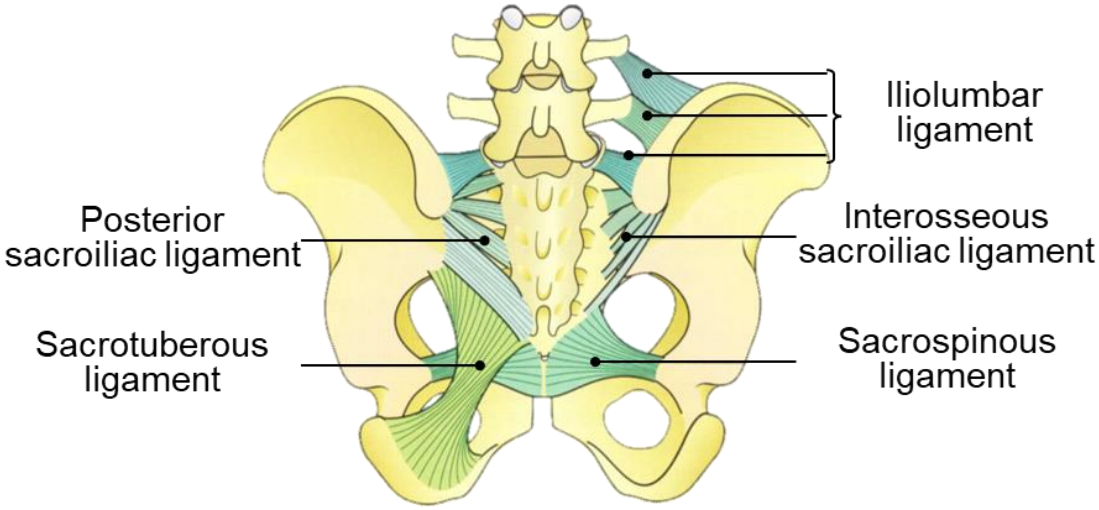

Fig. 1.9 Ligament positions with the posterior view (modified from Kapandji, 1974).

1.4 Sacroiliac joints (SIJs)

SIJs are composed of an anterior synovial joint and a posterior tough ligamentous region (Fig. 1.10) (Cohen, 2005). Morphologically, SIJs are classified as a synovial joint, however they have only a small range of motion for shock absorption because the ligaments support them strongly (Takayama, 1990). Cartilages on the synovial joint are fibrocartilage on the iliac side and hyaline cartilage on the sacral side. In addition, a large amount of fat is also contained in the ligamentous region behind the SIJs and may play a role as a shock absorber (Fig. 1.11). Since the articular surface of the SIJs is almost vertical to the gravity, the load from the trunk should cause strong shear forces on the SIJs (Murakami, 2018a).

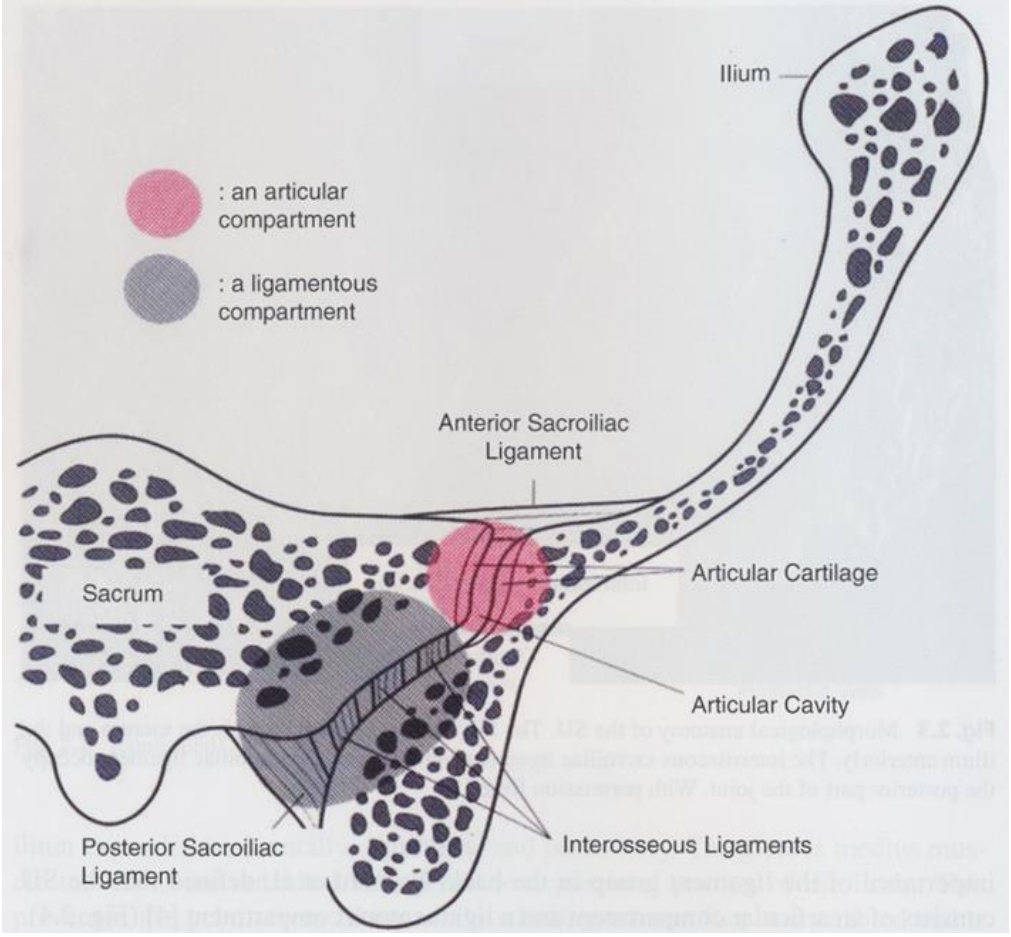

Fig. 1.10 Structure of sacroiliac joints on the transverse plane (Murakami, 2018a).

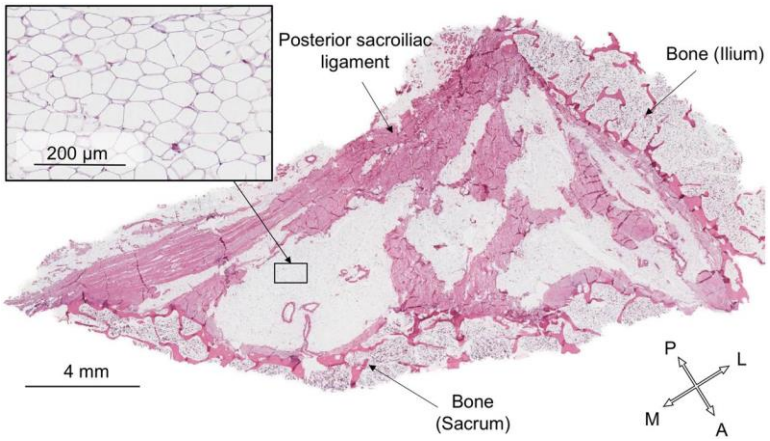

Fig. 1.11 Ligaments and fat in the posterior sacroiliac joint area (Poilliot et al., 2019a).

1.4.1 Articular surface morphology

Articular surfaces of SIJs are generally crescent-shaped, called an auricular surface, although the morphology varies greatly among individuals (Fig. 1.12). The major axis slopes from antero-superior-lateral to posterior-inferior-medial and is twisted caudally (Katada, 2019). In addition, the upper part of the joint is concaved toward the ilium and the lower part of the joint is concaved toward the sacrum (Fig. 1.13). Although the surface has fine irregularities, it is described as a flat rail structure, with a protrusion along the

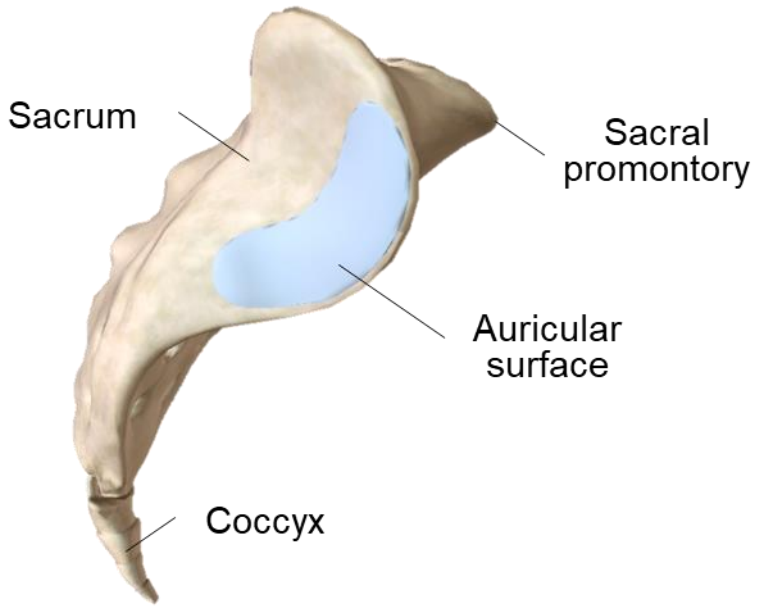

Fig. 1.12 Shape of sacroiliac joints (modified from “BioDigital Human”).

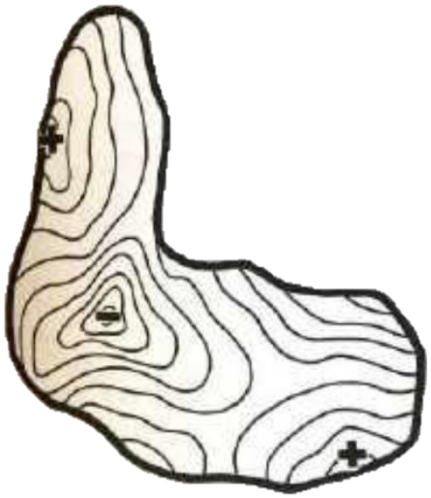

Fig. 1.13 Surface contours of the sacral articular facet (Kapandji, 1974).

long axis of the articular surface that divides depression into two. Although the articular surfaces may limit the slight movements of the joint, they are not always conforming to each other (Kapandji, 1974).

1.4.2 Joint motion

Although pelves can move depending on postures of bodies, SIJs mainly move within pelves because bony components and pubic symphysis have smaller mobility than SIJs. For example, when standing in a comfortable posture, the weight of trunk acting on the base of the sacrum pushes down the promontory, which rotates the sacrum forwardly (nutation) (Figs. 1.14(a), 1.15). This movement is quickly restricted by iliolumbar ligaments, anterior sacroiliac ligaments, sacrospinous ligaments and sacrotuberous ligaments (Fig. 1.16). At the same time, ground reaction forces are transmitted from the femur to the hip joint and produces a rotational moment. Consequently, the ilium tilts backward, enhancing the nutation movement. However, very little movement actually occurs due to the restriction of ligaments. The opposite movement (counter-nutation) is also restricted by ligaments (Fig. 1.14(b)). The counter-nutation position is a state in which the sacral wedge is deeply driven into the pelvic ring fixed by the pubic symphysis

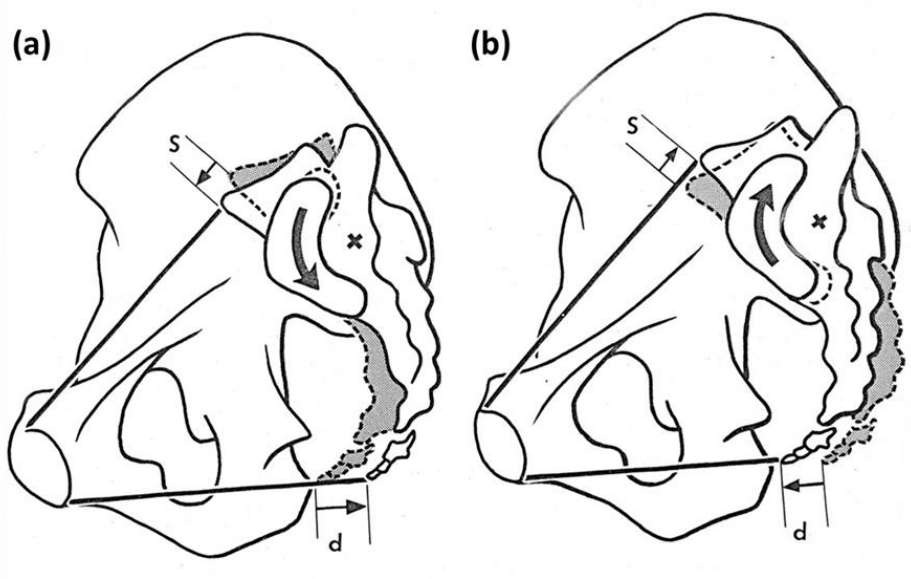

Fig. 1.14 (a) Nutation motion and (b) counter-nutation motion of sacroiliac joints (Kapandji, 1974).

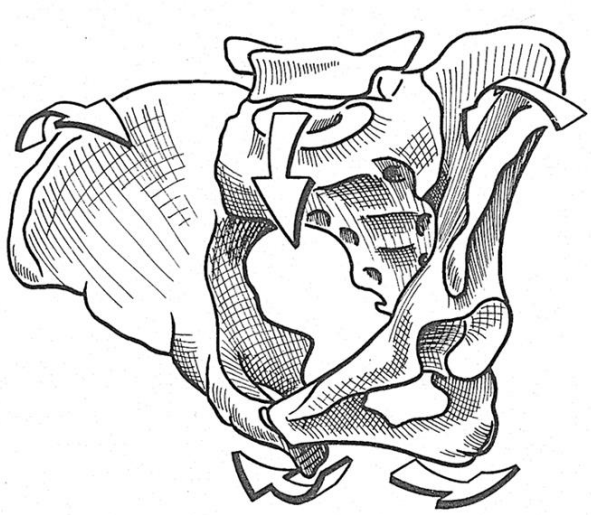

Fig. 1.15 Motion of pelves under loadings (Kapandji, 1974).

and the posterior ligaments. This position is considered to be the most rigid state (close-packed position), which does not move even when external force is applied. Therefore, it is a posture suitable for lifting heavy objects (Katada, 2019). In addition, nutation and counter-nutation movements are performed around lateral axes passing through the second sacral vertebra (Weisl, 1955).

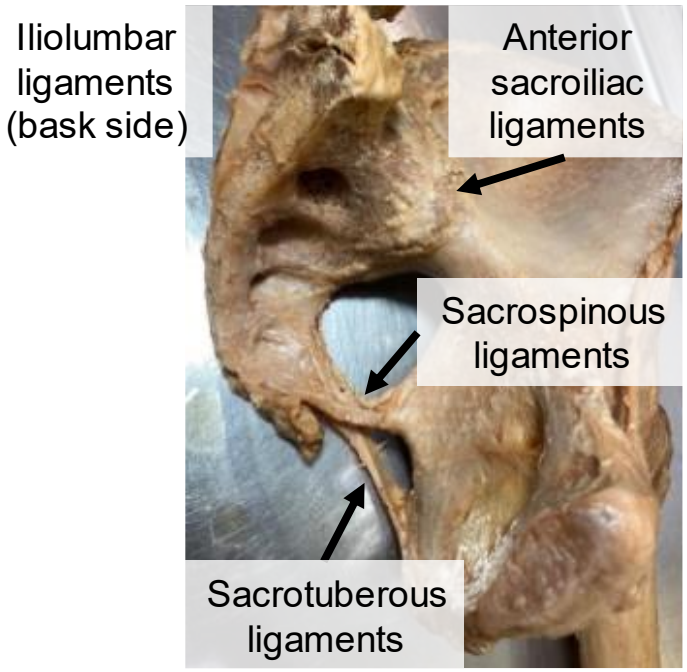

Fig. 1.16 Ligaments restricting nutation motion.

Furthermore, pelves are in various loading states depending on the postures of the whole bodies. When standing, the weight is supported by the acetabula which are the connection of foot. On the other hand, when sitting, the weight is supported by the ischial bones. In addition to this, pelves can be tilted forward or backward depending on the states of spines, that is, depending on the postures of upper bodies, which vary the loading directions on the pelves.

1.4.3 Sacroiliac joint dysfunction

Since SIJs need to stand a large load with a small range of motion, unexpected and/or repeated impacts can cause joint incompatibility, resulted in joint dysfunction. SIJ disease can be divided into arthritis and joint dysfunction, with the most cases being the latter. In the past, low back pain originating from SIJs was thought to be unique to women after childbirth, however, as shown in Fig. 1.17, it is not uncommon pain that can occur regardless of age or gender (Murakami, 2017).

Main actions that patients feel SIJ pain are in dorsal positions, in standing up, in sitting, in lying on the side with the affected side down and in starting to move in the morning. SIJ dysfunction is sometimes misidentified as an intervertebral disc disease because it causes pain in the lower limbs and in the lower back. Positions of SIJs are unclear to view from outside bodies and their movement can not be observed from the body surface. In addition, medical imaging tests such as X-ray and MRI can not provide strong findings indicating SIJ dysfunction, therefore, it is often overlooked (Murakami, 2017). One finger test is suggested as the main diagnostic method for SIJ dysfunction, in which doctors ask patients to point out the most painful part with one finger (Fig. 1.18). If the patients point near posterior superior iliac spines, they are likely to suffer from SIJ dysfunction. In addition, the diagnosis is confirmed by anesthesia for SIJs (Murakami et al., 2007).

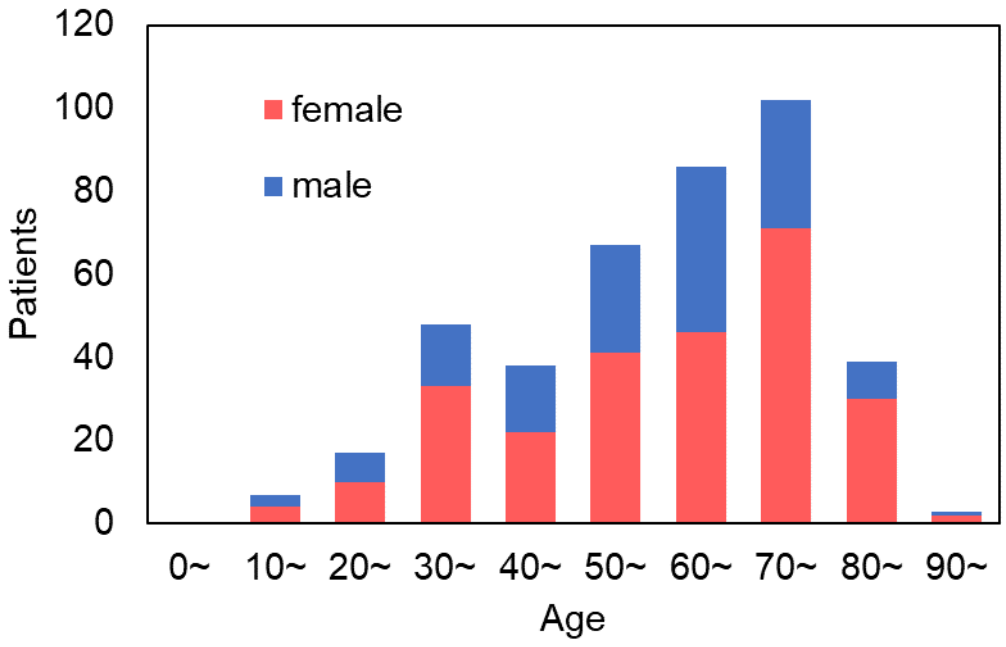

Fig. 1.17 Histogram between ages and patients with sacroiliac joint dysfunction (data from Murakami, 2018a).

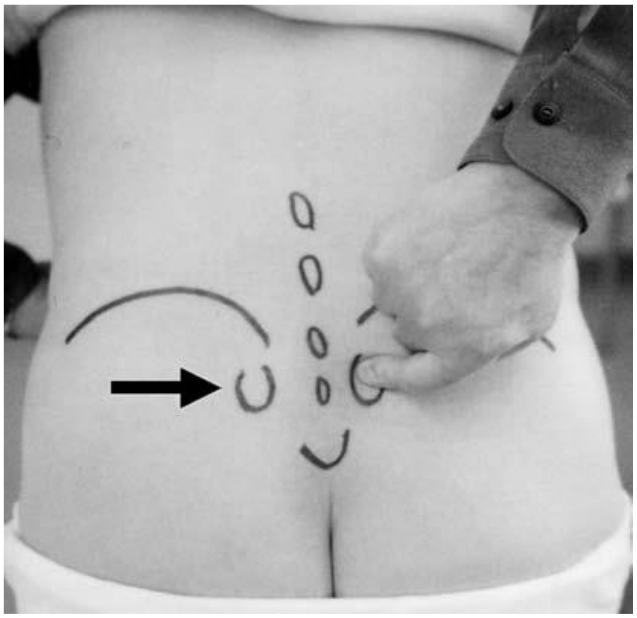

Fig. 1.18 One finger test (Murakami, 2017).

1.5 Treatments for sacroiliac joint dysfunction

1.5.1 Strategy of treatments

Excessive tension to the surrounding ligaments is believed to be a cause of pain due to SIJ dysfunction. According to Murakami et al. (2018b), an unexpected external force or repeated impact cause minor subluxation or incompatibility of SIJs, which makes the surrounding ligaments tense and nociceptors in the ligaments become hypersensitive. This causes pain signals. Immobilization of SIJs reduces loading that was previously supported by surrounding ligaments, which is believed to relieve pain. In other words, the stronger SIJs are fixed, the less ligaments are stretched, which reduces stress generation. This suggests that better fixation of SIJs reduces ligaments loading and relieves pain originating from ligaments. However, as fixation of SIJs means that they lose a little of their inherent mobility a better treatment may be needed to preserve that mobility.

1.5.2 Treatment options

There are several treatment options for curing or relieving pain in SIJ dysfunction, depending on the severity of pain and disease progression. The treatment methods are

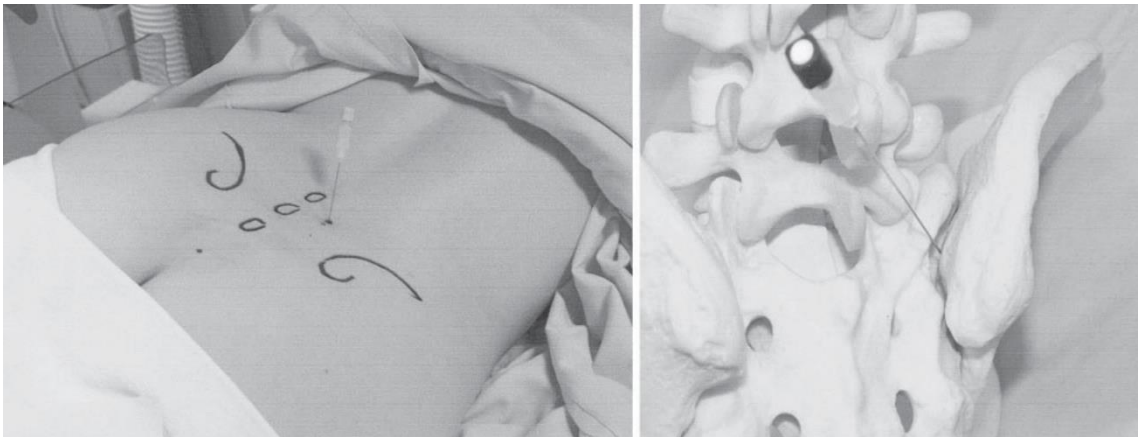

Fig. 1.19 Anesthesia injection on a patient (left) and on a skeletal specimen (right) (Murakami et al., 2007b).

classified into two types: conservative treatments and surgical treatments. Surgical treatments are generally performed when pain can not be sufficiently relieved by conservative therapy or when pain persists for a long time.

Anesthesia (conservative)

This treatment is performing injections to intra- or peri-articular SIJs and releave pain by blocking the nerve transmission pathways (Fig. 1.19). This is used for diagnoses as well as treatments. If pain is alleviated when a local anesthetic is injected into nerves (nerve block), the nerves can be identified as the source of pain. In addition, by mixing a local anesthetic with an anti-inflammatory agent, nerve inflammation can be calmed down, resulting in sustained pain relief.

SIJ injection often relieves pain over one week which greatly exceeds the effect duration of local anesthetics (approximately 2 hours). In addition, pain relief is often achieved in stages with repeated sessions. This can not be explained by the temporary effects of local anesthetics alone (Murakami, 2017). Local anesthetics relieve tension in the posterior ligaments and fluid volume widens the narrow posterior joint space, possibly contributing to the micro-incompatibility of the joint.

Fig. 1.20 Pelvic belts (Soisson et al., 2015).

Pelvic belt (conservative)

Pelvic belts (Fig. 1.20), attached on pelves under iliac crests, provides compression to pelves and partially replaces the supportive role of ligaments, restricting SIJs movement. This method is expected to be sufficiently effective (Murakami, 2017) and can be used to prevent recurrence when returning to work.

Physical therapy (conservative)

Asakura (2015) and Katada (2019) performed physical therapy to maintain and improve motor control function using physical means such as exercise therapy, manual therapy and electrotherapy. In the SIJ dysfunction, osteopathy is generally performed in combination with medical treatment such as pelvic rubber belts and anesthesia (Fig. 1.21).

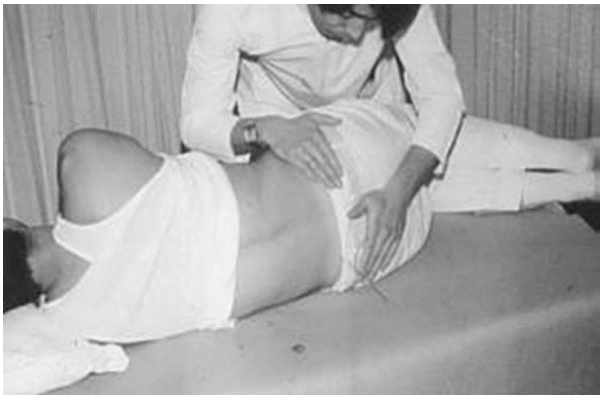

Fig. 1.21 Manual therapy (Katada, 2019).

Joint fixation (surgery)

When the previous treatments can not relieve the pain satisfactorily and severe pain interferes with returning to work or daily life, surgical treatments are performed. SIJ fixation (also called SIJ fusion) is, thus, used for a last resort for treatment. The actual surgical cases are 1% of all SIJ dysfunction cases (Murakami, 2017).

Generally, arthrodesis is an operation performed to connect diseased joints with bony tissues. Despite the complete loss of joint mobility, this treatment is performed when pain control is necessary even in sacrifice of joint function and widely used for various diseases (Canale et al., 2003). In order to perform joint fixation reliably, it is necessary to minimize displacement between bones by fixation using implants and to allow bone growth at the joint. Although SIJs have only a small range of motion, a strong fixation that does not allow even the slightest movement is required to obtain bone union (Bruna-Rosso et al., 2015). Since the early twentieth century, various surgical techniques have been tried for SIJ fixation and recently three methods are mainly used: anterior fixation using plates and screws from front sides of pelves (Fig. 1.22) (Murakami et al., 2018c), posterior fixation using screws and rods from the back sides of pelves (Fig. 1.23) (Venayre et al., 2021) and iFuse implant system using triangular implants from lateral sides of pelves (Fig. 1.24) (Miller et al., 2013). During surgery, it is necessary to fix the joint while avoiding damage to lumbosacral plexuses around SIJs, pelvic organs and blood vessels. The surgical techniques have not yet been completed and are being explored (Stark et al., 2011).

Fig. 1.22 Anterior fixation. (Left) Model. (Center) X-ray image. (Right) CT scan (Murakami et al., 2007a).

Fig. 1.23 Posterior fixation.

Fig. 1.24 iFuse implant system (Miller et al., 2013).

1.6 Previous research on sacroiliac joints

Few studies have been available for physiological functions on SIJs and structural features due to the small range of motion. In addition, the cause of SIJ dysfunction has not been well elucidated and therefore the treatment methods are largely not based on scientific evidences but based on opinions of clinicians. Many reports on SIJs are about clinical results and only a few studies have been conducted using computational biomechanical analysis and human cadavers. The followings are a summary of previous researches on three categories: SIJ motion, articular structure, dysfunction and treatments.

1.6.1 Sacroiliac joint motion

The small range of motion of SIJs has been mainly investigated using cadavers. Various research groups have performed experiments to apply body weight loading to intact healthy pelves (Fig. 1.25) and SIJs motion range was reported to be 0.8 mm (Miller et al., 1987) and 0.3 mm (Hammer et al., 2019c). On patients with SIJ dysfunction, Sturesson et al. (1989) showed to be 0.7 mm using radiographs. The SIJ mobility is thus considered to be less than 1 mm in both healthy subjects and patients. Furthermore,

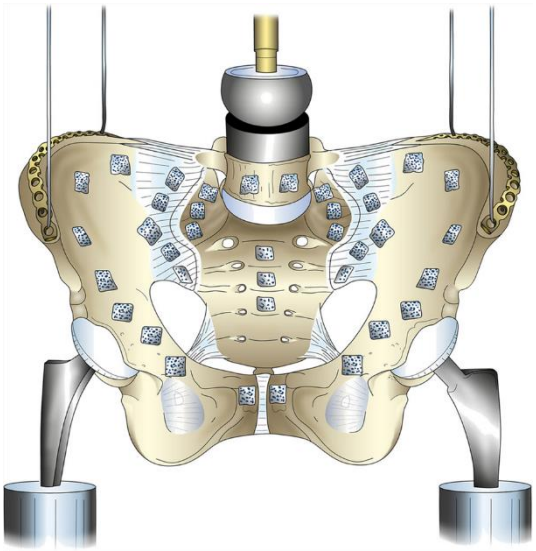

Fig. 1.25 Scheme of experimental setup for physiological load application (Hammer et al., 2019c).

loading experiments have also demonstrated the role of the ligaments using pelves with a removal of specific ligaments. Dall et al. (2019) removed the posterior sacroiliac ligament and showed that it was involved in the stability of SIJs. Hammer et al. (2019a) analyzed finite element models of pelves by removal of various ligaments. They reported that a pelvis with a removal of the sacrospinous and sacrotuberous ligaments increased overall pelvic motion, indicating that these ligaments played a stabilizing role (Fig. 1.26).

Sanaka et al. (2022) investigated the dynamics of SIJs during walking using an in-house android model with wires as ligaments and air cylinders as psoas major muscles (Fig. 1.27). In upright bipedal walking, they showed that the psoas major muscle plays a major role in swinging of legs and SIJs transmit an inertial force from the upper body to the lower body.

1.6.2 Articular surface structure

Several groups have investigated the articular surface structure of SIJs in recent years. Nishi et al. (2018) observed the articular surface on the ilium sides using one hundred cadavers and quantified the three-dimensional morphological characteristics of the joint surface. The SIJ high-degeneration group aged over 60 years showed lower concavities at the middle and lower parts and sharp angles at the posterior edge than the low-

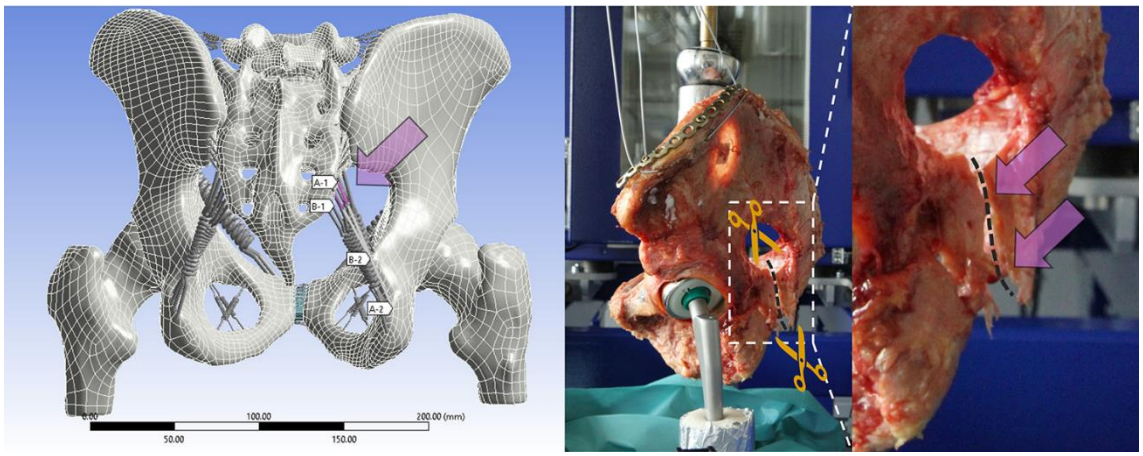

Fig. 1.26 A partial removal of the right complex of sacrospinous and sacrotuberous ligaments on a finite element model (left) and on a cadaver (right) (Hammer et al., 2019a).

degeneration group, indicating that individuals with a larger concavity of the posterior border of the SIJ surfaces may have difficulty in maintaining the stability mechanisms of SIJs as they become older.

Ito et al. (2020) investigated bony coordinate systems on SIJs to reveal the association between sacral morphology and SIJ conformity. The sagittal rotational angles on SIJs were measured using CT images of patients with unilateral SIJ pain, showing that the sacra rotated 2.1 degrees downwards on the symptomatic sides compared to the asymptomatic side. The nutation positions may be likely to cause SIJ pain.

Poilliot et al. (2020, 2021) investigated the bone mineralisation patterns of the articular SIJ subchondral lamella using CT osteoabsorptiometry (Fig. 1.28). Patients with SIJ dysfunction showed more mineralization in the inferior sacrum compared to healthy subjects, resulted from abnormal joint motion of SIJs.

Poilliot et al. (2019a) observed frozen slices of pelves to investigate the distribution of fat in SIJs. The ligamentous region at the posterior SIJs contains a large amount of fat tissue, which may have a shock-absorbing role for during the posterior SIJ compression.

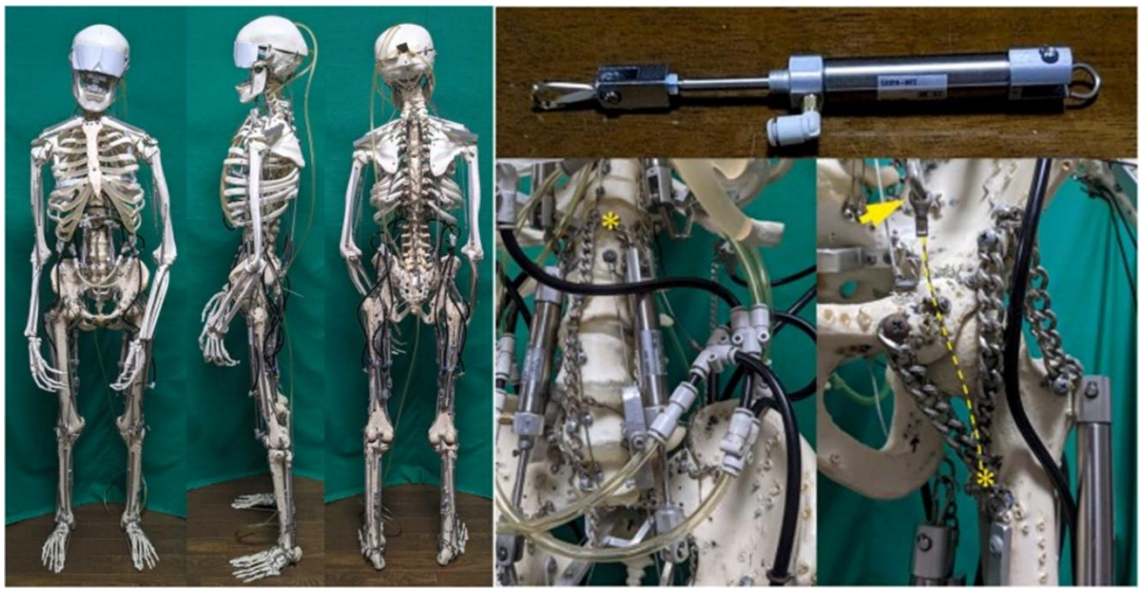

Fig. 1.27 (Left) An android model. (Right top) An air cylinder and (right bottom) an attachment position for psoas major muscles (Sanaka et al., 2022).

1.6.3 Sacroiliac joint dysfunction and treatments

SIJ dysfunction was difficult to diagnose due to the lack of imaging findings. Kurosawa et al. (2017) developed a simple clinical diagnostic scoring system based on pain areas, provocation test, etc., making diagnosis of SIJ dysfunction easier. In the US, definitive diagnosis is often made using intra-articular injection ("North American Spine Society"), which is a difficult procedure (Borowsky and Fagen, 2008; Liliang et al., 2014) and has a low diagnostic rate (Liliang et al., 2009). Without the SIJ sroring system, it may be impossible to diagnose SIJ dysfunction.

Most of previous reports on treatment methods are related to surgery. Murakami et al. (2018c) proposed anterior joint fusion surgery and showed good results. Venayre et al. (2021) numerically analysed this arthrodesis with a finite element analysis, demonstrating high fixation efficiency (Fig. 1.29). However, Sanaka et al. (2020) showed that the surgery inhibits efficient bipedal walking using the aforementioned android model. Recently, other types of surgical treatment have been suggested, with a triangle-shaped iFuse implant system designed specifically for SIJs ("iFuse: The Triangle-Shaped Implant

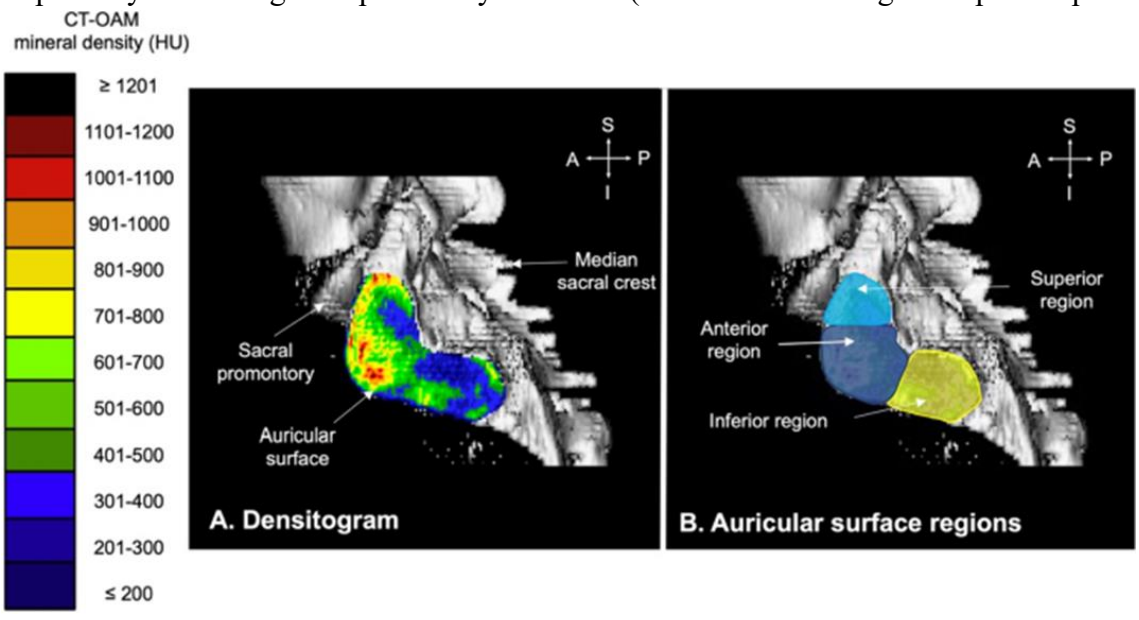

Fig. 1.28 (A) A sacral auricular surface densitogram with the Hounsfield unite (HU) scale. (B) The same densitogram divided into the three regions: superior, anterior and inferior region (Poilliot et al., 2021).

Designed Specifically for the SI Joint"). Casaroli et al. (2019) showed effective fixation for the iFuse implant system than for usual screw fixation systems. This implant system is minimally invasive and has many reports with good clinical results (Duhon et al., 2015). However, all suggested surgical treatments may have a risk of breaking articular structures of SIJs and leading to a loss of functions.

As mentioned above, there are many reports on surgical treatments, while there are few studies on conservative treatments. Murakami et al. (2007b) suggested periarticular injection, which was easier to insert block regions than intraarticular injection and showed higher improvement rate. In addition, Katada (2019) proposed manual therapy based on joint kinematics without any tools. Many techniques such as the Swing-Ishiguro method (Ishiguro and Ishiguro, 2017) have been developed, however the actual mechanisms of their treatments have not been elucidated.

Although a therapy with pelvic belts, one of the conservative treatments, is commonly used clinically, there have been few biomechanical studies to elucidate their effectiveness. Klima et al. (2018) mounted a pelvic belt on a cadaver pelvis and applied a body weight loading. They showed the pelvic belt increased extensional rotation of the sacrum on the sagittal plane and induced counter-nutation. Sichting et al. (2014) analyzed pelvic stress environment with pelvic orthosis using a finite element analysis and demonstrated that pelvic belts relieved tension of SIJ ligaments (Fig. 1.30). Pel et al.

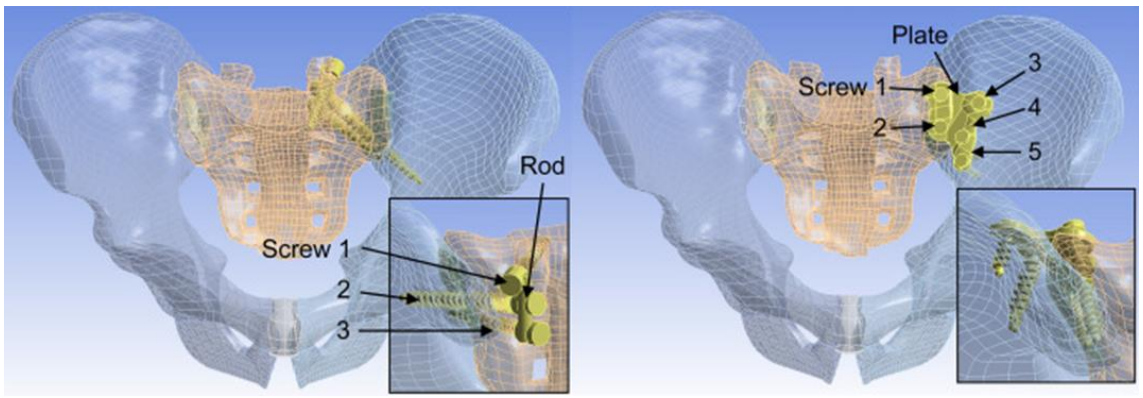

Fig. 1.29 Finite element models of (left) posterior and (right) anterior fixations (Venayre et al., 2021).

(2008) conducted a mathematical analysis of a pelvic model with ligaments and muscles and showed that muscle stress was reduced by pelvic belts.

In addition to the above, Endo et al. (Endo et al., 2020) and Mizuno (Mizuno, 2022) proposed application of extracorporeal shockwave therapy as a new treatment method. They aimed shockwaves to promote regeneration of ligament enthesis or to relive ligament loading temporarily for improving joint mobility, however, there are only clinical reports without any scientific evidences in the actual phenomena.

Therefore, a few research is available on conservative treatments although the mechanisms of some surgical treatments have been objectively demonstrated. Many treatments are based on the assumptions or idea from physicians. Understanding joint function and morphological characteristics, i.e., considering SIJ biomechanics is important for developing future treatments.

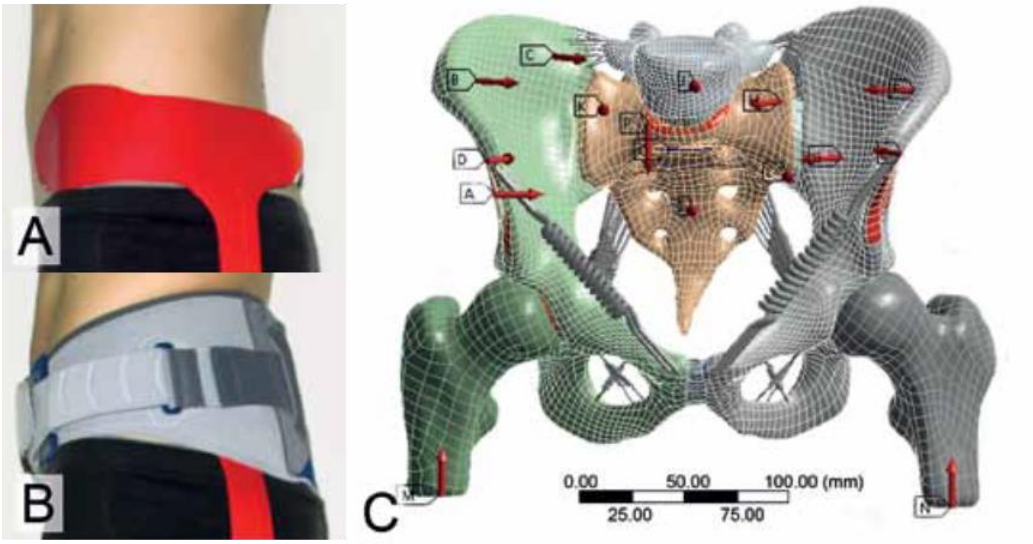

Fig. 1.30 A pressure measuring system (A) without and (B) with a pelvic belt. (C) A finite element model with resultant force vectors for pelvic compression (Sichting et al., 2014).

1.7 Research purposes

As mentioned above, mobility of SIJs is strongly limited and difficult to evaluate from outside the body. Researchers have tried to elucidate mechanical environment on SIJs and found that the range of SIJ movements at rest shown to be 1 mm or less. Recently, owing to this slight mobility, SIJs are considered to work as a shock-absorbing system and to play an important role during walking. For a better understanding of SIJ functions, some researchers have observed the surface morphological characteristics on SIJs using cadavers and suggested that SIJ surfaces can be affected by mechanical environment. It is also noted that conservative treatment options, even pelvic belts that are one of the most popular treatment options for pathological SIJs, have not been well investigated with a focus on stress environment. It is thus highly expected that investigation of detailed stress environment may show mechanical function and importance on pelvic structures with obvious evidence. This study may provide important and significant information useful for diagnosis and treatments. Most of the previous reports have been no more than clinical observations and few researchers have tried to understand mechanical environment on several treatment methods using finite element methods or cadavers.

The purposes of this study are to clarify mechanical functions of SIJs on physiological and pathological pelves and the effect of SIJ morphologies on mechanical environment in the pelves and to visualize stress environment caused by pelvic belts to clarify the treatment mechanism.

This study was conducted in collaboration with Dr. Daisuke Kurosawa (JCHO Sendai Hospital, Japan) and Prof. Niels Hammer (Medical University of Graz, Austria).

1.8 Thesis outline

This thesis is outlined to 6 chapters. The content of each chapter can be summarized as follows:

Chapter 1 introduces fundamental aspects of pelves and SIJs, including anatomical knowledge and SIJ dysfunction. In literature review, previous reports on mechanical environment of SIJs and treatment methods for SIJ dysfunction are summarized. In addition, the purposes of this study are described.

Chapter 2 discovers functions and importance of SIJs on mechanical environment. Due to low mobility of SIJs, few researches have been done on their function and movement. In this chapter, a 3D finite element model of a pelvis with detailed SIJ structure and ligament arrangement are used to perform stress analysis under walking conditions.

Chapter 3 investigates the relationship between SIJ surface morphology and joint motion resistance. SIJ surface has fine irregularities, however, is considered to restrict SIJ motion in a particular direction. In this chapter, SIJ surface models are fabricated based on X-ray CT data and used to measure shear resistance by using an in-house experimental setup.

Chapter 4 considers mechanical environment of SIJs on pathological conditions, using acetabular dysplasia pelves. Acetabular dysplasia is a pelvic morphological abnormality at hip joints, which should affect stress environment of SIJs. Clinically, patients with acetabular dysplasia complain of SIJ pain. In this chapter, finite element models of acetabular dysplasia pelves are created to determine stress distributions on SIJs.

Chapter 5 elucidates effectiveness of pelvic belts, one of treatment options for SIJ dysfunction. This treatment is frequently used in clinic, however, few studies have investigated the mechanism of its effect. Lumbar pressure distribution wearing pelvic belts is measured and stress environment of pelves is analyzed using a finite element model. It provides basic information for treatment strategy of pelvic belts.

Chapter 6 summarizes all results obtained in this study and provide prospects for future research.

Chapter 2

Finite element analysis of mechanical environment of sacroiliac joints during bipedal walking

2.1 Introduction

Sacroiliac joints (SIJs) are composed of synovial joints in the anterior third and tough ligaments in the posterior aspect (Cohen, 2005). Since SIJs are strongly supported by these strong ligaments, SIJs posess comparably low mobility. The range of their motion is generally considered to be a few millimeters and degrees (Egund et al., 1978; Sturesson et al., 1989; Takayama, 1990; Poilliot et al., 2019b). SIJs are largely assumed to serve as a damper, receiving impact between the upper and lower part of the body, thereby transmitting effectively. However, the joint line of SIJs runs roughly parallel to the line gravity, i.e., shear force is generated at SIJs from an upper body weight (Murakami, 2018a).

Bipedal walking consists of a period where only one leg supports the total body weight in the walking cycle. In this period, shear forces are stronger compared to standing on both legs in a resting state. During the swing phase, SIJs are pulled downward by the weight of the free leg. Therefore, SIJs are burdened with variant loads during walking. However, no methods could to date measure objectively how SIJs deform in vivo as well as in vitro during the different phases of walking. Previous researches have made attempts to quantify SIJ motion by three-dimensional computed tomography (3D-CT) and by loading tests on cadavers, reporting that SIJs move less than 1 mm and function as a joint (Takayama, 1990). These trials were however conducted under static conditions.

In this study, to determine the dynamic load transition on SIJs, computer simulations were performed using a finite element analysis during normal walking, resembling the five walking phases of a living body. It was hypothesized that the stress increases in the pelvis if SIJs are lost, indicating that SIJs play an important role during walking. A finite element model of a pelvis consisted of SIJs, the surrounding ligaments and both femora based on previous anatomical studies (Hammer et al., 2009, 2010, 2019c; Steinke et al., 2010; Ramezani et al., 2019). Simulations were performed with actual walking data.

2.2 Methods

2.2.1 Finite element model of pelves

A finite element model of a pelvis (Fig. 2.1) was created by using ANSYS 19.2 (Cybernet Systems Co., Ltd., Chiyoda, Japan) based on CT data of a healthy male (29 years old, 185 cm, 69 kg) (Sichting et al., 2014). The FE model included the fifth lumbar vertebra, the sacrum, the both hip bones, the proximal ends of the both femora, the both SIJ cartilages, the pubic symphysis, the both hip joints cartilages and the intervertebral disks. A total of 210 spring elements representing the ligaments surrounding the pelvis were modelled based on previous anatomical studies on more than 80 cadavers (Hammer et al., 2009, 2010; Steinke et al., 2010), considering the major fiber orientations. Twelve types of ligaments were modelled (Fig. 2.2, Table 2.1). The ligaments were defined in a way where they act only when they are subjected to tensile loads because they do not have a stabilization property on the pelvis and can not sustain the bones in the case of a compressive load.

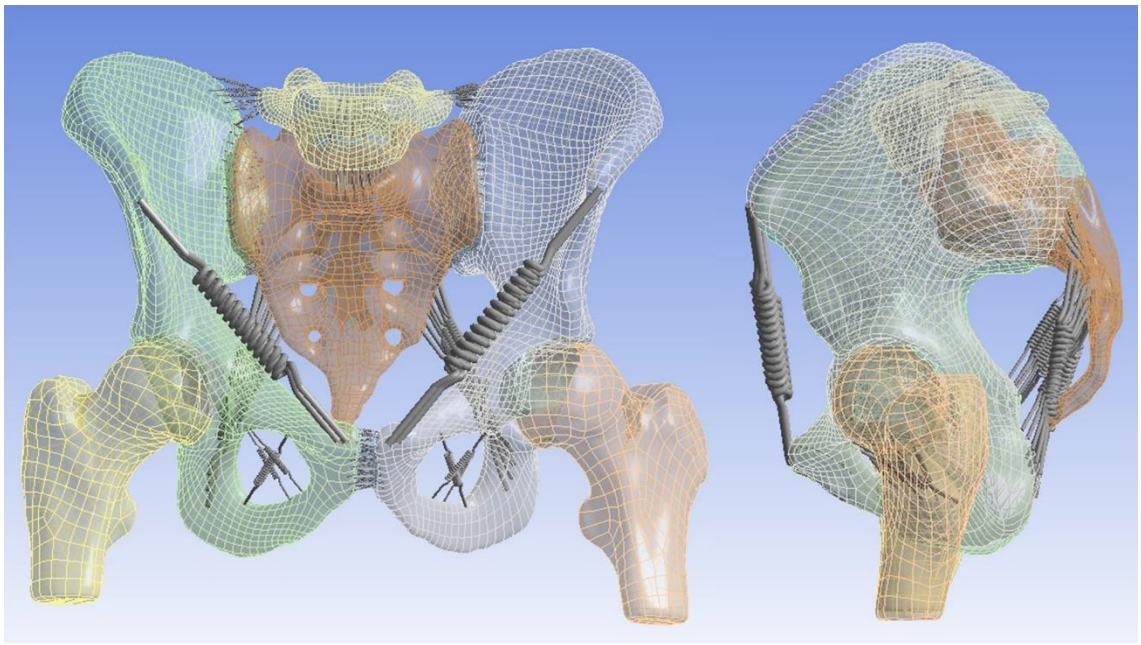

Fig. 2.1 Anterior view (left) and left lateral view (right) of the pelvic model used for finite elements simulations (Toyohara et al., 2020).

In order to determine the role of the SIJ in the pelvis, both models with and without the SIJ cartilage were created by changing the material property of both SIJ cartilage and were named “cartilage model” and “bone model”, respectively. The material property used for both SIJ cartilage was the one of the SIJ cartilage (hyper-elastic body) in the cartilage model and the one of the cortical bone in the bone model.

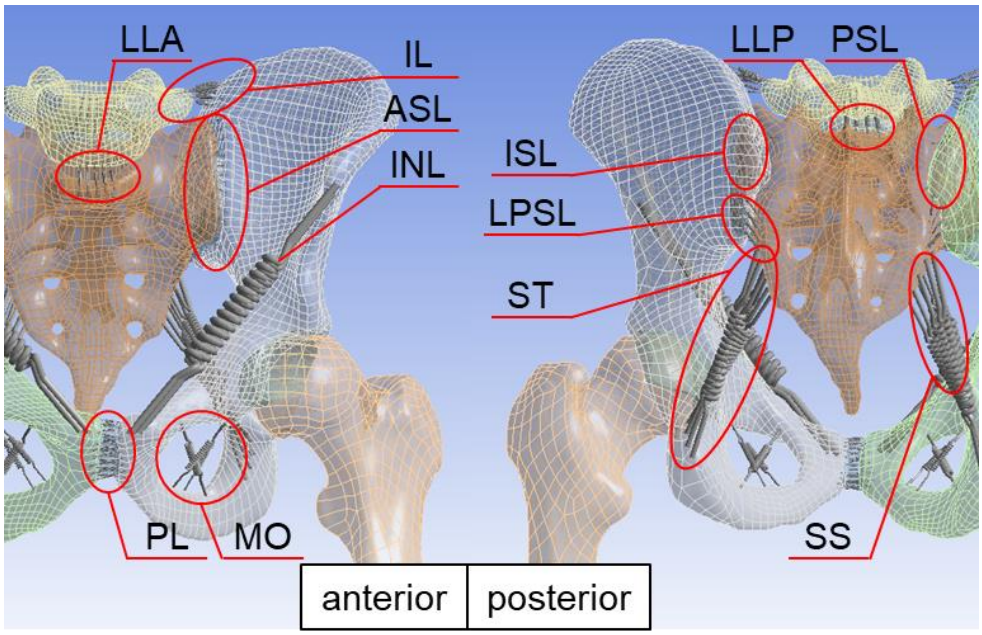

Fig. 2.2 Positions and names of ligaments in the pelvic model with anterior (left) and posterior (right) views (Toyohara et al., 2020).

Table 2.1 Names of ligaments.

Complete expression	Abbreviation	Complete expression	Abbreviation
Iliolumbar ligament	IL	Long posterior sacroiliac ligament	LPSL
Anterior longitudinal ligament	LLA	Inguinal ligament	INL
Posterior longitudinal ligament	LLP	Sacrospinous ligament	SS
Anterior sacroiliac ligament	ASL	Sacrotuberous ligament	ST
Interosseous sacroiliac ligament	ISL	Pubic ligament	PL
Posterior sacroiliac ligament	PSL	Obturator membrane	MO

2.2.2 Material properties

All tissues were defined as a uniform isotropic material for simplification and their material properties were referred from the papers (Wirtz et al, 2000; Sichting et al., 2014; Ramezami et al., 2019) and in part by personal communication with Prof. Hammer (Table 2.2). The hyper-elastic material properties based on Mooney-Rivlin model, which is the strain energy density function W given by the following formula as a complete non-compressional body. Here, C_{10} and C_{01} are material constants. I_1 and I_2 are the first and second invariant of the distortion, respectively.

$$W = C_{10}(I_1 - 3) + C_{01}(I_2 - 3) \tag{2.1}$$

Table 2.2 Material properties. C_{10}, C_{01} and C_{11} mean the parameters of Mooney-Rivlin model for hyper-elastic bodies (modified from Toyohara et al., 2020).

Material	Tissue	Young's Modulus[MPa]	Poisson's ratio	C10 [MPa]	C01 [MPa]	C11 [MPa]
Cortical bone (Wirtz et al., 2000)	Both hip bones, Sacrum Both femora, Both SIJ cartilage 5th lumbar vertebra	11,000	0.2	-	-	-
Cartilage (elastic body) (Sichting et al., 2014)	Both hip joints cartilage intervertebral disks	150	0.2	-	-	-
SIJ cartilage (hyper-elastic body) (by personal communication)	Both SIJs cartilage	-	-	4.1	0.41	0
Symphysis cartilage (hyper-elastic body) (by personal communication)	Pubic symphysis	-	-	0.1	0.45	0.6
Ligament (Ramezani et al., 2019)	All ligaments	350	-	-	-	-

2.2.3 Mesh generation

The bones and joints were meshed using tetrahedral elements consisting of 10 nodes each. The total number of elements and nodes was 141,672 and 80,578, respectively. The average element quality is 0.75, indicating good mesh quality.

2.2.4 Walking Loads

Walking parameters were obtained with 3D walking analysis (MAC 3D, Motion Analysis Corporation, Rohnert Park, CA, USA) of six healthy people (4 males, 2 females, an average of 26.7 years old) by Department of Physical Medicine and Rehabilitation, Tohoku University Graduate School of Medicine (Tohoku University hospital ethics committee, approval number 2018-1-552) (Honda et al., 2019). All methods were performed in accordance with relevant guidelines and regulations and all participants provided written informed consent before participating in the experiment. Walking parameters were divided into five phases (Table 2.3), focusing on the right leg. The walking phases were named phases 1 to 5 (Table 2.4).

2.2.5 Boundary conditions

To simulate walking conditions properly, the joint moments were applied on both femoral heads and surface loads were applied on adhesive surfaces of both femoral heads and both hip bones cartilage and on the base of the sacrum (Fig. 2.3(a)). The surface loads on the base of the sacrum were calculated from the ones on both femoral heads with the principal of action and reaction. By changing the angle of joint moments and surface loads, the tilt, drop and rotation of the pelvis were reproduced during walking. The anterior aspect of the second sacral spine was fixed in space in order to reproduce movements of the sacrum: nutation and counter-nutation (Fig. 2.3(b)). For contact type, all surfaces in contact were defined as “bonded”, which means the surfaces are fixed to each other.

Table 2.3 Mean values of joint moments, surface loads, and pelvic angles (modified from Toyohara et al., 2020).

			Phase 1	Phase 2	Phase 3	Phase 4	Phase 5
Joint moments[1] [Nm]	Right femur	sagittal plane	10.9 (19.9, 1.8)	-18.9 (-16, -21.2)	-21.3 (-17.4, -29.1)	-2.5 (-1.2, -3.9)	0.5 (1.6, -0.5)
		coronal plane	17.8 (23.1, 11.9)	44.5 (50.1, 35.9)	16.5 (22.8, 13.9)	0.5 (0.8, 0.2)	0.1 (0.2, -0.1)
		transversal plane	5.8 (9.2, 3.8)	0 (1.4, -1)	9.5 (15.9, 5.7)	-0.2 (-0.1, -0.3)	0.1 (0.4, 0)
	Left femur	sagittal plane	-17 (-13.2, -24)	-0.8 (-0.5, -1.1)	16.1 (21.3, 9.4)	-5.7 (1.8, -12.8)	-28.1 (-20.6, -41)
		coronal plane	16.4 (20.7, 11)	0.3 (0.5, 0.2)	15 (21.5, 10.9)	45 (51.6, 36.3)	41.6 (52.3, 32.7)
		transversal plane	10.2 (18, 3.8)	0 (0, -0.1)	-6.4 (-1.9, -11.6)	-5.1 (-1.7, -9.9)	3.2 (5.5, 0.4)
Surface loads[2] [N]	Right femur	medio-lateral	13.9 (21.3, 6.5)	36.1 (48.9, 25.4)	16.7 (29, 8.9)	1.7 (2.4, 1.1)	1.7 (2.6, 1)
		anterior-posterior	53 (65.6, 40.9)	-0.8 (3.6, -6.7)	-74 (-62.7, -101.7)	-3.9 (-2.7, -5.1)	2.6 (3.3, 1.7)
		vertical	344.6 (422, 244.5)	558.3 (659.1, 438)	319 (424.8, 255.6)	-26.5 (-21.2, -31.2)	-25.6 (-20.8, -30.1)
	Left femur	medio-lateral	-18 (-10.3, -26.3)	-1.7 (-1.3, -2.2)	-11 (-6.3, -17.6)	-33.7 (-24.6, -45.1)	-34.3 (-22.1, -45.3)
		anterior-posterior	-66.9 (-57.6, -82)	-0.4 (0.2, -1)	46.8 (66.9, 28.1)	40.4 (55.8, 30.7)	-31.3 (-25.4, -48.7)
		vertical	289 (368.8, 235.7)	-25.8 (-20.5, -30.1)	318.6 (403.9, 237)	550.5 (657.5, 424)	553.8 (648.5, 428.5)
	Base of sacrum	medio-lateral	4.1 (8.2, 0.8)	-34.4 (-23.8, -46.9)	-5.7 (-1.9, -12.1)	32 (42.7, 23.5)	32.6 (43.6, 21.1)
		anterior-posterior	13.9 (20.4, 0.3)	1.2 (7.3, -3.3)	27.2 (45.9, 14.6)	-36.5 (-28.1, -51)	28.7 (45.4, 22.9)
		vertical	-633.6 (-480.2, -760.4)	-532.5 (-417.5, -629.1)	-637.6 (-492.6, -773.1)	-524 (-402.8, -626.3)	-528.2 (-407.5, -619.7)
Pelvic angles[3] [°]		sagittal plane	8.1 (12, 3.8)	8.1 (11.2, 5.3)	8.3 (11.5, 4.6)	7.7 (11, 3.8)	7.8 (10.9, 4.6)
		coronal plane	-3.8 (-1.9, -5.9)	-1.7 (0.6, -4.1)	1.6 (3.1, -0.4)	1.3 (3.8, -0.5)	-2.3 (-0.1, -3.9)
		transversal plane	-5 (-1.8, -9)	-0.8 (0.9, -3)	3.4 (7.6, -1.2)	2.6 (7.1, -1.2)	-3.1 (-0.6, -5.4)

[1] sagittal plane : flextion [+] / extension [-], coronal plane : abduction [+] / adduction [-], transversal plane : external rotation [+] / internal rotation [-]
[2] medio-lateral : left [+] / right [-], anterior-posterior : posterior [+] / anterior [-], vertical : superior [+] / inferior [-]

[3] sagittal plane : anterior tilt [+] / posterior tilt [-], coronal plane: elevation [+] / depression [-], transversal plane: forward rotation [+] / backward rotation [-], on right leg

Table 2.4 Walking phases.

	Phase1	Phase2	Phase3	Phase4	Phase5
Right limb	Stance Phase			Swing Phase	
Left limb	Stance Phase	Swing Phase	Stance Phase		
Gait phase	Heel contact	Single leg support	Opposite heel contact	Single leg support	

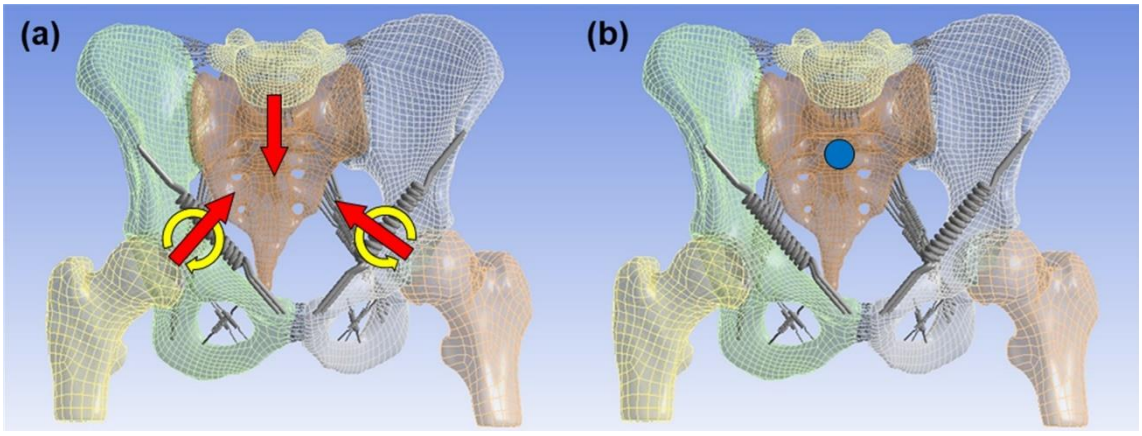

Fig. 2.3 (a) The yellow arrows indicate where the joint moments are applied, the red arrows indicate where the surface loads are applied, and (b) the blue point indicates where the pelvis is fixed (Toyohara et al., 2020).

2.2.6 Analytical parameters

In this study, the resultant displacement of the pelvis and SIJ cartilage and the equivalent stress (Von Mises Stress) of the SIJ cartilage were investigated. The resultant displacement shows a 3D displacement value and direction. The equivalent stress is a scalar value that is calculated from normal stresses and shear stresses without any distinction between tension and compression. This stress is given by the following formula.

$$\sigma_{eqv} = \sqrt{\frac{1}{2}\left\{\left(\sigma_{xx} - \sigma_{yy}\right)^2 + \left(\sigma_{yy} - \sigma_{zz}\right)^2 + (\sigma_{zz} - \sigma_{xx})^2 + 6\left(\sigma_{xy}^2 + \sigma_{yz}^2 + \sigma_{xz}^2\right)\right\}} \quad (2.2)$$

Here, σ_{eqv} is Von Mises stress. σ_{xx}, σ_{yy} and σ_{zz} are normal stress in X, Y and Z direction, respectively. σ_{xy}, σ_{yz} and σ_{xz} mean shear stress in XY, YZ and XZ direction, respectively.

In addition, the maximum elastic force of spring probes was investigated for loads on ligaments and summed for each of the ligaments.

2.3 Results

As the data obtained from 3D walking analysis yielded consistent results, one of the datasets (33-year-old male, 175 cm, 72 kg) was used for the modeling.

2.3.1 Displacement of pelves

The difference in displacement between the sacrum and ilium in all walking phases averaged 0.23 mm in the cartilage model and 0.04 mm in the bone model, respectively (Fig. 2.4). In the cartilage model, this difference increased to approximately 5.4 times compared to the bone model. The displacement differed greatly between the sacrum and the both hip bones on the SIJ as the boundary.

During maximum displacement of the pelvis (Fig. 2.5), mean values in all walking phases averaged 1.9 mm in the cartilage model and 1.1 mm in the bone model, indicating a decrease in displacement to approximately 57 % compared to the cartilage model throughout all walking phases.

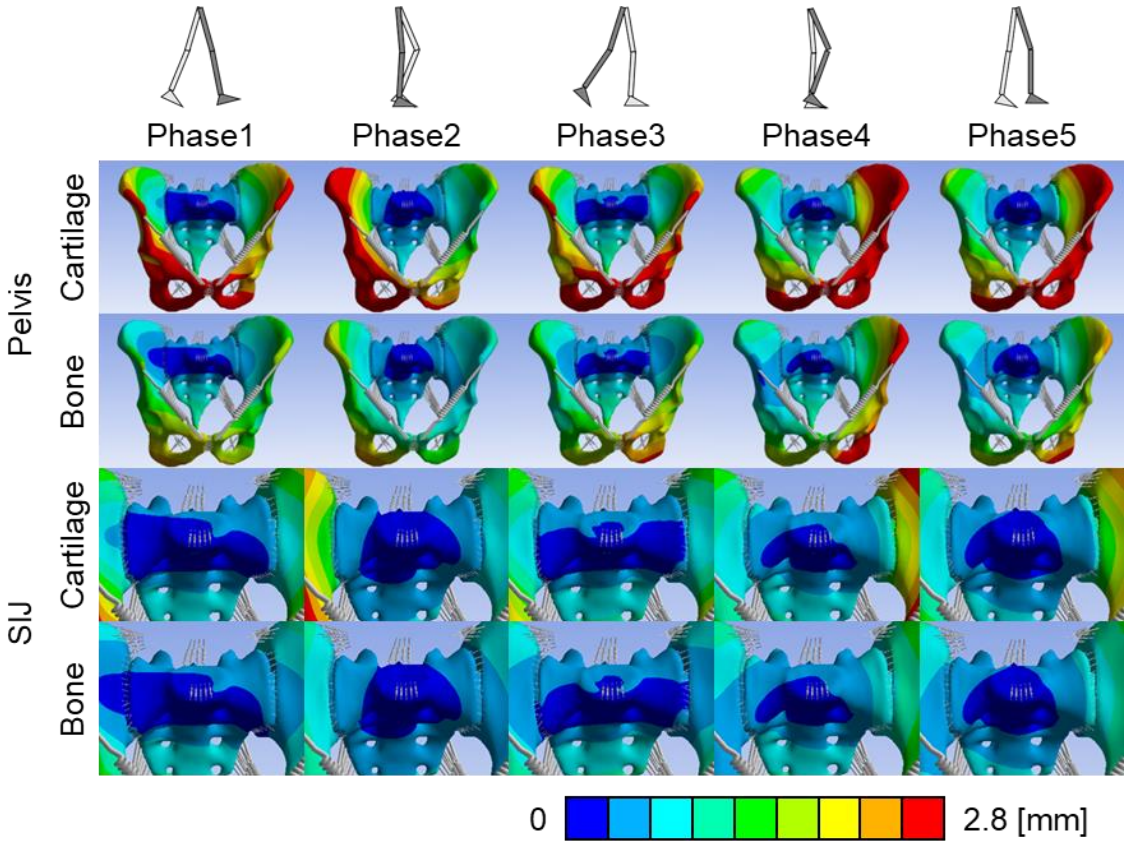

Fig. 2.4 Resultant displacement distribution of pelvis excluding femora (top 2 lines) and pelvis surrounding sacroiliac joints (bottom 2 lines) on a representative example (Toyohara et al., 2020).

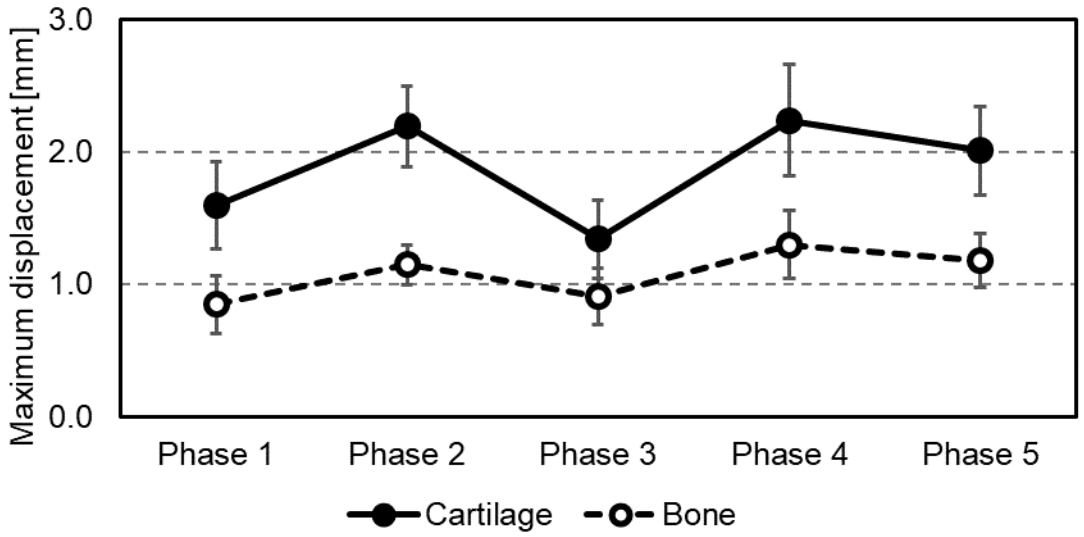

Fig. 2.5 Change of mean values of maximum resultant displacement in pelvis excluding femora (Toyohara et al., 2020).

2.3.2 Rotational motion of sacroiliac joints

As shown in Fig. 2.6, during the stance phase (phases 1, 2, 3), the ilium was elevated relative to the sacrum and the sacrum had a nutation movement relative to the ilium. Meanwhile, during the swing phase (phases 4, 5), the ilium was lowered relative to the sacrum and the sacrum moved in a counter-nutation sense relative to the ilium.

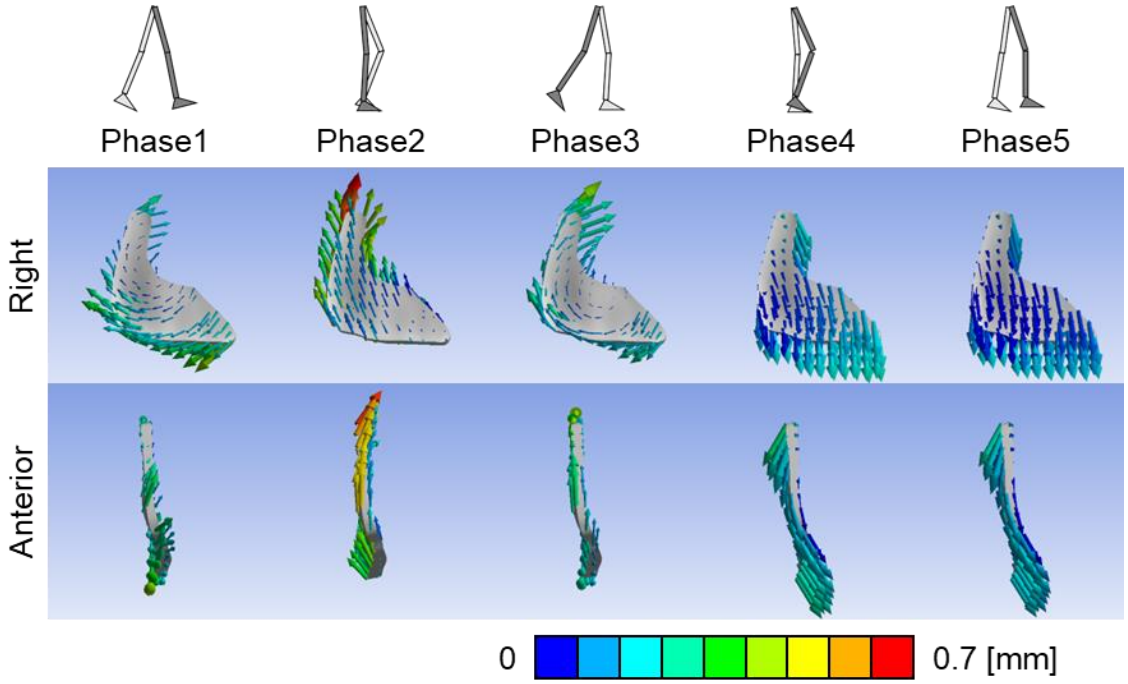

Fig. 2.6 Resultant displacement vector diagrams of sacroiliac joints (SIJs) with the cartilage model on a representative example (Toyohara et al., 2020).

2.3.3 Displacement of sacroiliac joints

During the stance phase (phases 1, 2, 3), the SIJ cartilage was mainly deformed cranially centered on the lower part of the SIJ cartilage and the ilium went away from the sacrum on the same part. Meanwhile, during the swing phase (phases 4, 5), the SIJ cartilage was mainly deformed caudally centered on the upper part of the SIJ cartilage and the ilium went away from the sacrum on the same part (Fig. 2.6). The maximum displacement of the SIJ cartilage was approximately 0.3 mm and 0.6 mm during the swing and stance phase (phases 1, 2, 3), respectively (Fig. 2.7).

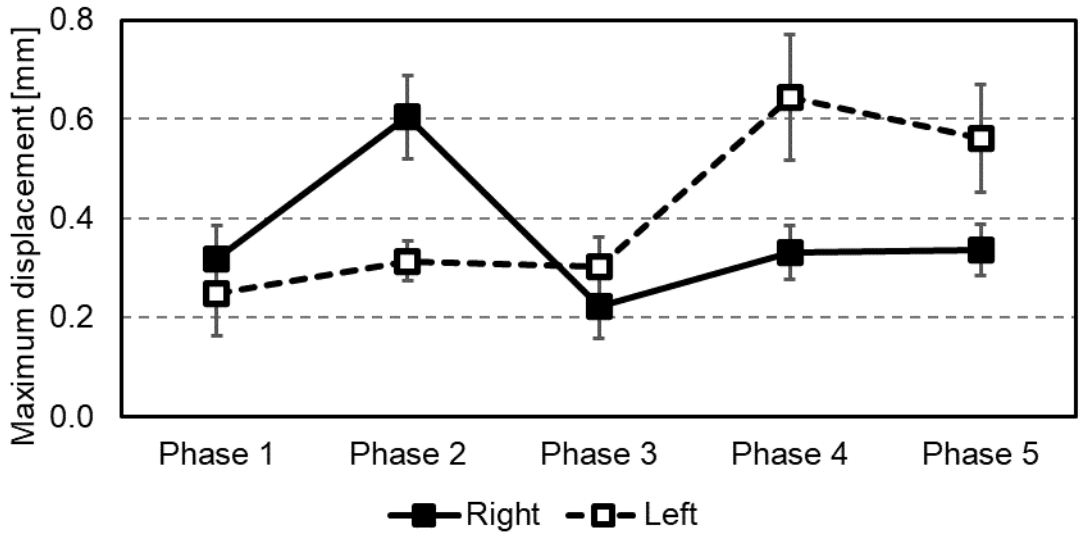

Fig. 2.7 Change of mean values of maximum resultant displacement of right and left SIJs (Toyohara et al., 2020).

2.3.4 Equivalent stress on sacroiliac joints

In the cartilage model, equivalent stresses were concentrated in the front of the SIJ cartilage throughout all walking phases and increased to approximately 5.8 MPa in the upper part of the SIJ cartilage during the stance phase (phases 1, 2, 3) (Fig. 2.8). During phase 2, where only a single leg supports the whole-body weight, the equivalent stresses increased remarkably to approximately 3.8 x the extent compared to the other walking phases and averaged 5.8 MPa (Fig. 2.9). In the swing phase (phases 4, 5), the equivalent stress was similar at the lower aspect of the SIJ cartilage compared to the stance phase (phases 1, 2, 3) at approximately 1.0 MPa and the maximum values decreased as a whole. Regarding the maximum equivalent stress of the right SIJ cartilage, the values at phase 2, when the maximum equivalent stress was highest, averaged 41.2 MPa in the bone model, i.e., in phase 2 the values of the bone model increased to approximately 700% of the cartilage model.

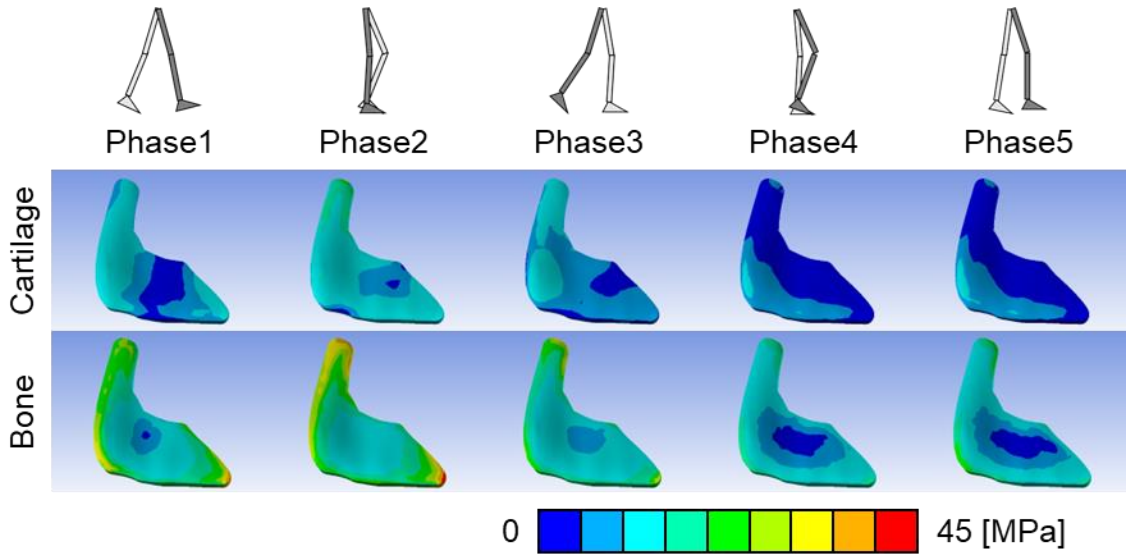

Fig. 2.8 Equivalent stress distribution of right sacroiliac joints (SIJs) on a representative example viewed from sacral sides (Toyohara et al., 2020).

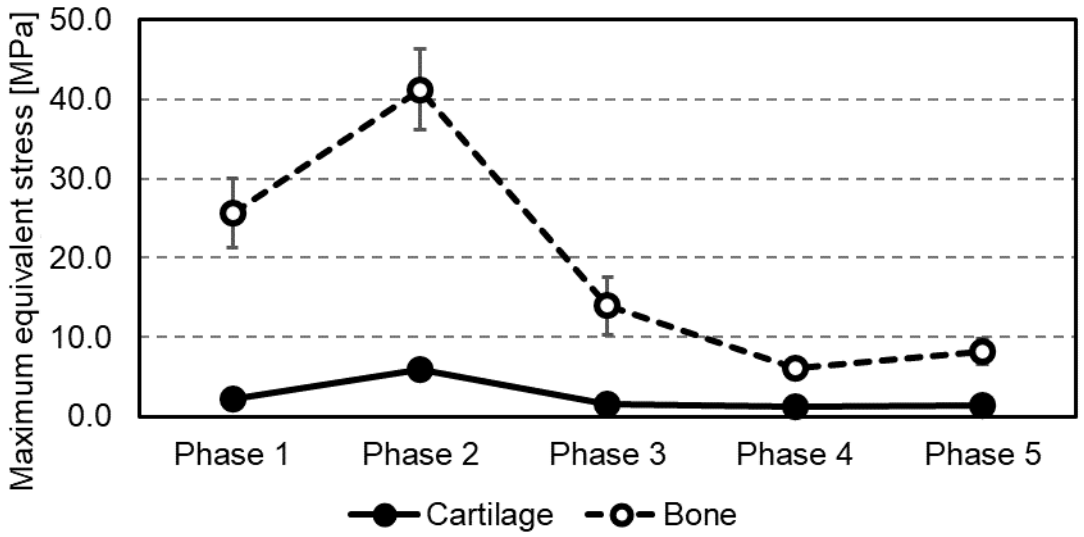

Fig. 2.9 Change of mean values of maximum equivalent stress in right SIJs (Toyohara et al., 2020).

2.3.5 Loads of pelvic ligaments

Although the loads varied depending on the walking phase and the ligament, the loads of the bone model decreased to approximately 23% compared to the cartilage model. In particular, the loads on the ASL, ISL and PSL as well as the SS and ST decreased to less 23% and only the ISL and PSL decreased remarkably more than 200 N. In the cartilage model, the loads increased in the swing phase (phases 4, 5) and decreased in the stance phase (phase 1, 2, 3) (Fig. 2.10(a)). The loading rate on PSL and ISL accounted for 81% (maximum PSL 45%, ISL 62%) and was much higher than others throughout all walking phases. In addition, only on the stance phase (phases 1, 2, 3) the ST was loaded and its load rate was approximately 11% (Fig. 2.10(b)).

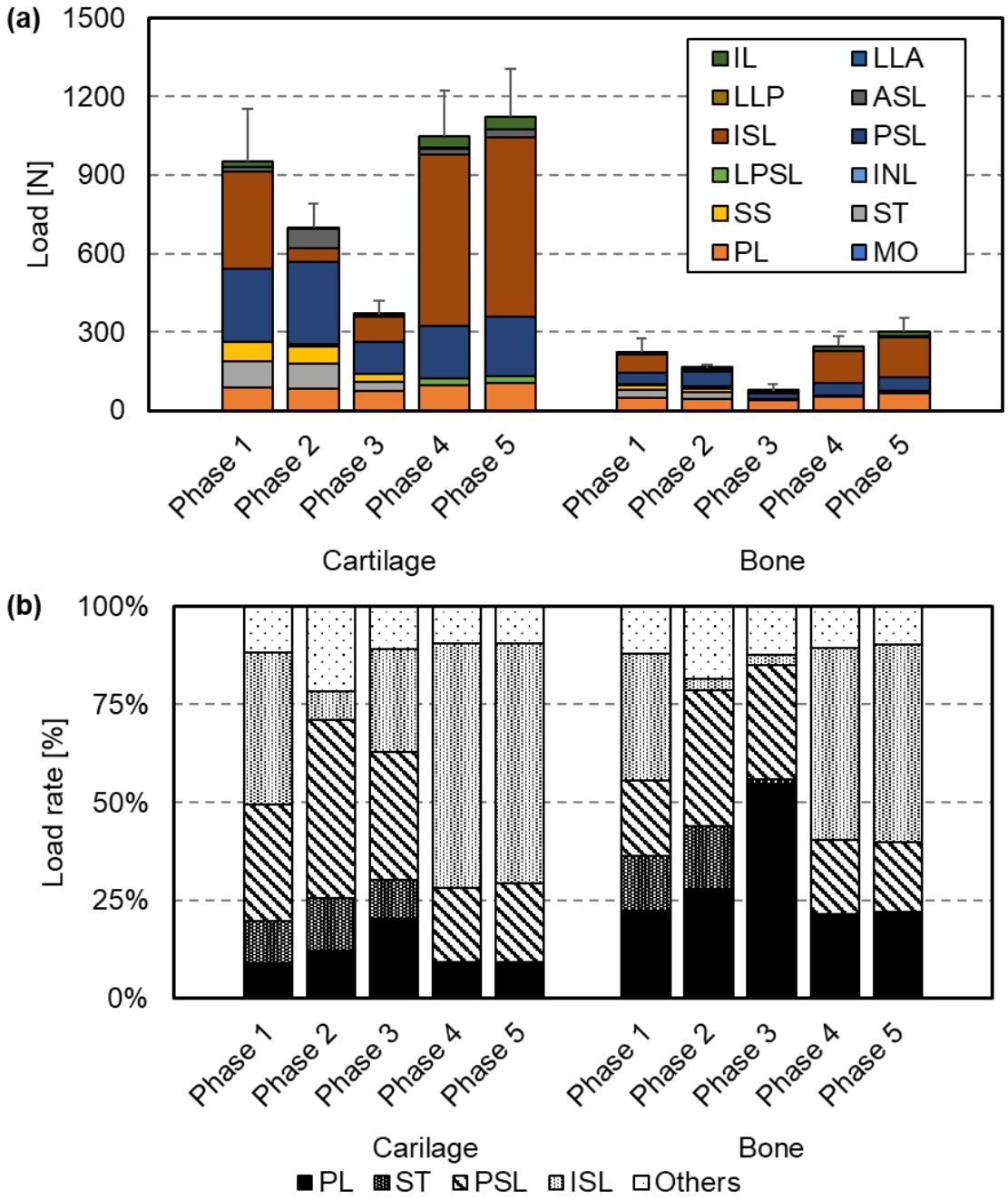

Fig. 2.10 Comparison of (a) the mean loads and (b) the mean load rates on ligaments of the right part of the pelvis between the bone and cartilage model. The loads of ligaments are the sum of each ligament, which has 2 to 30 spring components. Here, the loads on pubic ligament PL, anterior longitudinal ligament LLA, and posterior longitudinal ligament LLP were halved due to their location at the center of the spinopelvic complex (Toyohara et al., 2020).

2.4 Discussion

2.4.1 Motion of sacroiliac joints during bipedal walking

On the finite element analysis, the pelvis of the free leg moved relatively inferiorly when walking. This corresponds to a report stating that the pelvis is depressed to a swing leg on walking (Kapandji, 1974). In addition, the SIJ had small motion of less than 1 mm, and moved separately on the left and right SIJ. The range of the SIJ movements has been investigated with various methods; on patients with SIJ disorders 0.7 mm by Sturesson et al. (1989), 0.7 mm by Jacob and Kissling (1995) and 0.3 mm by Sturesson et al. (2000), on healthy individuals 0.47 mm by Kibsgård et al. (2012), on cadavers 0.8 mm by Miller et al. (1987), less than 1 mm by Takayama (1990) and 0.3 mm by Hammer et al. (2019c) and on FEM 0.3 mm by Bruna-Rosso et al. (2015). This study showed that the displacement of the SIJ cartilage was ranged from 0.3 mm to 0.6 mm, which was similar to the previous studies. It was previously demonstrated that most of the sacral movement takes place around a transverse axis, situated at the level of the second sacral vertebra. Iliac rotation relative to the sacrum was later named nutation and counter-nutation (Vleeming et al., 2012), thought ambiguity exists as nutation was also named the combined rotation and translation movement of the sacrum relative to both innominate bones (Kapandji, 1974). The above studies (Sturesson et al., 1989, 2000; Jacob and Kissling, 1995; Kibsgård et al., 2012; Hammer et al., 2019c) have reported that the sacrum rotates approximately 2 degrees on the sagittal plane, which seems to indicate such movement. Bruna-Rosso et al. have shown the rotation of the sacrum with vector diagrams in a finite element model (Bruna-Rosso et al., 2015). In this study, the relative nutation and counter-nutation movements of the sacrum during bipedal walking were visualized, which had not been clarified so far. On the side of the stance leg, the sacrum moved into the nutation position. Meanwhile, on the side of the free leg, the sacrum moved into the counter-nutation position. The nutation is a movement in which the sacrum rotates forward when the load from an upper body is applied on the upper of the sacrum and pushes down the promontory. At this time, the ground reaction force is

applied via the femora to both hipbones, and the ilium tilts backwards. This promotes the nutation. However, the ligaments restrict the movements in order to avoid too ample the nutation (Kapandji, 1974). This nutation mechanism is based on both legs standing and can not be fully replicated when walking. From these results, the nutation mechanism during walking was interpreted as follows: On the standing leg, the nutation was facilitated by the load from an upper body and the ground reaction force as in the case of double-leg standing. Meanwhile, in the swing leg, this movement was not facilitated and the sacrum performed a counter-nutation, as the ilium was pulled down by the weight of the lower limb. It is impossible that the left and right SIJs perform individual nutation or counter-nutation movements if the pelvis is only modelled as one bone. Given the left and right SIJ showed separate movements, it was possible to walk on a human bipedal walking with a standing leg and a free leg alternatively. This suggests that the SIJs plays an important role in the human bipedal walking mechanism, however, very little information is to date available on the nutation and counter-nutation during walking, and these findings need to be substantiated further.

2.4.2 Load transition of sacroiliac joints

In the bone model, the difference in displacement between the ilium and sacrum was minute (0.04 mm), resulting in a continuous displacement between these bones. In this model, as a result, the equivalent stress of the SIJ cartilage defined at the cortical bone was comparably high. This equivalent stress indicates load concentrations at the bony transition, to the end that in a “fused condition” premature failure of the adjacent bone may occur.

In the cartilage model including the SIJ, the difference in displacement between the ilium and sacrum was 0.23 mm, which seemed high when compared to the bone model. Loading across the bones seemed discontinuous, with the SIJ acting as a damper. These results were in line with the work by the group of Takayama (1990). Therefore, the role of the SIJ as a shock absorber can be confirmed based on the findings presented here.

Potentially, the fat situated within the interosseous ligaments plays an important role in shock absorption (Poilliot et al., 2019a; b). Owing to this, the pelvis obtains additional elasticity. The ligaments surrounding the posterior do work additionally to help distribute the loads from the upper to the lower body parts by means of increased areas of force transmission, while may at the same time be the potential failure site in case of injury (Hammer et al., 2019b). These findings strongly suggest that the SIJs forming part of the pelvis help dissipate loads and therefore be vital for non-traumatic loading at the spine-leg transition. The SIJ was found to be an area where stress peaked on the pelvic ring from the bone model. It is therefore speculated that it may be important for the structure of the pelvic ring to have a joint structure that relieves stress concentration at this area.

The load rates at the PSL and ISL were approximately 70% throughout all walking phases and much higher than in other areas. In phase 2 of the gait cycle when only a single leg supports the whole-body weight and when the equivalent stress of the SIJ peaked, their load rate decreased to approximately 52%. On the other word, when the stress of the SIJ cartilage increases, the loads of the pelvic ligaments decrease. This mechanical finding is in line with the morphology of the SIJ which is composed of an anterior synovial joint region and a posterior ligamentous region (Vleeming et al., 2012; Poilliot et al., 2019b). In particular, it was considered that the anterior synovial joint region helps carry the compression load from an upper body weight and the ligamentous region the tensile load from the lower limb in a simplified model.

It can be assumed that in the humans walking upright and bipedal, the SIJ has become more resilient to support the weight of the upper body even under relatively unfavourable levers which constantly change when walking (Murakami, 2018a). Cohen proposed that the SIJ was designed primarily for stability (Cohen, 2005). However, if the SIJ is too tightly connected for stability, this may result in a biased load with peak effects. Like the current SIJ, although supported by tough ligaments, the SIJ was considered to need to have some mobility.

Surgical SIJ fixation is a treatment that minimizes SIJ motion (Dreyfuss et al., 2004; Murakami, 2018a) and there are fixation methods aiming the ossification on the articular surface following surgery (Wise and Dall, 2008; Smith et al., 2013). These experiments have been performed with cadavers (Dall et al., 2019) or FEM (Bruna-Rosso et al., 2015; Lee et al., 2017; Casaroli et al., 2019) in order to assess the fixation. However, these only indicate only one condition immediately after the surgery. In the medium to long term time frame, the actual post-fixation state may be close to the bone model presented here. The SIJ fixations suppress the SIJ deformation and relieve pain, however, it could be assumed that stress of the SIJ increased due to the ossification, which may further promote bone formation and damage the SIJ when a sudden or unexpected external force is applied.

2.5 Conclusions

This simulation was performed for the first time by implementing actual 3D walking data into a finite element model of the pelvis elaborated from large-scale anatomical studies. As a result, the mechanical state of SIJs during bipedal walking was visualized, and the movements of the SIJ and the loads of the SIJ cartilages and surrounding ligaments could be quantified. The walking loads caused distortion of the whole pelvis and the stress concentrated at the SIJ due of the morphology of the pelvic ring. Modeling the SIJ into the pelvic ring, stress concentrations was received and surrounding ligaments carried the loads. It was found that the SIJ had the shock absorbing mechanism during walking. For the first time, this study, the extent of motion of the SIJ and the relative nutation and counter-nutation movements of the sacrum during bipedal walking were visualized. This novel information provides a scientifically informed basis for clinical discussions regarding the state of the SIJ dysfunction caused from the timing of pain induction during walking, gait changes and surgical intervention.

Chapter 3

Experimented analysis of relation between articular surface and motion resistance on sacroiliac joints

3.1 Introduction

Sacroiliac joints (SIJs) located in the pelvis are composed of synovial joints in the anterior third and tough ligaments in the posterior aspect (Fig. 3.1) (Cohen, 2005). Due to the strong ligaments, SIJs have comparably low mobility. The range of their motion is generally considered to be a few millimeters and degrees (Egund et al., 1978; Sturesson et al., 1989; Poilliot et al., 2019b). The SIJs are largely assumed to serve as a damper, receiving impact between the upper and lower part of the body, thereby transmitting effectively (Toyohara et al., 2020). Unexpected or repeated impacts are believed to cause pain from the SIJ (Murakami et al., 2018b). Since SIJ dysfunction is hypothesized to be caused by joint misalignment, fixing the SIJs and preventing excessive motion is considered effective in relieving the pain.

In the synovial joint area, the articular surface has fine irregularities, however, it is considered to form a flat rail (Katada, 2019). In addition, it is thought to affect the synovial fluid flowing through the joint gap (Yoshida, 1999). One of the representative movements of the SIJ is nutation and counter-nutation, which are forward and backward

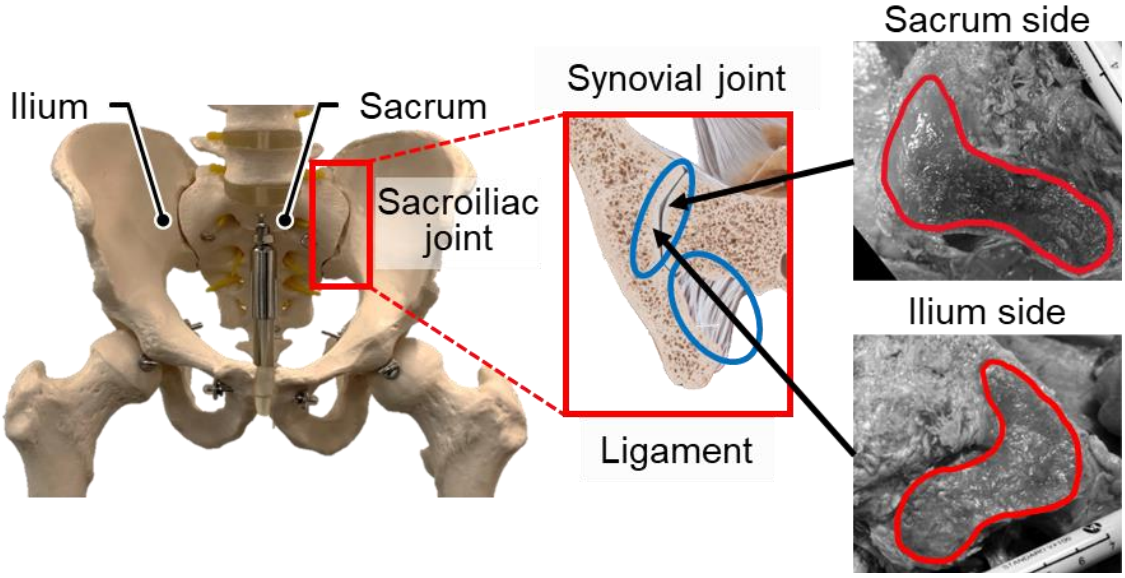

Fig. 3.1 The anterior and posterior sides are synovial joints and ligamentous regions, respectively (modified from Schünke et al., 2017). The edges of synovial joint area are shown in red lines.

rotations of the sacrum on the sagittal plane, respectively. The sacrum is standing and the wedge is deeply driven into the pelvic ring fixed by the pubic symphysis and the posterior ligaments. This state is considered to be the most stabilized form for SIJs (Katada, 2019). Articular surfaces of the SIJ are to date poorly characterized in relation to the mobility of SIJs. This study aims to clarify how the SIJ surface affects motion resistance. From previous anatomical research using cadavers, it was hypothesized that the surface shape potentially restricts the direction and range of motions in the SIJs.

3.2 Materials and methods

3.2.1 Pelvic surface model with sacroiliac joints

Lumbar CT data of three patients were provided from the JCHO Sendai Hospital (Sendai, Japan) for this study. Two of them suffered from unilateral SIJ dysfunction and the contralateral unaffected sides were provided for this modeling. All patients provided the signed informed consent for use of the data. The whole pelves were automatically segmentated to construct a pelvic surface model. Articular surfaces of the sacrum and

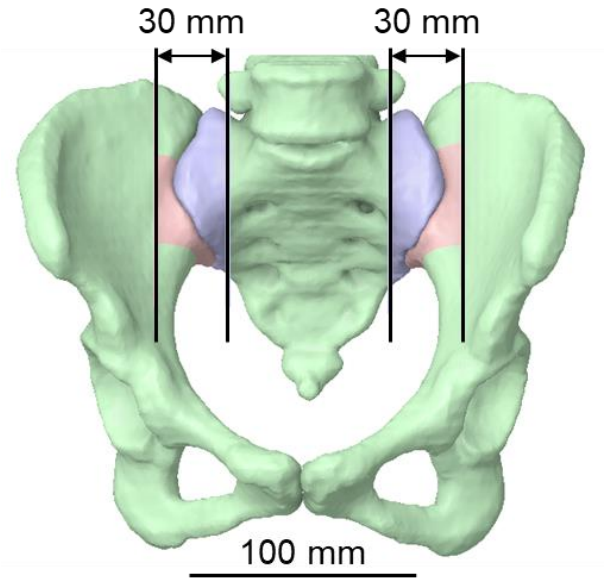

Fig. 3.2 A pelvic model. The blue and red models are the sacrum and ilium models, respectively. The black lines are the cuting lines with intervals of 30 mm.

ilium were manually segmentated with 1 mm slices. The SIJs were cut in the sagittal planes at intervals with 30 mm centered on the articular surfaces (Fig. 3.2). The right SIJ models were reversed and all SIJ models were assumed to be on the left sides.

3.2.2 Extraction of articular surface

The above articular surface models were extracted only for the synovial joint regions (Fig. 3.3). To compare motion resistance with difference in alignments of joints, the sacrum models were rotated 5 degrees clockwise and counterclockwise around the center of their articular sufaces. As summarized in Table 3.1, the clockwise rotated models imitated counter-nutation positions on the right sides and nutation positions on the left sides, while the counterclockwise rotated models imitated counter-nutations positions on the right sides and nutation positions on the left sides.

The combinated articular surface models were imported into open-source software, CloudCompare v2.10.2, which is 3D point cloud and mesh processing software ("CloudCompare"). The articular gap height distribution was measured on the sacrum models from the ilium models and then colored on the sacrum models depending on gap heights (Fig. 3.4).

Table 3.1 Joint states on surface models.

	Ilium model	Sacrum model	SIJ state
Right side	Fix	Clockwise	Counter-Nutation
	Fix	Counterclockwise	Nutation
Left side	Fix	Clockwise	Nutation
	Fix	Counterclockwise	Counter-Nutation

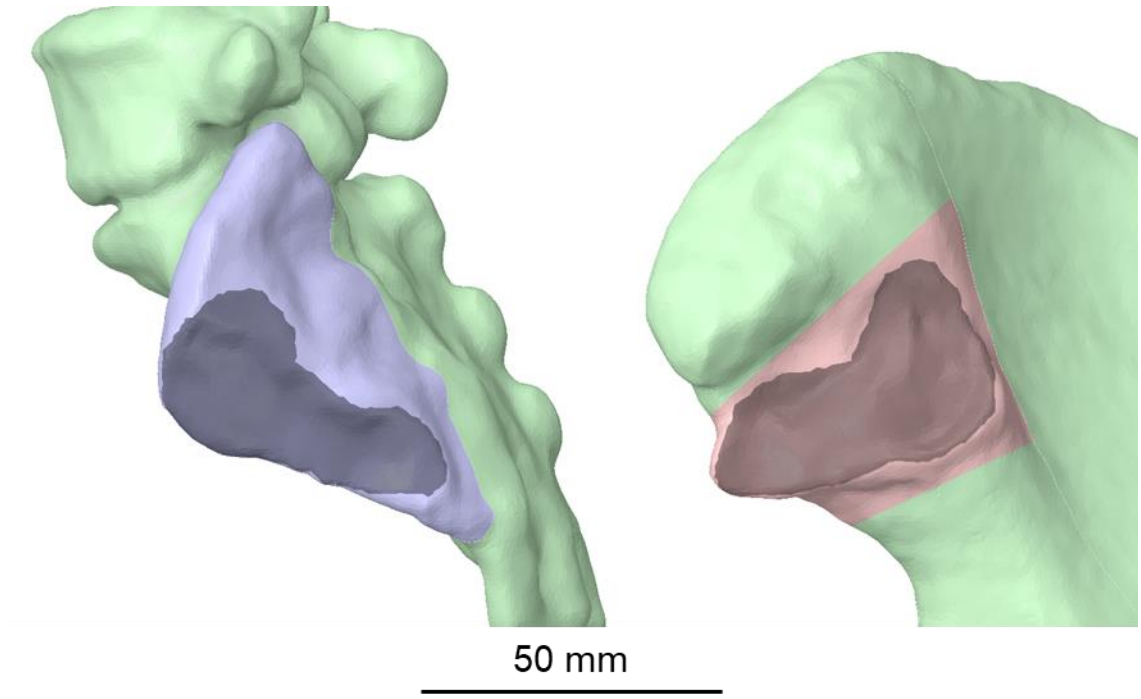

Fig. 3.3 Surface models of a sacrum (blue, left) and ilium (red, right). The dark areas indicate surface regions.

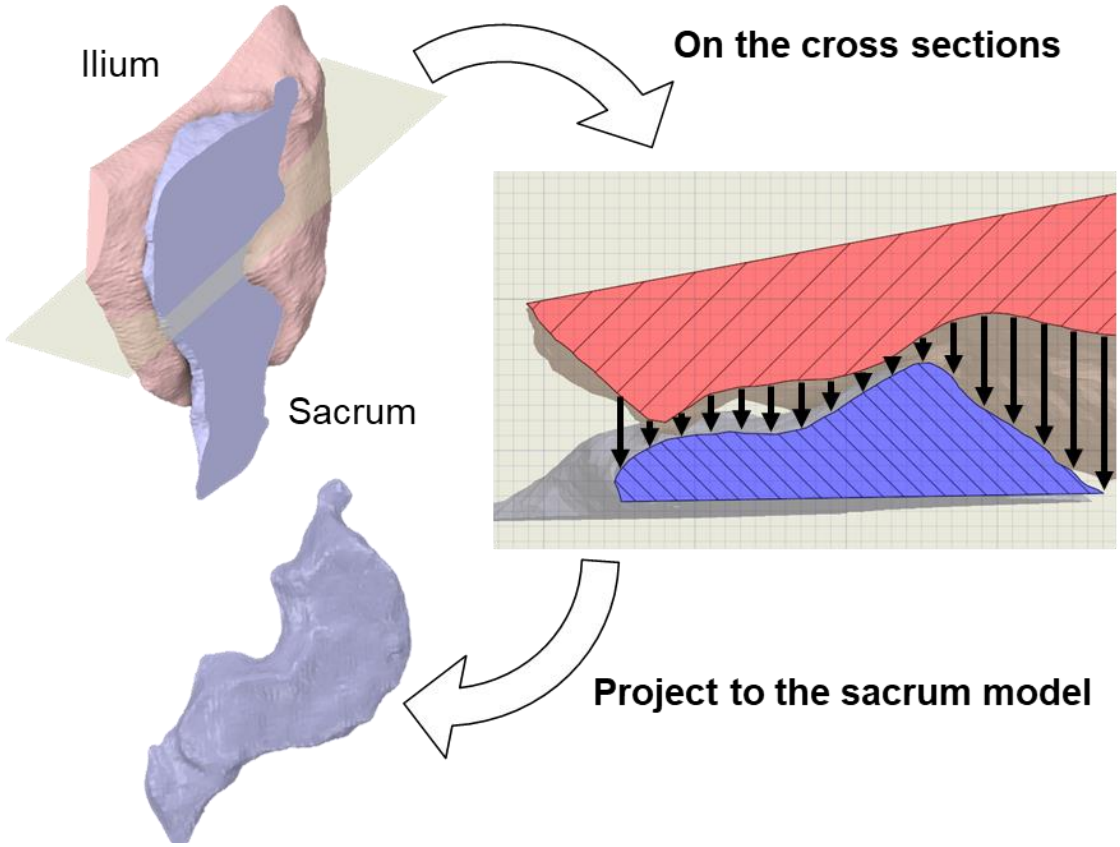

Fig. 3.4 Investigation procedure of articular gap height distribution.

3.2.3 Joint sliding test

Preparation of test model

The SIJ articular surface models were placed on a base (100 mm wide, 100 mm long, 2 mm depth) (Fig. 3.5). All surface models were 3D printed in ABS resin using a 3D printer (da Vinci 1.0 Pro 3D Printer, XYZ printing Inc., Tokyo, Japan). The printed models were exposed to acetone in vapor form for one hour to get smooth surfaces (Fig. 3.6). After drying sufficiently, casts were made with silicon (Elastosilm M8012, Wacker Asahikasei Silicone Co., Ltd., Tokyo, Japan) and the articular surface models were duplicated with polyester resin (PROST Co.,LTD., Ibaraki, Japan) (Fig. 3.7).

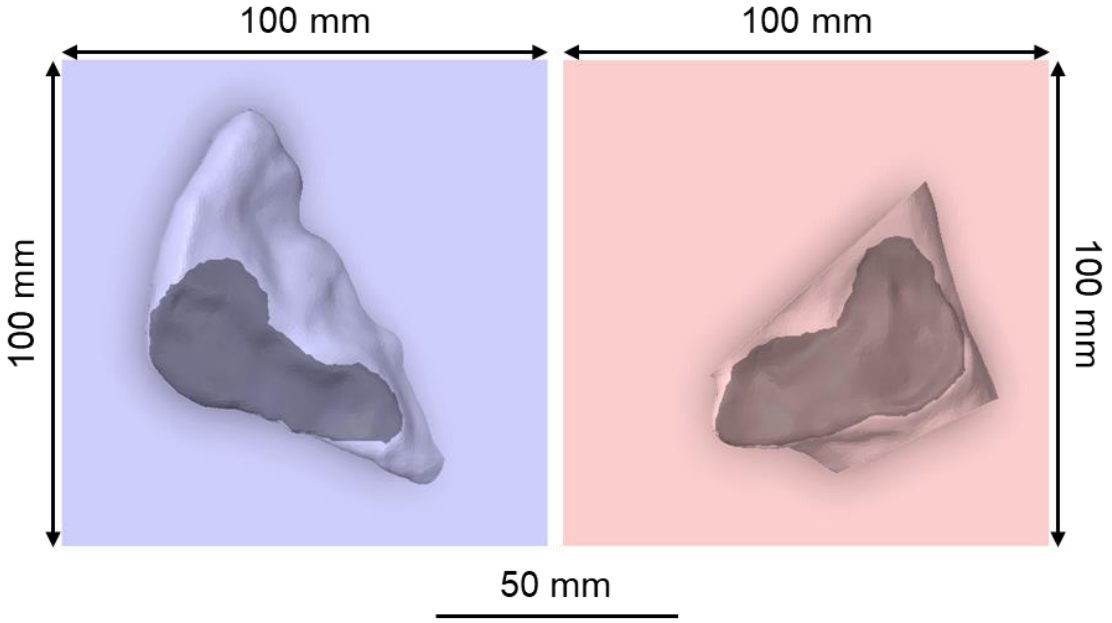

Fig. 3.5 Surface models with bases of a sacrum (blue, left) and ilium (red, right).

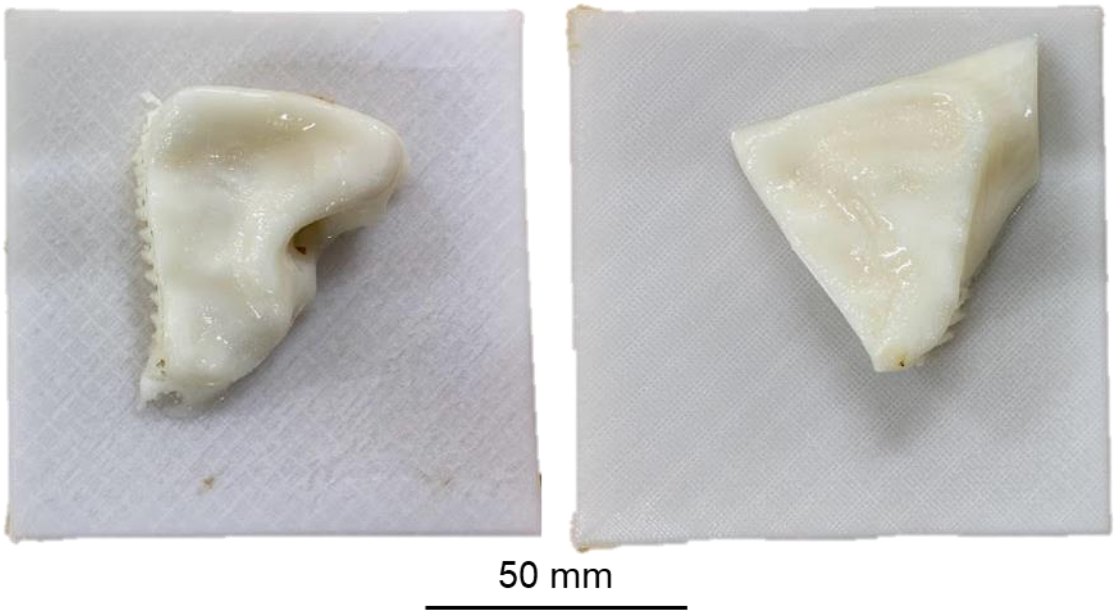

Fig. 3.6 Surface models of ABS resin after acetone vapor process. (Left) A sacrum and (right)ilium.

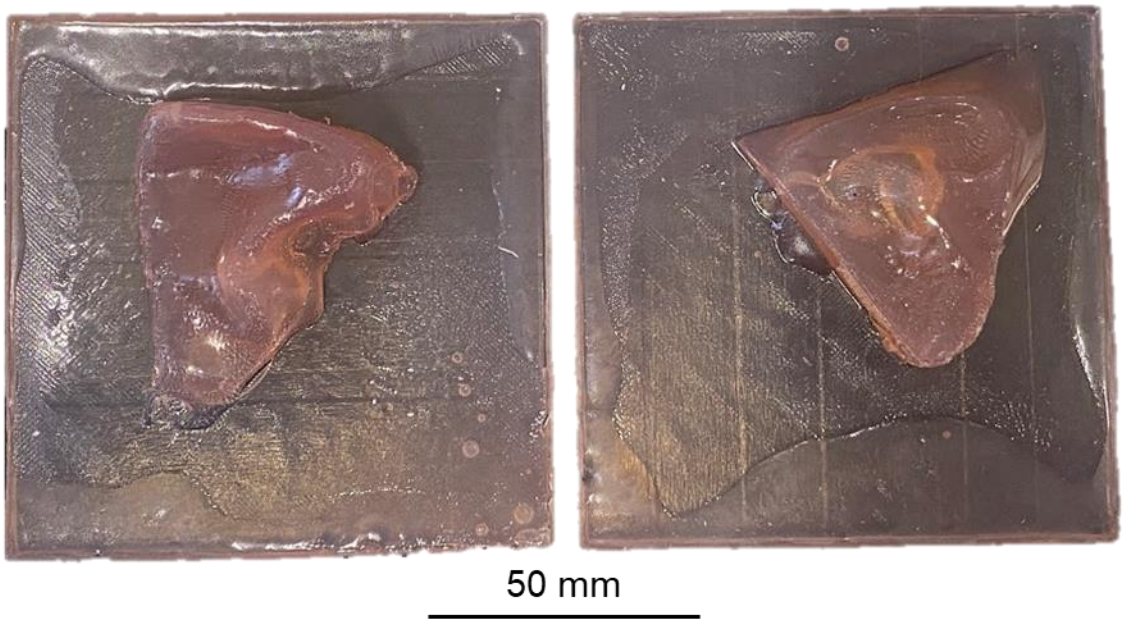

Fig. 3.7 Surface models of polyester resin. (Left) A sacrum and (right) ilium.

Test device

A test device (Fig. 3.8) was developed for this study. Since the SIJ is exposed to compressive and shear stress, the tests were designed to mimic that stress environment. It was mainly comprised of the force gauge (DTG-100N, Digitech Co., Ltd., Osaka, Japan), digital camera (DSC-WX500, Sony Corp., Tokyo, Japan), springs and surface models. The force gauge pulled the models to apply and measure shear force. The springs caused the surface models to compress and pull them back to initial positions. The camera tracked the displacement of the models. In addition, vinyl was placed between the models to prevent the resin models from sticking to each other. Shear resistance coefficients are given by the following formula.

$$\mu = \frac{S}{N} \tag{3.1}$$

Here, μ is a shear resistance coefficients and S and N are shear force by the force gauge and compression force by the springs.

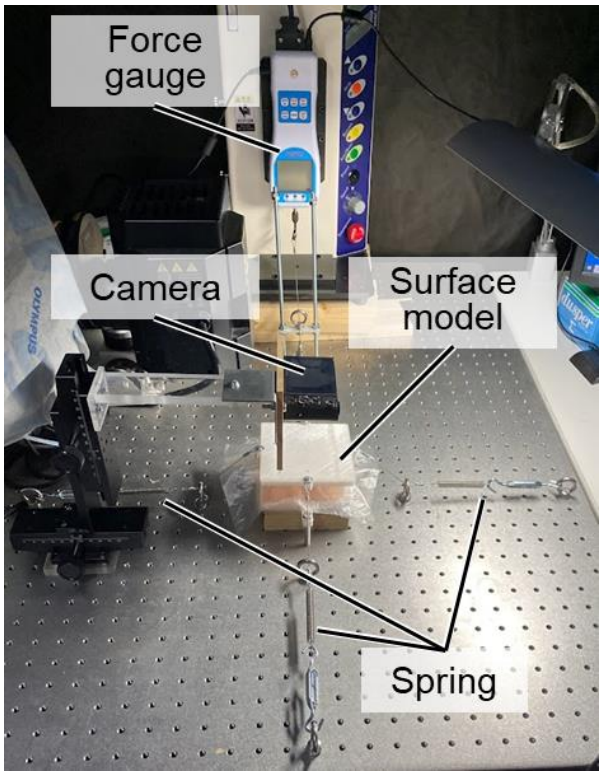

Fig. 3.8 A joint motion resistance test device.

Joint motion resistance test

The force gauge pulled the models at a speed of 60 mm/min in four directions, the vertical and anteroposterior direction of the articular surface (Fig. 3.9) and was set to stop at a maximum of 20 N. The sacrum and ilium models were used as the moved and fixed sides, respectively. The force gauge recorded force histories and the camera tracked the displacement of the sacrum models. In addition, to investigate the difference in resistance due to the joint surface alignment, the ilium model was rotated 5 degrees to reproduce the nutation and counter-nutation positions. All tests were performed three times for each condition.

Joint repositioning test

The force gauge pulled the models to certain forces, 2 to 20 N in 2 N increments and returned to 0 N with a speed of 60 mm/min in the four directions (Fig. 3.9). After each experiment, the device was returned to its original position and the next experiment was conducted. Likewise, the sacrum and ilium models were used as the moved and fixed sides, respectively. The force gauge recorded force histories and the camera tracked the displacement of the sacrum models. In addition, to investigate the difference in repositioning capacities due to the combination of joint surfaces, the ilium model was rotated 5 degrees to reproduce the nutation and counter-nutation positions. All tests were performed one times for each condition.

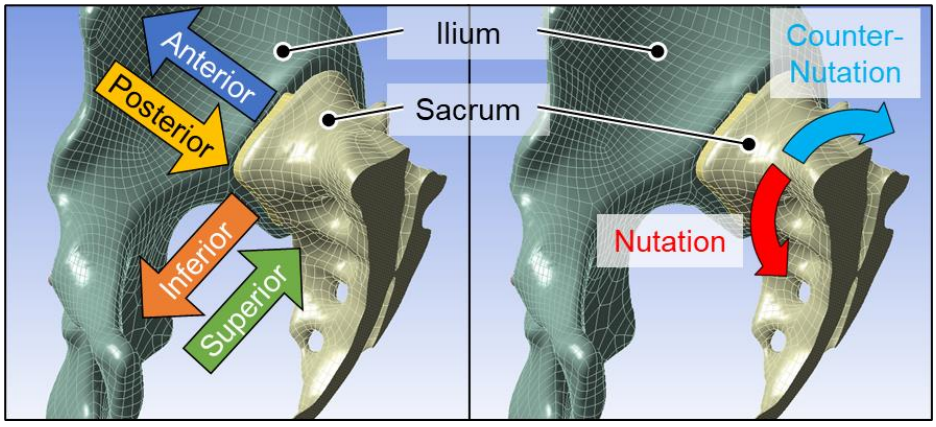

Fig. 3.9 Experimental conditions on (left) directions and (right) alignments.

3.3 Results

3.3.1 Articular gap height distribution

The articular gap height of the SIJ were narrow at the inferior edges and center points, and wide at the anterior and posterior regions of the joint (Fig. 3.10). On the nutation and counter-nutation positions, the intervals changed at the anterior and posterior areas. Meanwhile, the inferior and center regions showed narrow areas.

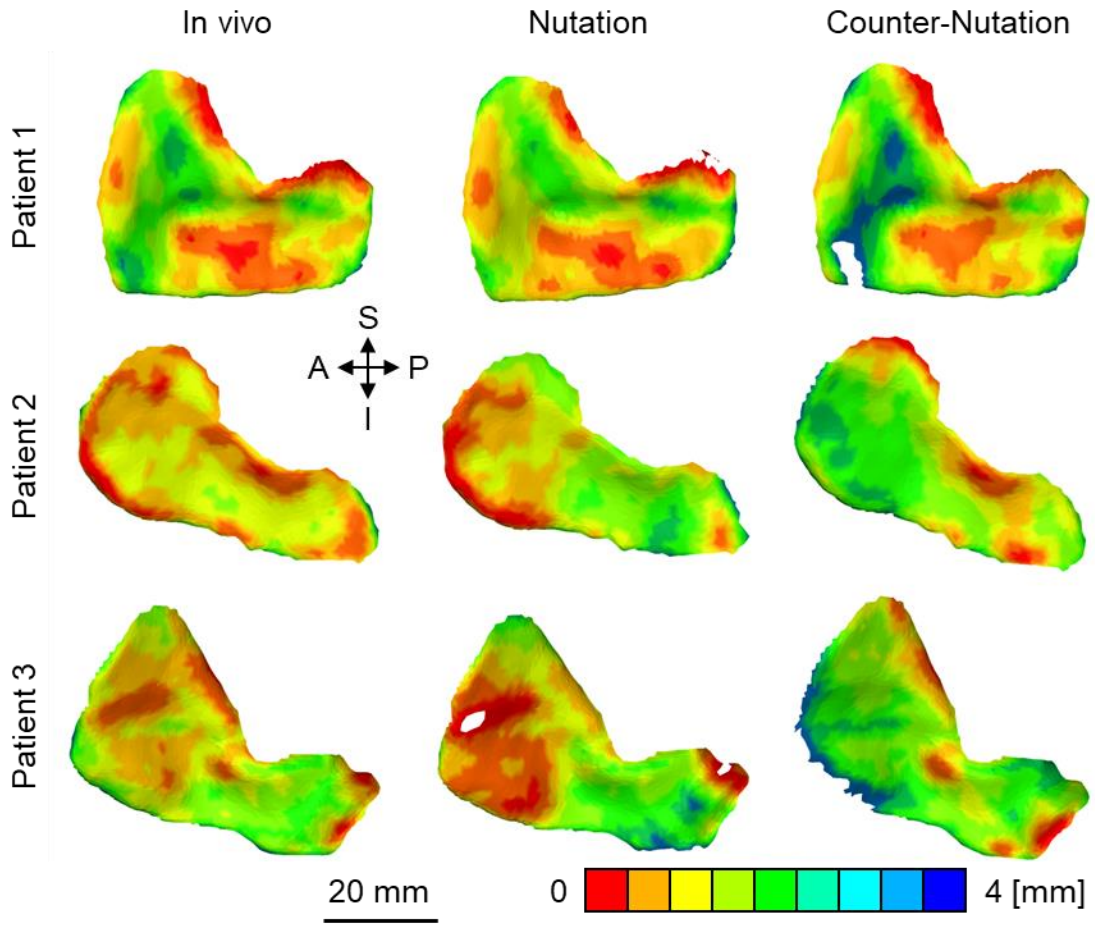

Fig. 3.10 Articular gap height distribution on the sacrum. The gap height increases from red to blue. A: anterior, I: inferior, P: posterior, S: superior.

3.3.2 Joint motion resistance

The compression forces were 31 N. In the anterior direction, the change in the friction coefficients was less than 7% at any displacement position. The friction coefficients in the anterior and superior directions were around 0.1. The friction coefficients varied depending on the pulling direction (Fig. 3.11). The order of friction coefficients is as follows: S→I, A→P, P→A, I→S (Fig. 3.12(a)). The friction coefficient also changed depending on the joint surface alignment. Furthermore, the friction coefficients increased in the anterior and superior directions at the nutation position, hardly changed in the anterior, posterior and superior directions at the counter-nutation position and decreased on others (Fig. 3.12(b)).

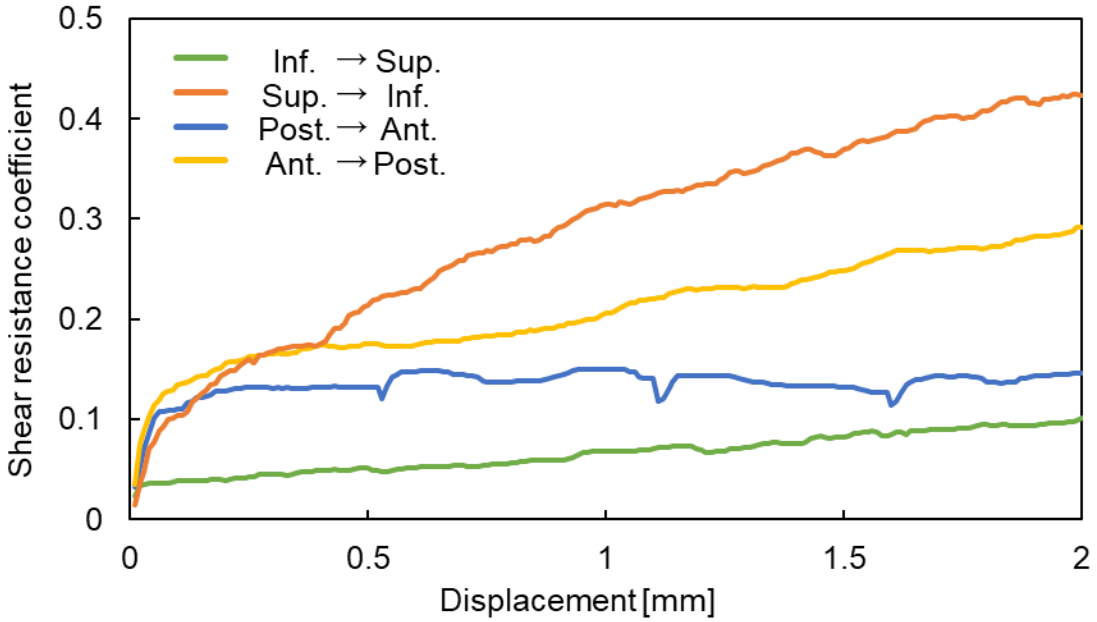

Fig. 3.11 A representative shear coefficient on the in-vivo condition.

Inf.: inferior, Sup.: superior, Ant.: anterior, Post.: posterior.

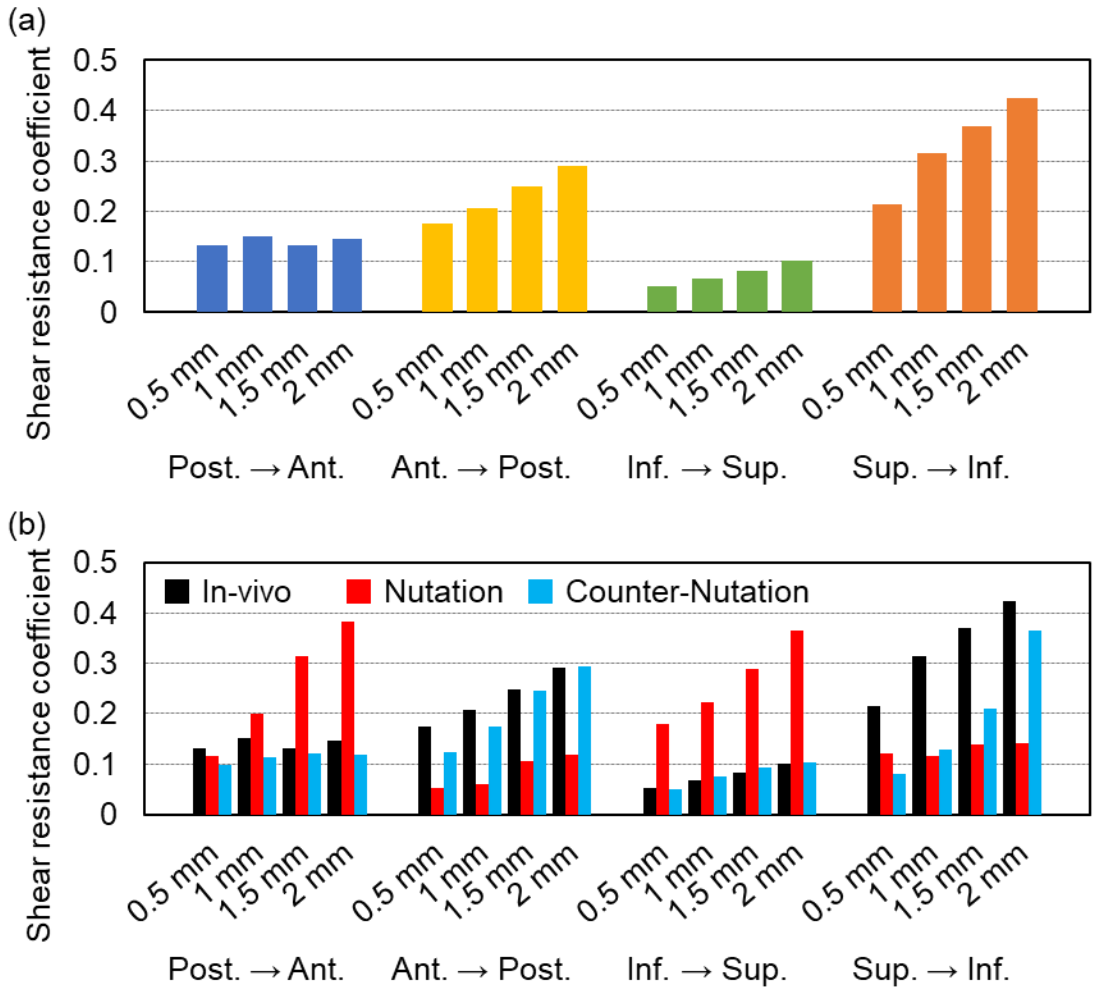

Fig. 3.12 Shear coefficients at four displacement points from initial positions (a) on the in-vivo conditions and (b) on all conditions. Inf.: inferior, Sup.: superior, Ant.: anterior, Post.: posterior.

3.3.3 Joint repositioning

The compression forces were 31 N. Figures 3.13 and 3.14 show that the surface models could not return to their original positions after unloading with a load exceeding threshold. The load that caused displacements from the initial positions of more than 2 mm in the direction parallel to the pulling direction was 10 N (to posterior) and 12 N (to superior) on the in-vivo condition, 12 N (to superior) and 14 N (to anterior) on the nutation condition and 8 N (to anterior) and 10 N (to superior) on the counter-nutation condition. The load that caused displacements from the initial positions of more than 2 mm in the

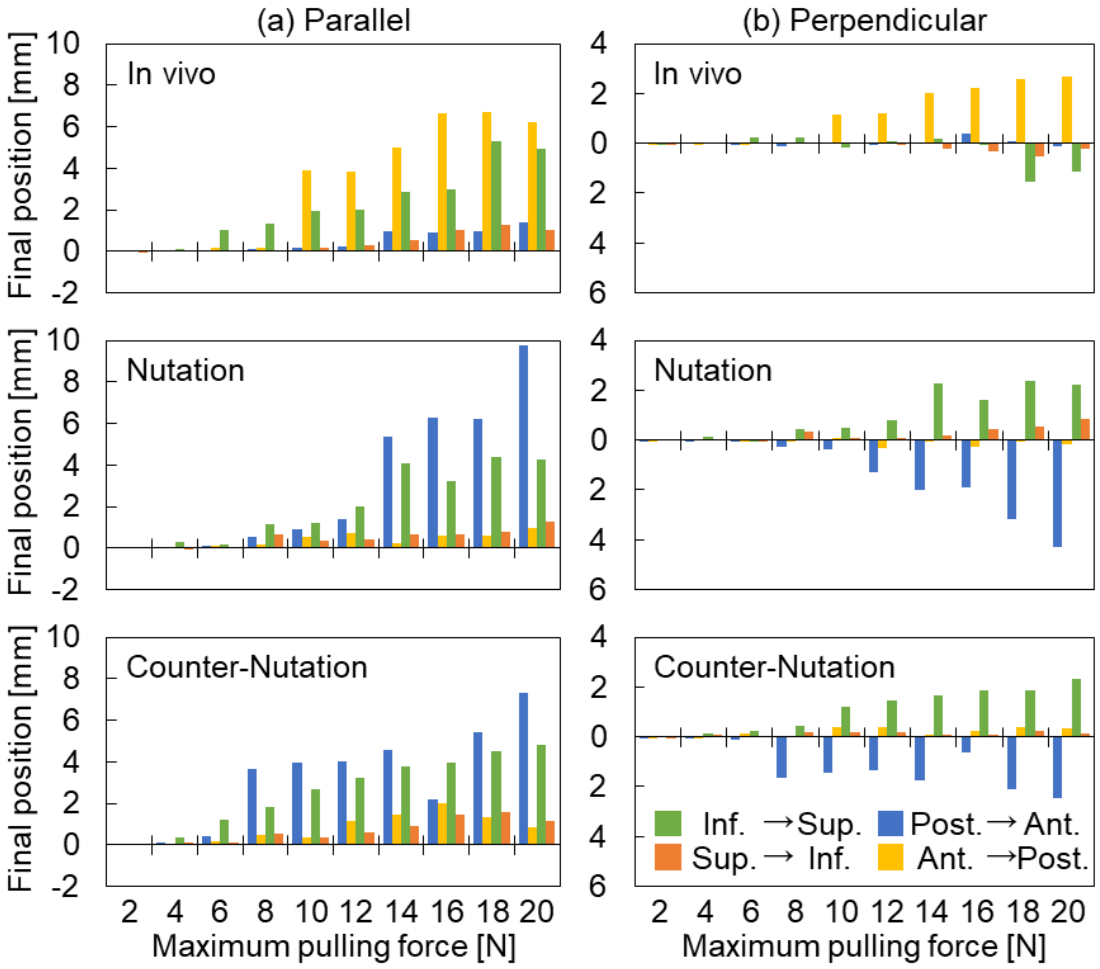

Fig. 3.13 Repositioning on in-vivo (top), nutation (center) and counter-nutation (bottom) conditions. The horizontal axes are maximum pulling force in increments of 2N. The vertical axes are finnal posision returned 0 N on (a) parallel and (b) perpendicular to pulling directions. Inf.: inferior, Sup.: superior, Ant.: anterior, Post.: posterior.

direction perpendicular to the pulling direction was 14 N (to posterior) on the in vivo condition, 14 N (to superior) on the nutation condition and 20 N (to superior) on the counter-nutation condition.

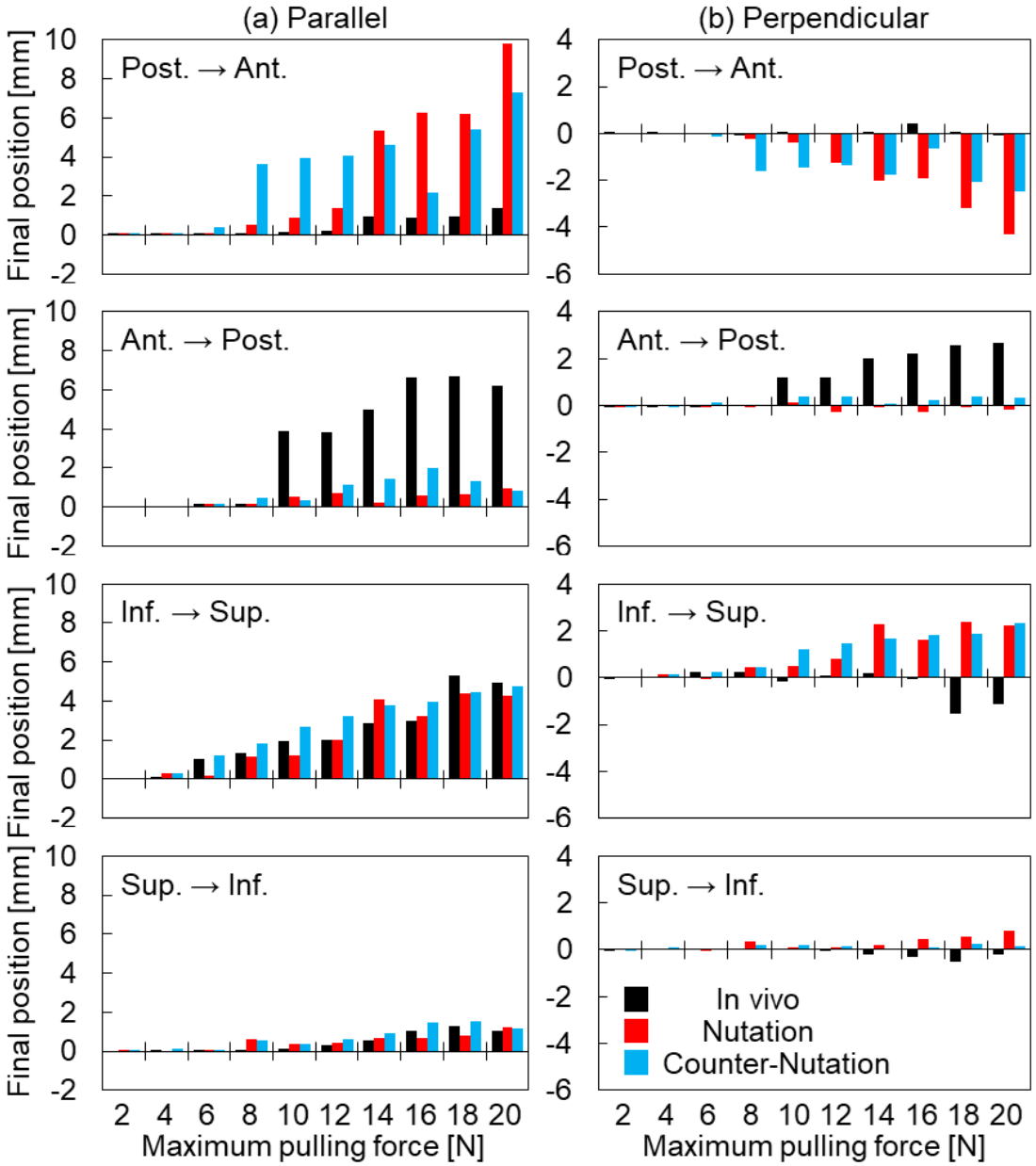

Fig. 3.14 Repositioning on the posterior to anterior (1st line), anterior to posterior (2nd line), inferior to superior (3rd line) and superior to inferior (4th line) directions. The horizontal axes are maximum pulling force in increments of 2N. The vertical axes are finnal posision returned 0 N on (a) parallel and (b) perpendicular to pulling directions. Inf.: inferior, Sup.: superior, Ant.: anterior, Post.: posterior.

3.4 Discussion

There are to date few studies on the SIJ surface morphology. This study for the first time investigates the motion resistance depending on alignments of the joint surfaces and the directions of the slding motion. The upper part of the joint is concaved toward the ilium, while the lower part of the joint is concaved toward the sacrum. In addition, the major axis slopes from antero-superior-lateral to posterior-inferior-medial and is twisted caudally (Katada, 2019). The sacra, that consist of SIJs, are divided into five sacral spines at birth, however, in adults, they become one sacrum by osseointegration (Tortora and Derrickson, 2012). Whole-body motion during growth may contribute to bone formation and may determine the SIJ morphology. It is considered, therefore, that there is a close relation between articular surface morphology and joint motion. SIJ disease is generally regarded as a joint dysfunction due to a misalighnment of joint surfaces (Murakami, 2017). Manual therapy, one of the conservative treatments, reduces pain by resolving joint incompatibility (Asakura, 2015; Ishiguro and Ishiguro, 2017; Katada, 2019), the combinated position of the joint surfaces may affect the function of SIJs.

In this study, the articular gap height distribution was visualized and the shear resistance was experimentally investigated. The maximum articular gap height was apporoximately 3 mm, which is similar to the literature values: 1.5 mm on bilateral joints of patients with unilateral SIJ disease (Ito et al., 2020), 2.49 ± 0.66 mm on healthy young people (Demir et al., 2007), 3.17 ± 1.54 mm on healthy young female (Kalenderer et al., 2017). The articular surfaces on sacra are convex at the top and bottom and concave at the center (Kapandji, 1974) and the joint interval distances were narrow at the inferior and center areas. In the anterior and posterior regions, however, the joint gap was wide, which may not directly contribute to shear resistance. Since the intervals changed depending on the alignment of the joint surfaces, it is suggested that the wide joint gap may contribute to fluid resistance of synovial fluid on narrow flow passages.

In the SIJ surface, the upper and lower parts are original sacral vertebrae and the central part is formed by bone fusion. Since mechanical stimulation promotes bone formation, the morphology of the SIJ surface should be formed mainly by load environment in growth periods although it changes with aging (Nishi et al., 2018). The fusion of the sacrum, however, begins around puberty and completes by the ages of 25 to 30 (Anatomy, Back, Sacral Vertebrae). In addition, quadrupeds do not have the SIJ structure. It is considered, therefore, that the SIJ surface was caused by the load of upright bipedal walking peculiar to humans. Since humans need to support the trunk load at the SIJ during standing, the downward motion of the sacrum should be strongly restricted. On the other hand, the upward motion of the sacrum is not beneficial for the potential energy loss on efficient swing phase during walking. It is reasonable for bipedal walking that the friction coefficients were high during downward motion and consistently low during upward motion. In addition, lifting while bending forward is likely to cause low back pain and the results of this study suggested that this movement had a low coefficient of friction in SIJs and a large load may be applied to ligaments and muscles. The counter-nutation position is considered to be the most stabilized state (Katada, 2019), which was not in agreement with this study. Although there are individual differences, it is necessary to investigate not only the SIJ surface friction resistance but also the pelvic structure including ligaments for further research.

The repositioning tests show that the joint become inconfamity due to unevenness of the surfaces and can not return to its original position when a large load is applied. The range of SIJ motion has been reported to be less than 1 mm (Miller et al., 1987; Sturesson et al., 1989, 2000; Takayama, 1990; Jacob and Kissling, 1995; Kibsgård et al., 2012; Bruna-Rosso et al., 2015; Hammer et al., 2019c; Toyohara et al., 2020), which is considered to be the physiological range. In this study, the displacement of 2 mm or more, which is twice the physiological range after the unloading of shear force, was regarded as pathological range, i.e., subluxation. Table 3.2 shows the results of a preliminary study with the finite element model used in Chapter 2 (analytical condition: 70 kg body weight,

Table 3.2 Summary of preliminary study for shear and compressive forces.

	Shear force				Compressive force
	Anterior	Posterior	Superior	Inferior	
Maximum	684 N	733 N	39 N	1104 N	2422 N
Average	98 N (to posterior)		283 N (to inferior)		537 N

double leg standing). In this study, a compressive force of 31 N was applied, which corresponds to a shear force of 5.6 N (backward) and 16.3 N (downward). Permanent displacement occured with a relatively small load in the anteroposterior directions. Subluxation is, however, easy to occur in the upward direction, which does not receive a large load in vivo and it may be necessary to pay attention to impacts such as landing from a high place. The articular surface morphology diplaced the models in the directions other than shear direction. Depending on the loading direction, large displacements occured, which may increase the risk of subluxation. The alighment position of the joint changes the load that can cause subluxation. Especially in the forward load, the nutation and counter-nutation were greatly displaced even with a small load, suggesting that there is a high possibility that a sudden backward fall may cause SIJ dysfunction.

There are some limitations in this study. First, the bony surfaces of SIJs are covered with cartilage; the cartilage thickness is 4 mm on the sacral sides and 2 mm on the ilium sides (Bowen and Cassidy, 1981; Kampen and Tillmann, 1998; Vleeming et al., 2012). The joint surfaces are softer than bones and should be deformed by friction. This study, however, used a resin model and did not consider deformation behavior of cartilage. In addition, mineralization of cartilage varies on the joints (Poilliot et al., 2020, 2021), which may affect sliding motion. Next, the surface models were created based on X-ray CT data and printed out using a 3D printer with a pitch of 0.2 mm. This study can not reflect the surface geometry with submillimeter accuracy. The surface morphology of the whole joint, however, was reproduced, which was sufficient to investigate relation between the

complicated curved surface of SIJs and joint motion resistance. Thirdly, ligament orientations were not considered, although they vary from place to place (Tortora and Derrickson, 2012) and may affect joint motion. Finally, the sample size in this study was three. The surface morphology of SIJs varies greatly among individuals (Kapandji, 1974; Katada, 2019). For further research, more patients data are needed.

3.5 Conclusions

The articular gap height distribution of SIJs was visualized and the articular shear resistance was experimentally investigated. A test device was developed for joint motion resistance tests in this study. It was suggested that the shear resistance of SIJs changed depending on the shear direction and the alignment position of the surfaces. The SIJ surface morphology may be designed to accommodate an upright bipedal walking and joint misalignment could adversely affect walking.

Chapter 4

Finite element analysis of effect of pelvic morphology on stress environment of sacroiliac joint: acetabular dysplasia pelvis

4.1 Introduction

Acetabular dysplasia (Fig. 4.1) is one of the most influential factors to progress to osteoarthritis (OA) of the hip joint due to insufficient bony coverage of the femoral head (Reijman et al., 2005; Jacobsen et al., 2005; Jingushi et al., 2010, 2011). As a characteristic of acetabular dysplasia, it has been reported that the iliac bone has an inward morphological abnormality (Fujii et al., 2011). The posterior part of the iliac bone constitutes the sacroiliac joints (SIJs). In the pelves, the SIJs have a small range of motion to work as a shock absorber between the spine and the lower extremities (Lovejoy, 2007; Vleeming et al., 2012). In humans, the SIJs play a crucial role in the ability to walk upright on the two legs (bipedal walking) (Toyohara et al., 2020), as they dissipate loads effectively. Repetitive and/or unexpected movements may cause minor subluxation of the SIJs, which has been hypothesized to lead to joint dysfunction (Murakami, 2018a). In general, a joint dysfunction can be defined as a functional disorder of the joint without known specific cause (Mennell, 1694), i.e., modern medical standards including imaging equipment and surgical technology are unable to detect the morphological changes (Katada, 2019). When SIJ dysfunction occurs, nerve endings, mainly in the posterior ligaments of the joint (Murakami et al., 2018b), may be involved in the generation of pain as an alarming sign of SIJ dysfunction. Several clinical reports mentioned that hip disorders could affect the SIJ condition and pain (Morgan et al., 2013; Asada et al., 2019; Krishnamoorthy et al., 2019). The mechanical effects on both the cartilaginous and the ligaments of the SIJs in patients with acetabular dysplasia may differ from those in the healthy pelves.

Peri-acetabular osteotomy is a mainstay in the surgical treatment of acetabular dysplasia to prevent the progression of OA of the hip. This surgery transects the iliac and the ischial bones that are in contact with the hip joints; here the osteotomized bone is rotated outward and anteriorly to improve the bony and cartilaginous coverage of the femoral head. Acetabular osteotomy, such as rotational acetabular osteotomy and

periacetabular osteotomy, has been performed and good, long-term results have been reported clinically in improving hip pain and suppressing OA progression (Clohisy et al., 2009; Hasegawa et al., 2014; Kaneuji et al., 2015; Yasunaga et al., 2016). It is believed that acetabular osteotomy alters stress distribution at the hip joint (Vukasinovic et al., 2012), however, it is unclear to date whether mechanical changes to the SIJs would occur.

In this study, stress distribution of whole pelves was analyzed using preoperative and postoperative models of the osteoligamentous pelvis of four patients who underwent unilateral spherical periacetabular osteotomy (Kaneuji et al., 2021). The study aimed to investigate the stress environment of the SIJs in acetabular dysplasia.

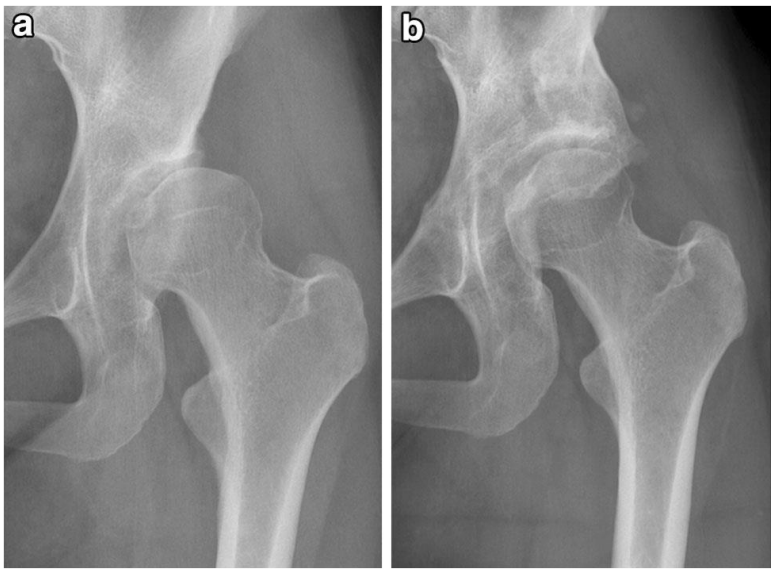

Fig. 4.1 Radiographs of a (a) preoperative and (b) postoperative acetabular dysplasia pelvis (Iwai et al., 2014).

4.2 Methods

4.2.1 Finite element model of acetabular dysplasia pelves

Finite element models of acetabular dysplasia pelves (Fig. 4.2) were created based on computed tomography (1-mm slice thickness) of preoperative (named pre model) and postoperative (post model) pelves of four female patients (18 - 41 years old). All methods were carried out in accordance with relevant guidelines and regulations and all patients provided the signed informed consent for use of the data. This study was approved by Institutional Review Board committee of Kanazawa Medical University. The bones and cartilage components were segmented in MECHANICAL FINDER ver. 10 (Research Center of Computational Mechanics, Inc., Tokyo, Japan) including the lumbar vertebra, the sacrum, the both hip bones, the proximal ends of both femora, the both SIJ cartilages, the pubic symphysis, the both hip joint cartilages and the intervertebral disks. These geometries were modified and the SIJ cartilage was adapted to the bone shape in

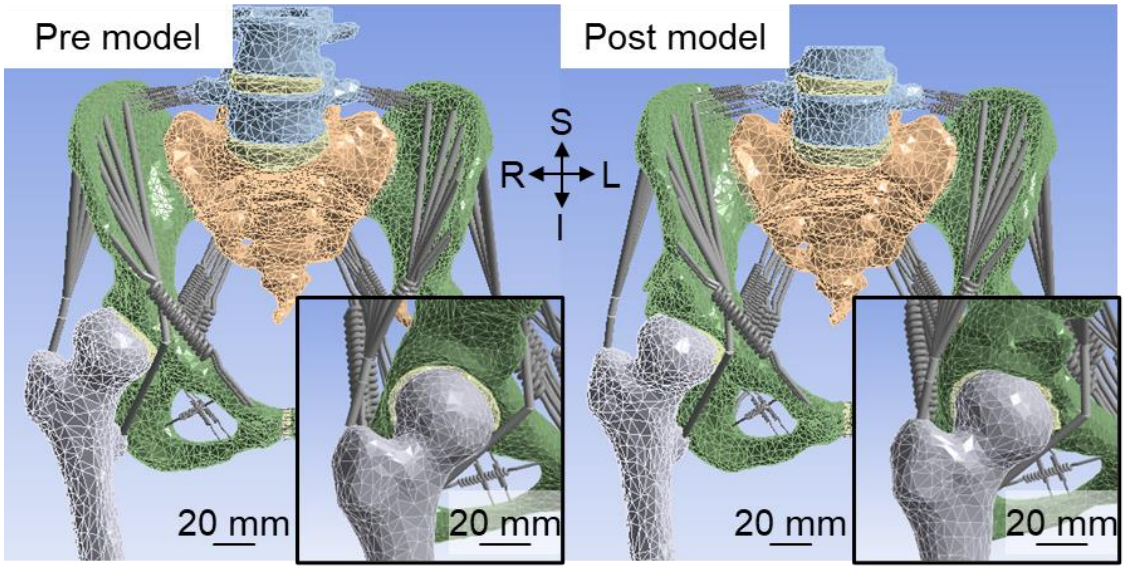

Fig. 4.2 Finite element models of the preoperative (left) and postoperative (right) pelves of patient 1. The right is the surgical side. The insets are enlarged views of the right hip joints. The scale bar: 20 mm. I: inferior, L: left, R: right, S: superior. In the pre model, the acetabulum does not cover the femoral head sufficiently. In the post model, the acetabulum widens by the surgical intervention (Toyohara et al., 2022b).

SpaceClaim 2021R1 (Cybernet Systems Co., Ltd., Tokyo, Japan). All models were then imported into ANSYS 2021R1 (Cybernet Systems Co., Ltd.). The twelve types of ligaments and the two types of muscles surrounding the pelvis were modelled by a total of 210 spring elements (Toyohara et al., 2020) and 20 beam elements, respectively (Fig. 4.3). The ligaments were defined in a way where they could respond only when they are subjected to tensile loads. Tensile forces of 720 N and 100 N were applied on the gluteus medius muscle and iliacus muscle on both sides, respectively (Takano et al., 2011).

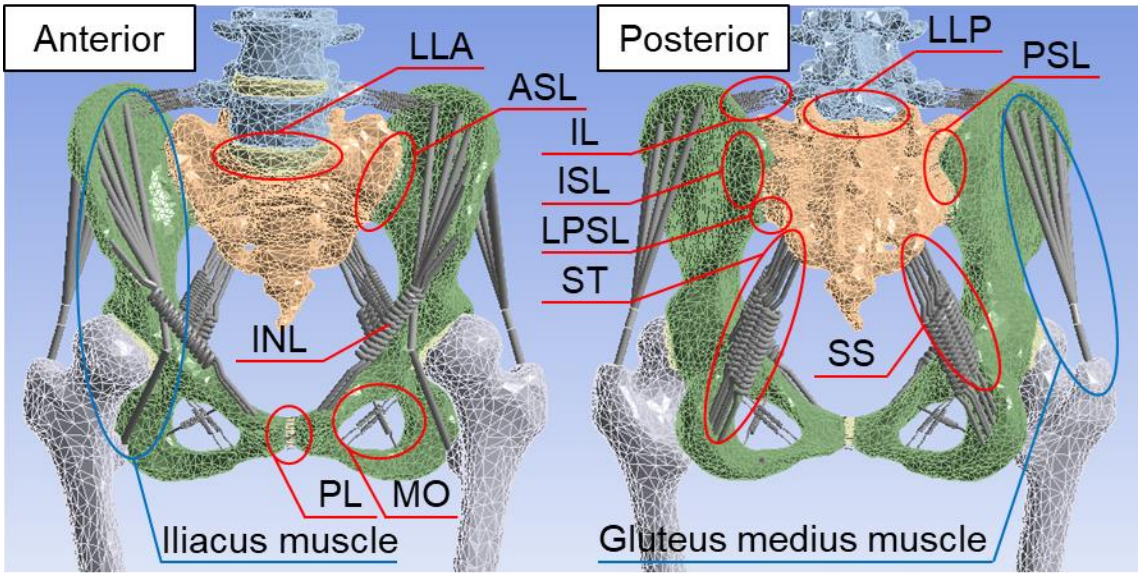

Fig. 4.3 The positions and names of ligaments (red circles) and muscles (blue circles) in a pelvic model of patient 1 with anterior (right) and posterior (left) view. The ligaments modelled are as follows: anterior longitudinal ligament (LLA), anterior sacroiliac ligament (ASL), inguinal ligament (INL), pubic ligament (PL), obturator membrane (MO), posterior longitudinal ligament (LLP), posterior sacroiliac ligament (PSL), iliolumbar ligament (IL), interosseous sacroiliac ligament (ISL), long posterior sacroiliac ligament (LPSL), sacrotuberous ligament (ST) and sacrospinous ligament (SS) (Toyohara et al., 2022b).

4.2.2 Material properties

The material properties used in this study were cited from previous studies (Wirtz et al., 2000; Sichting et al., 2014; Ramezani et al., 2019) (Table 4.1). All tissues were defined as being uniform and isotropic materials for simplification. Hyper-elastic material properties were defined using Mooney-Rivlin model, which is the strain energy density function W given by the following formula, as a complete non-compressional body. Here, C_{10} and C_{01} are material constants. I_1 and I_2 are the first and second invariant of the distortion.

$$W = C_{10}(I_1 - 3) + C_{01}(I_2 - 3) + C_{11}(I_1 - 3)(I_2 - 3) \quad (4\text{-}1)$$

Table 4.1 Material properties for finite element models. C_{10}, C_{01} and C_{11} mean the parameter of Mooney-Rivlin model for hyper-elastic bodies (modified from Toyohara et al., 2022b).

Material	Young's Modulus[MPa]	Poisson's ratio	C10 [MPa]	C01 [MPa]	C11 [MPa]
Cortical bone (Wirtz et al., 2000)	11,000	0.2	-	-	-
Cartilage (elastic body) (Sichting et al., 2014)	150	0.2	-	-	-
SIJ cartilage (hyper-elastic body) (by personal communication)	-	-	4.1	0.41	0
Symphysis cartilage (hyper-elastic body) (by personal communication)	-	-	0.1	0.45	0.6
Ligament (Ramezani et al., 2019)	350	-	-	-	-

4.2.3 Mesh generation

Meshing was performed using tetrahedral elements consisting of ten nodes each (Table 4.2).

4.2.4 Loading and boundary conditions

Mimicking double-leg stance, 300 N and 600 N of loads were applied via the lowers ends of both femora, which were shortened to two thirds of the total length and the base of the sacrum, respectively. The superior aspect of the second sacral spine and both femora were fixed in space. For contact type, all surfaces in contact were defined as “bonded”, which means the surfaces are fixed to each other.

Table 4.2 Number of nodes and elements and average element quality of each finite element models (modified from Toyohara et al., 2022b).

		Number of nodes	Number of elements	Average element quality
Patient 1	Pre model	253,909	144,502	0.72
	Post model	227,920	128,871	0.72
Patient 2	Pre model	242,013	138,004	0.71
	Post model	253,002	144,887	0.72
Patient 3	Pre model	249,850	142,448	0.71
	Post model	242,042	138,512	0.72
Patient 4	Pre model	219,098	124,072	0.71
	Post model	223,523	127,029	0.71

4.2.5 Analytical parameters

Acetabular head index (AHI, A/B) (Fig. 4.4) is used for an assessment of acetabular dysplasia and is the ratio of acetabular coverage to the femoral head (Heyman and Herndon, 1950). Upper coverage (upper) and posterior coverage (posterior) of the femoral head diameter were measured. The resultant displacement of the pelves, equivalent (Von Mises) stress of the SIJ cartilages, the normal stress on lateral axes, the angles of rotation on the SIJs, the maximum elastic force of spring probes and acetabular head indices were investigated. Equivalent stress is a scalar value that is calculated from normal stresses and shear stresses without any distinction between tension and compression. Normal stress on the lateral axes indicates the stress on the normal direction of the contact surfaces. The maximum elastic force of the spring elements was measured and summed for each of the ligaments as loads on ligaments.

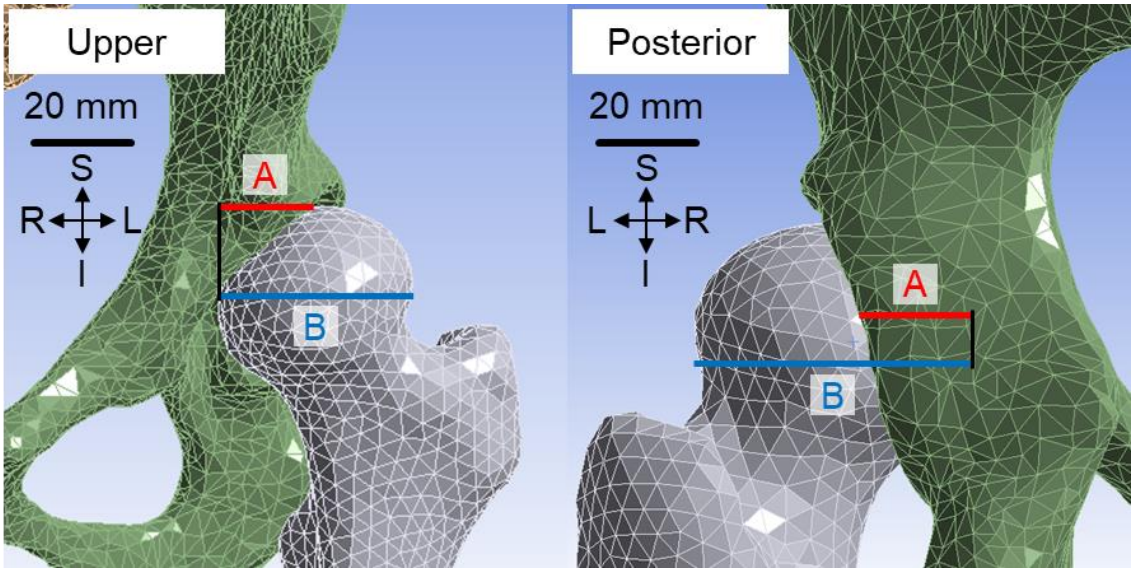

Fig. 4.4 The upper (left) and posterior (right) acetabular head index (AHI) measurement positions with anterior (upper) and posterior (posterior) views. AHI is a ratio of A to B. A means a coverage of acetabulum on the top (upper) or center (posterior) of the femoral heads, and B means a diameter of the femoral head. The left femur and innominate bone are shown in grey and green, respectively. The scale bar: 20 mm. I: inferior, L: left, R: right, S: superior (Toyohara et al., 2022b).

4.3 Results

4.3.1 Acetabular head indices

The AHIs improved mainly in upper coverage of acetabulum. The AHIs on the side which underwent surgery improved – 1 % to 22% (average 12.5%) in the upper area coverage and – 4 % to 12% (average 5%) and in the posterior area coverage (Table 4.3). Coverage improved on both sites only in patient 1. Patients 2 and 4 improved in upper coverage and patient 3 improved in the posterior coverage.

Table 4.3 Measured acetabular head indices (AHI) of upper and posterior coverage on the surgical sides. Improve means an increase of AHI from pre model to post model, respectively (Toyohara et al., 2022b).

		Upper		Posterior	
		AHI	Improvement	AHI	Improvement
Patient 1	Pre model	48%	22%	41%	10%
	Post model	70%		51%	
Patient 2	Pre model	56%	13%	48%	2%
	Post model	69%		50%	
Patient 3	Pre model	54%	-1%	44%	12%
	Post model	53%		56%	
Patient 4	Pre model	46%	16%	48%	-4%
	Post model	62%		45%	

4.3.2 Displacement of pelves

The acetabular dysplasia pelves tended to rotate inward, called the ‘inflare’. The displacement vector diagrams (Fig. 4.5) of the pelves showed that the post models of all patients showed the innominate bones were deformed posteriorly. In the pre models derived from the patient datasets 1, 3 and 4, however, the innominate bones were deformed laterally to anteriorly. On the other hand, patient 2 in the pre models showed that the innominate bone was deformed posteriorly more than the post models. In the pre models of patients 1, 3 and 4 on acetabular dysplasia, the pelves rotated inward in the state of inflare as indicated by the red arrows in Fig. 4.6. In the post models, the iliac crest was more rotated outward than in the pre models as indicated by the blue arrows in Fig. 4.6. The maximum displacement on the iliac crest of surgical sides decreased by approximately 19% from pre models to post models in patients 1 and 3 which had a high improvement in posterior AHIs more than 10%.

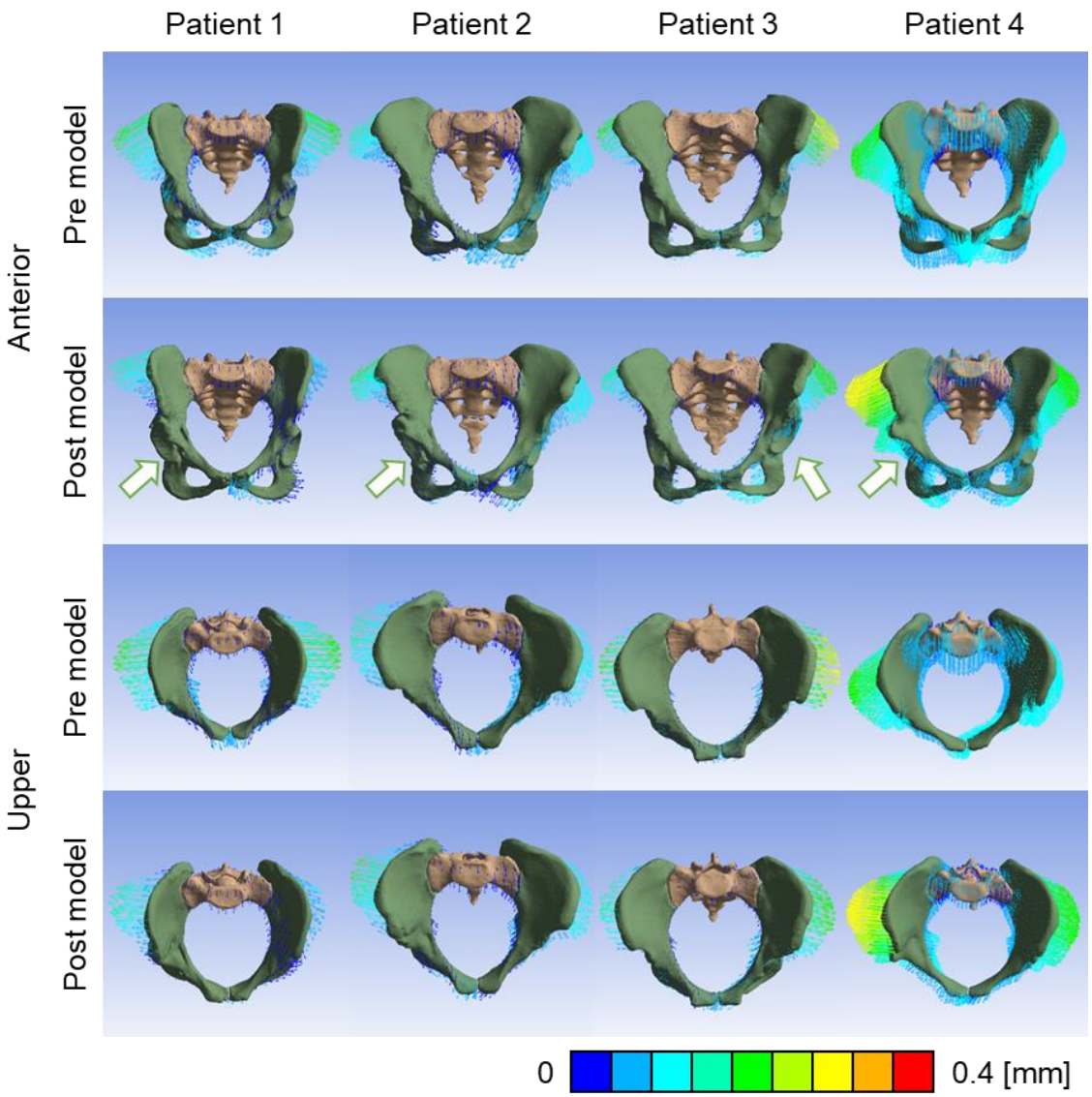

Fig. 4.5 Resultant displacement vector diagrams of the pelves on anterior (top 2 lines) and upper (bottom 2 lines) views. ‘Pre’ and ‘post’ reflect pre models and post models, respectively. The arrows indicate the sides of surgical intervention (Toyohara et al., 2022b).

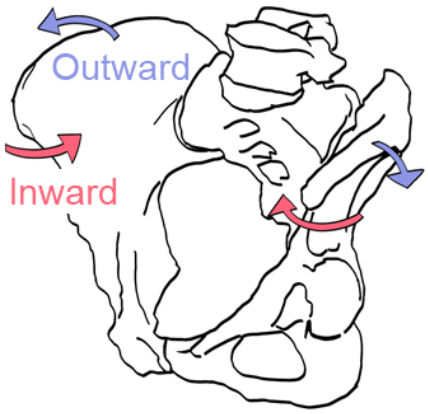

Fig. 4.6 Scheme of pelvic deformation. The red and blue arrows indicate inward rotation (inflare) and outward rotation, respectively (Toyohara et al., 2022b).

4.3.3 Rotational motion of sacroiliac joints

Sacral nutation decreased when increased acetabular coverage. In the surgical sides of post models, the rotation of SIJs decreased in patients 1 and 3 and increased in patients 2 and 4 compared to each pre models (Fig. 4.7). In addition, sacral nutation movement is decreased with posterior acetabular coverage and the overall improvement of the coverage led to counter-nutation (upper: r = - 0.39, posterior: r = - 0.68) (Fig. 4.8).

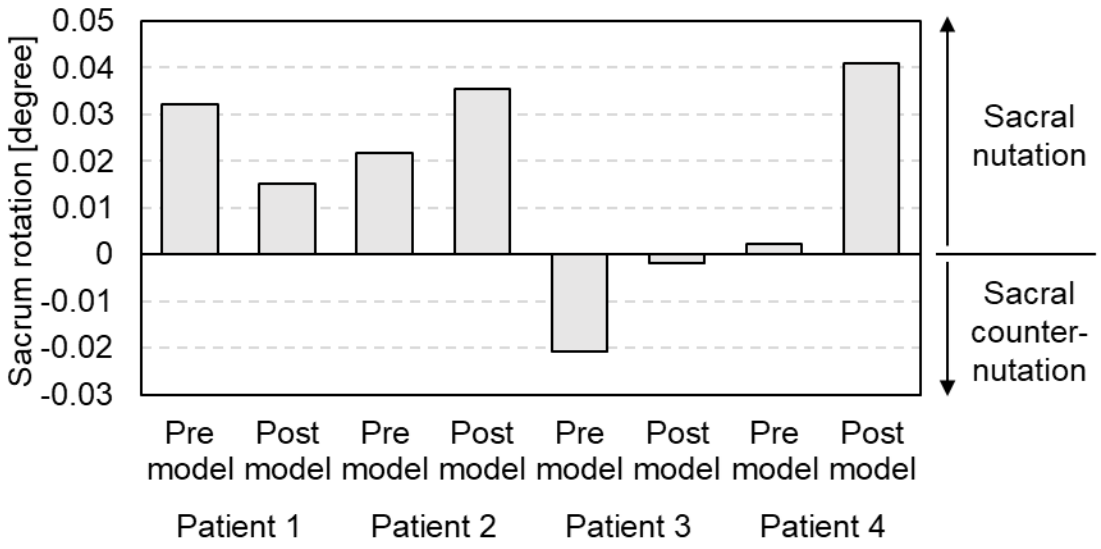

Fig. 4.7 Degree of rotation at the sacroiliac joints on the sides of surgery in all patients, i.e., is the angle of rotation on the sacrum for ilium. The positive and negative values mean the nutation and counter-nutation, respectively (Toyohara et al., 2022b).

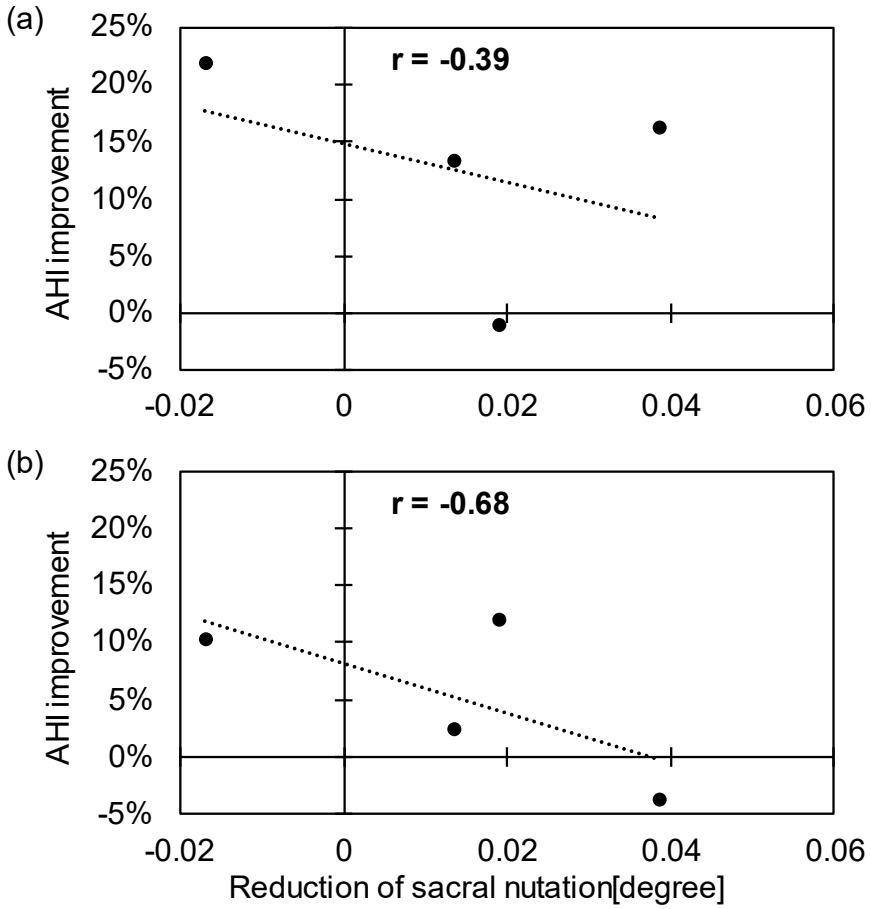

Fig. 4.8 The scatter plots of reduction of sacral nutation on the surgical sides vs. improvement of acetabular head index (a) on upper coverage and (b) on posterior coverage (Toyohara et al., 2022b).

4.3.4 Equivalent stress on sacroiliac joints

The equivalent stress on the SIJ cartilages decreased when increasing acetabular coverage. The equivalent stress of the SIJ cartilages decreased on the posterior regions in patient 1 and increased in the superior regions in all four cases (Fig. 4.9). Maximum equivalent stress of the SIJ cartilages ipsilateral to the surgical sides of pre models decreased by 80% in patient 1, while it increased by 67 – 2,834% in the other cases compared to the post models (Fig. 4.10). Posterior acetabular coverage improvement reduced the maximum equivalent stress and minimum normal stress (r = 0.26 (upper), 0.71 (posterior)) (Fig. 4.11).

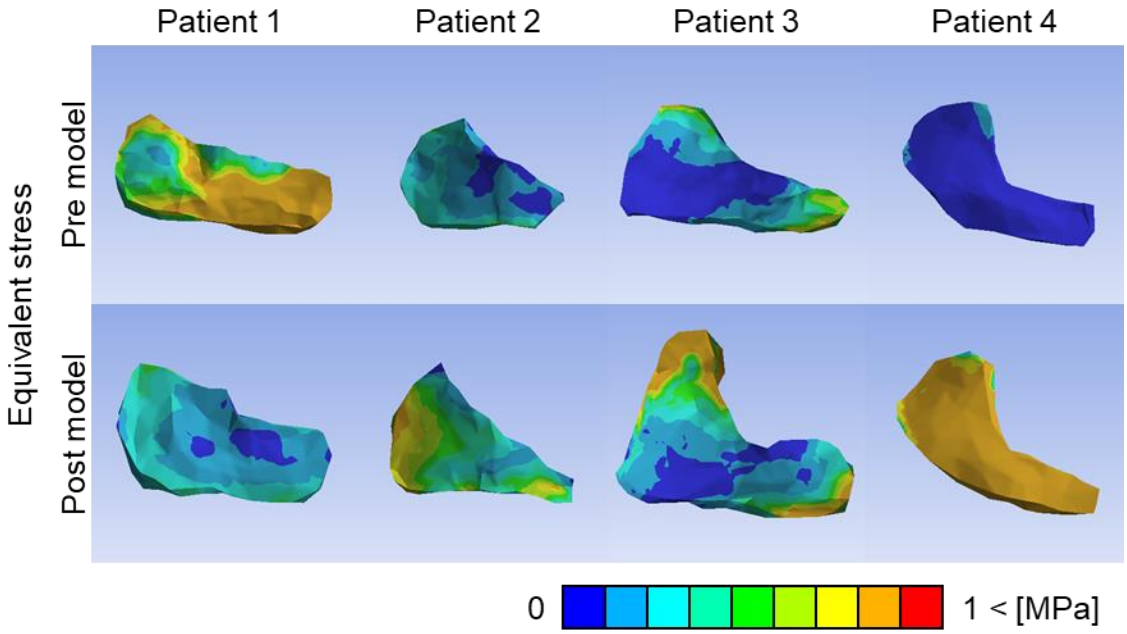

Fig. 4.9 Equivalent stress distribution of the contact surfaces in sacroiliac joints on surgical sides (Toyohara et al., 2022b).

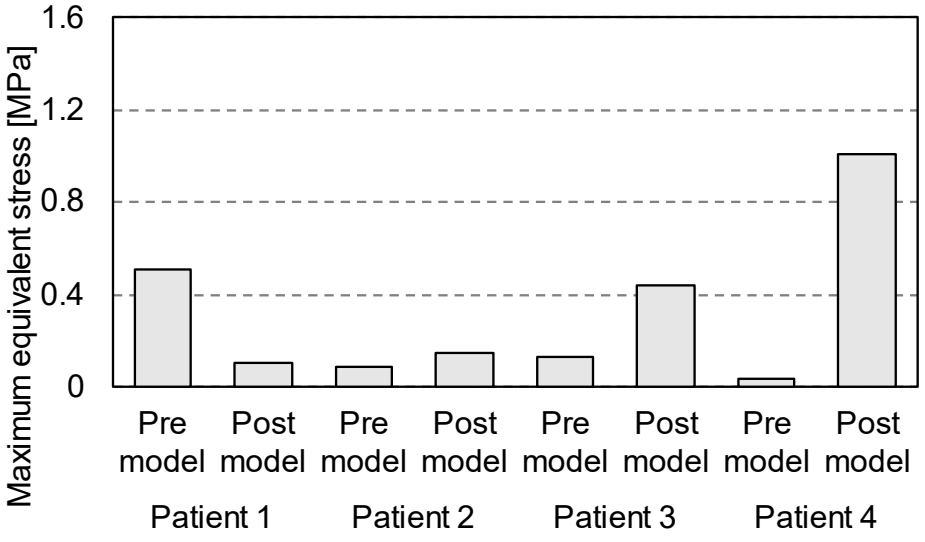

Fig. 4.10 Maximum equivalent stress in sacroiliac joints on surgical sides (Toyohara et al., 2022b).

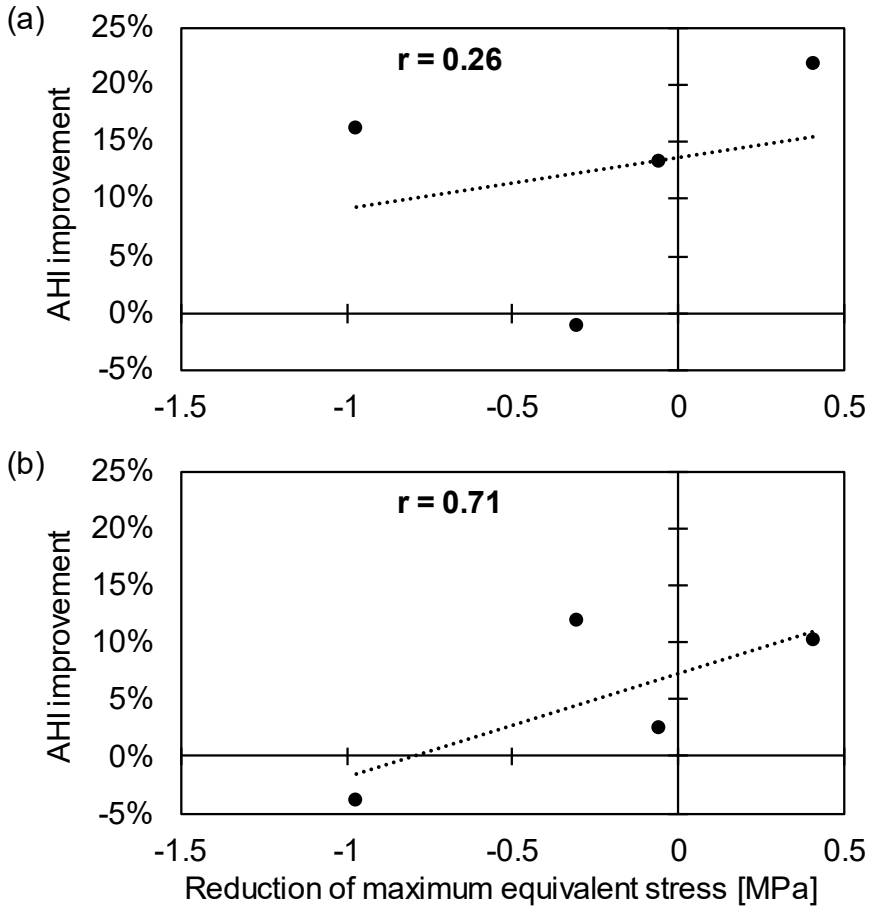

Fig. 4.11 The scatter plots of reduction of maximum equivalent stress in the sacroiliac joint on the surgical sides vs. improvement of acetabular head index (a) on upper coverage and (b) on posterior coverage (Toyohara et al., 2022b).

4.3.5 Compressive stress on sacroiliac joints

The compressive stress on the SIJ cartilages decreased when increasing acetabular coverage. Normal stresses yielded that the SIJs were compressed on the inferior and extended on the superior regions (Fig. 4.12). The minimum normal stress on the surgical sides decreased by 90% in patients comparing the pre models to the post models, and increased by 36 – 11,204% in the other cases (Fig. 4.13). In patients 1 and 3, the posterior coverages were highly increased (10% and 12% increase) and the stresses decreased or slightly increased. Patients 2 remained the posterior coverage (2% increase) and patient 4 were decreased (4% decrease). These models showed slightly or dramatically increment.

Thus, posterior acetabular coverage improvement reduced the minimum normal stress (r = 0.13 (upper), 0.83 (posterior)) (Fig. 4.14).

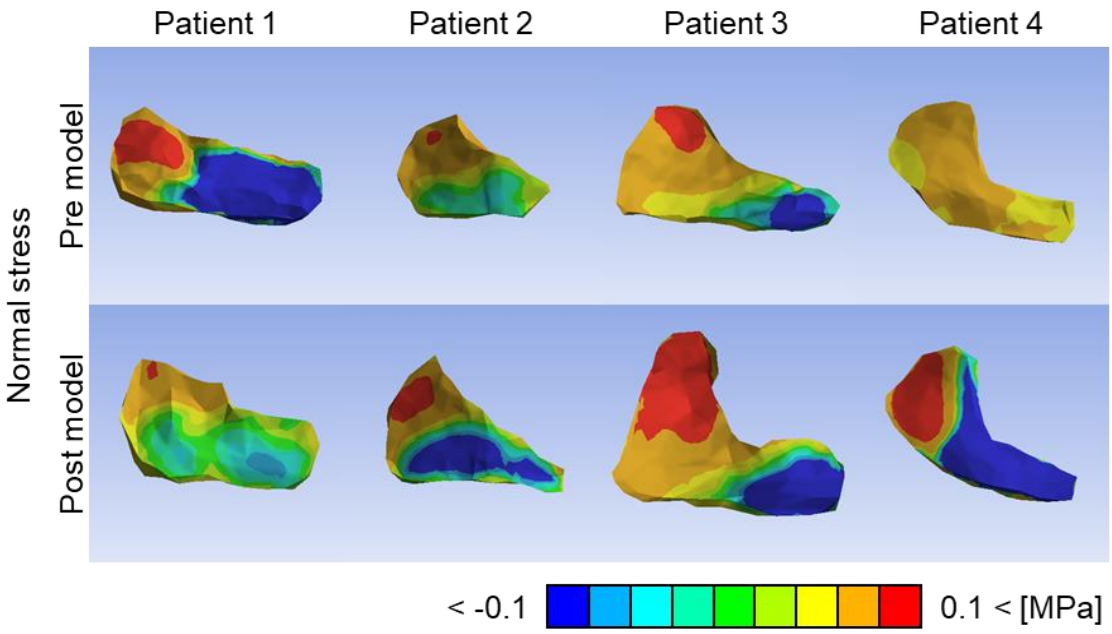

Fig. 4.12 Normal stress distribution on the normal direction of the contact surfaces in sacroiliac joints on surgical sides (Toyohara et al., 2022b).

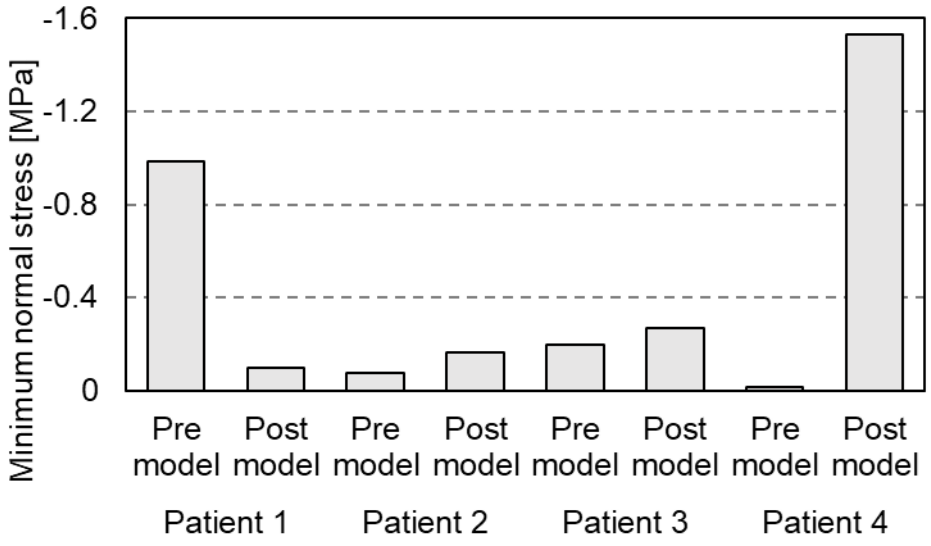

Fig. 4.13 Minimum normal stress in sacroiliac joints on surgical sides (Toyohara et al., 2022b).

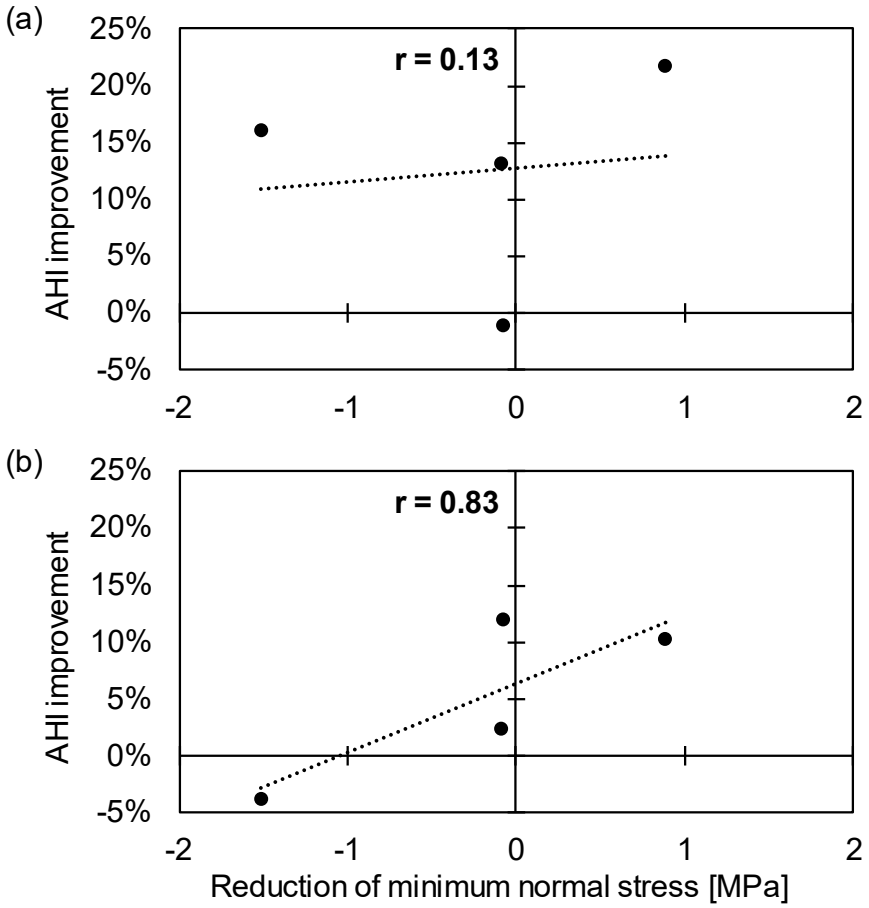

Fig. 4.14 The scatter plots of reduction of minimum normal stress in the sacroiliac joint on the surgical sides vs. improvement of acetabular head index (a) on upper coverage and (b) on posterior coverage (Toyohara et al., 2022b).

4.3.6 Loads on pelvic ligaments

Loading of the pelvic ligaments was reduced when acetabular coverage was increased. The ligament loading on the sides of surgical intervention of the pre models compared to the post models decreased by approximately 36% in patients 1 and 3 and increased by 27% in patients 2 and 4. The change was mainly due to a decrease in posterior sacroiliac ligament (PSL) loading and an increase in interosseous sacroiliac ligament (ISL) loading (Fig. 4.15). In relation to the decrease in the ligament loading and the improvement of acetabular coverage, sacrotuberous ligaments (ST) and sacrospinous ligaments (SS) loading decreased with increased posterior coverage and interosseous

sacroiliac ligaments (ISL) and posterior sacroiliac ligaments (PSL) loading increased with increased upper coverage (upper: r = - 0.19, - 0.08, 0.67, 0.70, posterior: r = 0.96, 0.89, 0.02, - 0.46, respectively) (Figs. 4.16, 4.17).

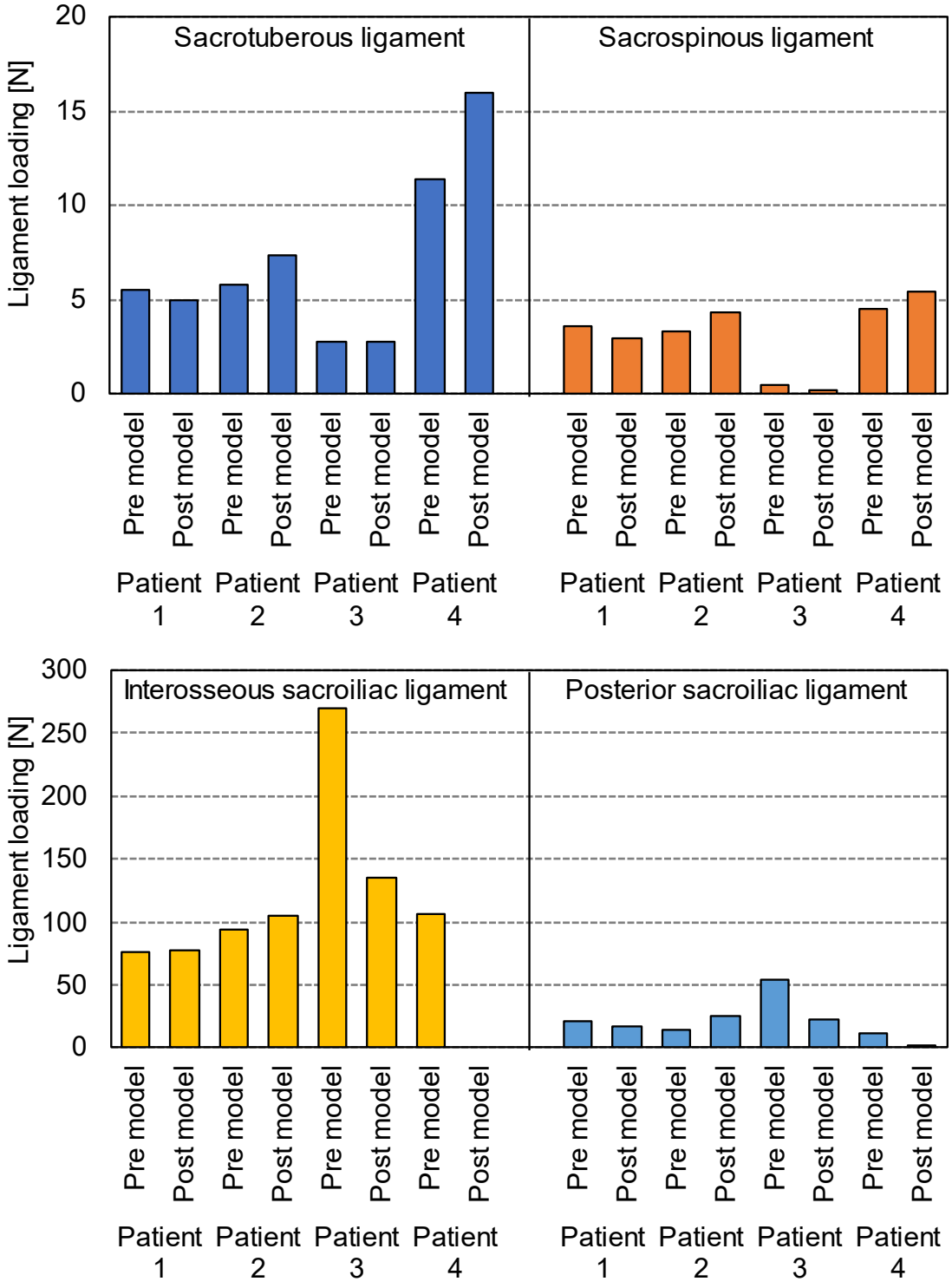

Fig. 4.15 Sacrotuberous ligament (ST), sacrospinous ligament (SS), interosseous sacroiliac ligament (ISL) and posterior sacroiliac ligament (PSL) loading on the surgical sides of all patients (Toyohara et al., 2022b).

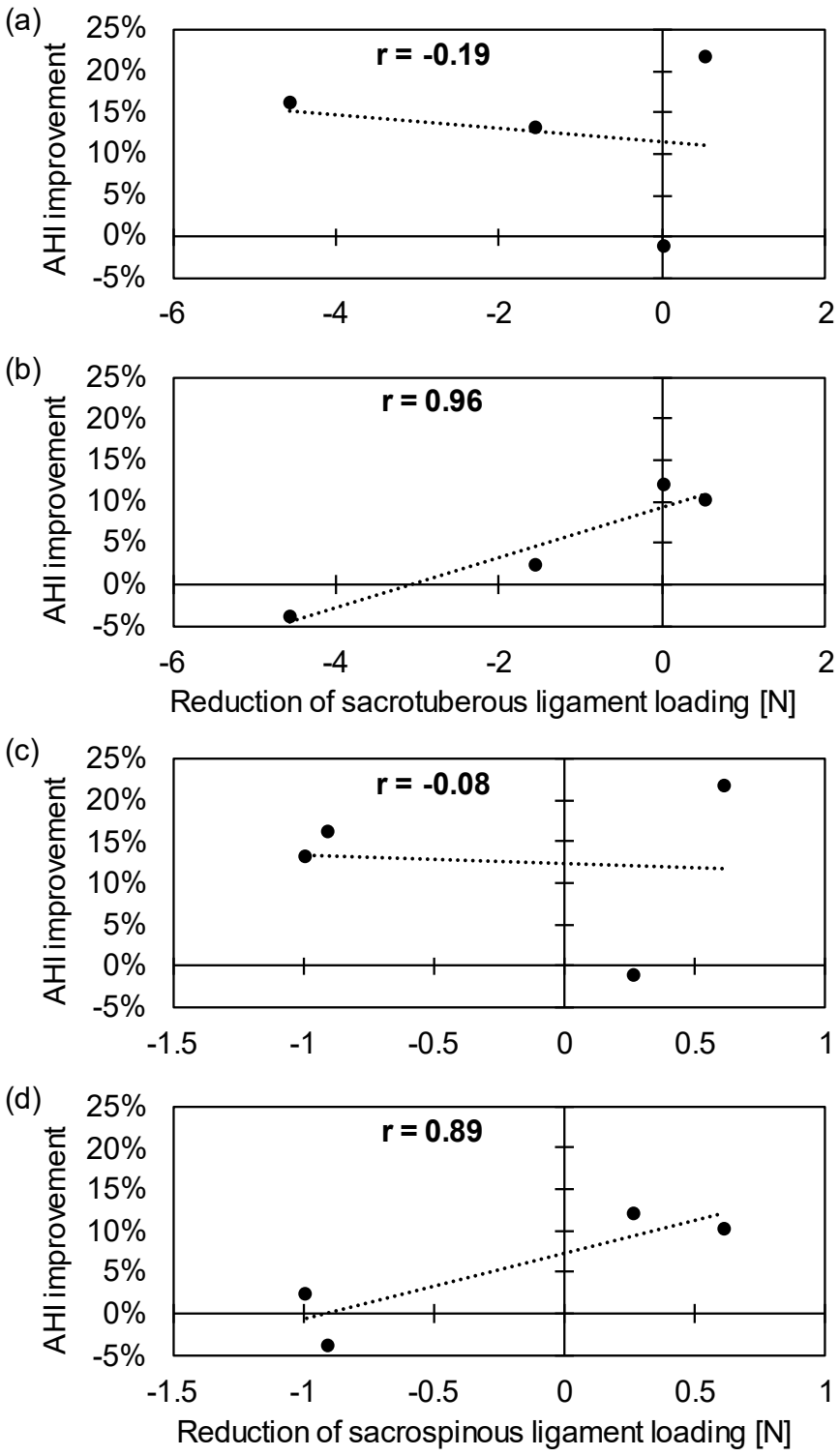

Fig. 4.16 The scatter plots of reduction of sacrotuberous ligament (ST) and sacrospinous ligament (SS) loading on the surgical sides vs. improvement of acetabular head index (a) (c) on upper coverage and (b) (d) on posterior coverage (Toyohara et al., 2022b).

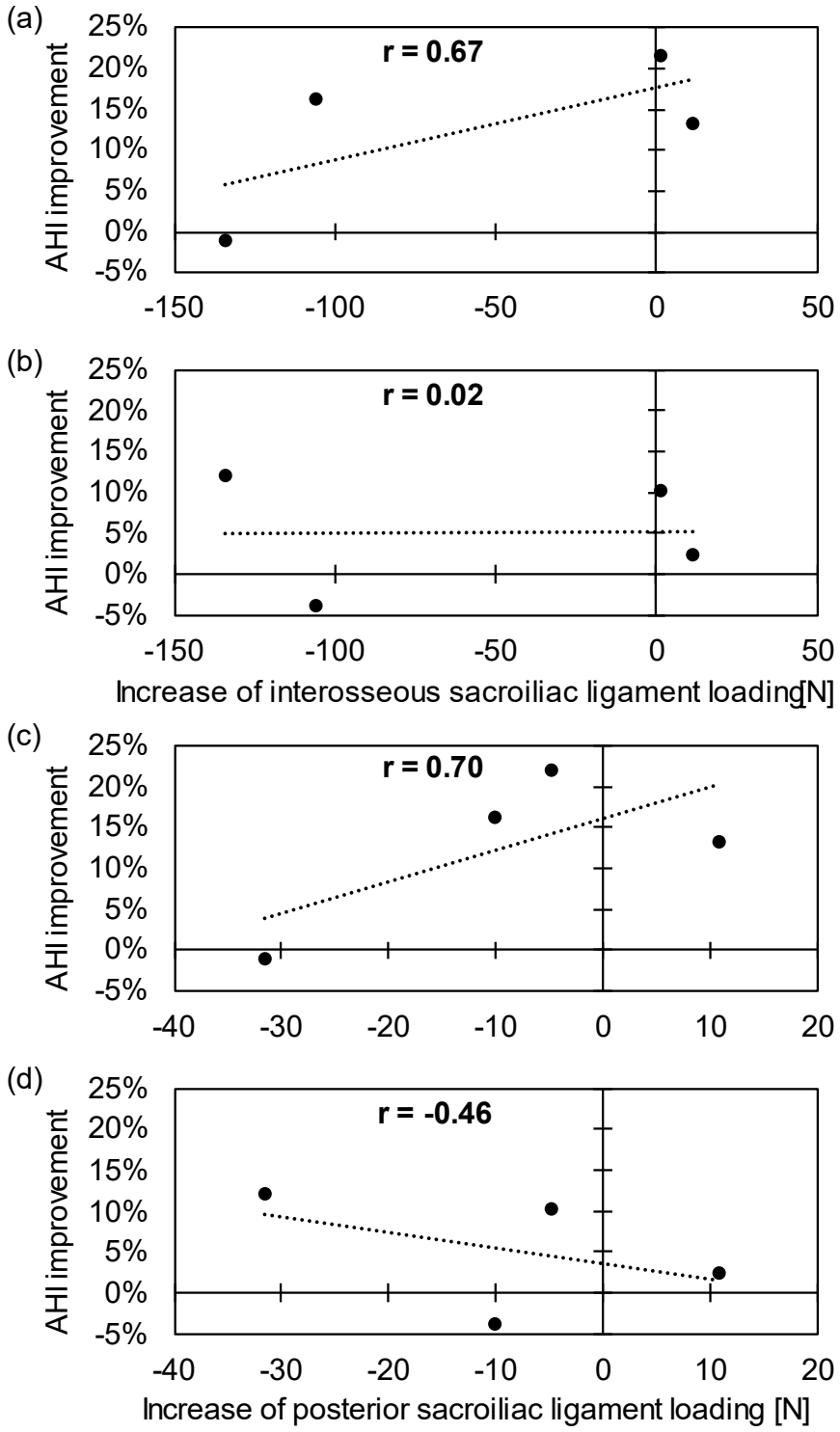

Fig. 4.17 The scatter plots of increase of interosseous sacroiliac ligament (ISL) and posterior sacroiliac ligament (PSL) loading on the surgical sides vs. improvement of acetabular head index (a) (c) on upper coverage and (b) (d) on posterior coverage (Toyohara et al., 2022b).

4.4 Discussion

There have to date few studies regarding to the morpho-mechanical coupling between the hip joints and the SIJs under instances of physiological loading (Joukar et al., 2019; Kozaki et al., 2021). To our best knowledge, this is the first report investigating the effects of acetabular dysplasia on the stress environment of the SIJs. In a pelvis with acetabular dysplasia, the innominate bone rotates inward (Fujii et al., 2011), called in-flare. The morphological results of the preoperative models obtained from bone scanning also showed in-flare and similar results were observed. Following the surgical intervention, this deformation was restored to a non-pathological anatomy including a normal or out-flare state, except for patient 2 of this given study. The in-flare state seems to open the posterior part of the SIJs, thereby increasing the load on the posterior ligaments and increasing the compressive load onto the superior part of the SIJs. On the other hand, in the out-flare state, the superior side of SIJs is thought to be opened and to be exposed to high tensile load. In patients 1, 3 and 4, the loading of posterior sacroiliac ligament (PSL) decreased by 22 - 91% from the preoperative to the postoperative state, indicating that the in-flare state changed to the out-flare state by peri-acetabular osteotomy for normalization of the acetabular bone coverage of the femoral head. Since the equivalent stress of the SIJ cartilages decreased only in patient 1, the equivalent stress state of the SIJ cartilages was determined by an increase in compressive loading due to the in-flare position and an increase in tensile loading due to the out-flare position. The equivalent stress is considered to increase or decrease depending on the extent of rotation. However, the normal stress of the SIJ cartilages decreased only in patient 1 following the surgery, which was inconsistent with an increase in tensile loading due to out-flare. This may be explained as follows: the gluteus medius muscle pulls the iliac crest outward, therefore the ilium is pressed against the sacrum at the lower part of the SIJs to generate compressive force. In consequence, the tensile load should not increase at the anterior aspect of the SIJs even though out-flare was induced. In addition, since the compressive

force at the SIJs tended to decrease with the improvement of the acetabular coverage, it was considered that the in-flare tended to result in lowered compressive loads. In this analytical model, the improvement of the posterior coverage was small and the compressive load region tended to widen.

Interestingly, some researchers have suggested that the cause of pain originating from the SIJs is a consequence of overloading of the joint's cartilaginous region and its stabilizing ligaments (Murakami et al., 2007, 2018b; Borowsky and Fagen, 2008). The lower part of the SIJ cartilaginous regions has been shown to be particularly stressed in patients with SIJ dysfunction (Poilliot et al., 2021). At the same time, the SIJs have the role of transmitting the load from the trunk to the lower limbs in the sense of form and force closure, which requires compressive forces to fulfill this function (Vleeming and Schuenke, 2019). Therefore, two possible pathways may exist to explain the stress environment at the SIJs due to acetabular dysplasia: relieved in-flare reduced the equivalent stress of the SIJ cartilage and ligament loading (patient 1); additional force closure due to the site of compressive loading may likewise increase stability (increased considerable stress) and decreased ligament loading (patient 3). In finite element analyses of the healthy pelvis, it has been reported that high equivalent stress is concentrated in the superior part of the SIJ cartilages (Toyohara et al., 2020; Venayre et al., 2021). In this given study, the postoperative model showed that following surgery, similar equivalent stress distribution was close to that of a healthy person. With surgery, the equivalent stress environment trended to become normal. At the same time, the pre models showed relatively low equivalent stress in the superior region of the SIJ cartilage. It has been observed in Japan that patients with acetabular dysplasia secondary progress the hip OA (Okuzu et al., 2021) and Asada et al. (2019) have reported that the volume of vacuum phenomena in the SIJs, which indicates the SIJ degeneration, was significantly larger in the hip OA and the vacuum areas were localized in the antero-superior region of the SIJs. The abnormal low equivalent stress at the same part may relate to the SIJ degeneration in acetabular dysplasia pelvis. The high equivalent stress distribution in the lower part of the

SIJ cartilages before surgery seemed to be characteristic of acetabular dysplasia. Compared with the report that patients with SIJ dysfunction were loaded at the same position (Poilliot et al., 2021), it is suggested that acetabular dysplasia may impair the stress environment in the SIJs.

Various indices such as center-edge angle (CEA) (Wiberg, 1939), acetabular roof angle (ARO) (Massie and Howorth, 1950), acetabular head index (AHI) (Heyman and Herndon, 1950) and sharp angle (Sharp, 1961) are used clinically to assess the extent of acetabular dysplasia. Physicians diagnose acetabular dysplasia at a CEA of 20 degrees or less (Wiberg, 1953). In this study, AHI was investigated on upper and posterior coverages of acetabulum. The improvement of the coverage of the posterior acetabulum was considered to lead to counter-nutation, which is assumed to stabilize the pelvis and to reduce the equivalent stress on the SIJs and the load on the main ligaments around the pelvis. The SS, ST and ASL were suggested to have a defined function of limiting the nutation movement (Kapandji, 1974; Hammer et al., 2019a) and a decrease in these ligaments' loading can be observed with the improved posterior coverage of the acetabulum, indicating that nutation movement weakens. The results were similar to those of the counter-nutation induction obtained from the measurement of the rotation of the SIJs. The decrease in displacement at the iliac crest after surgery indicated that the load from the femora could be stable be stably transmitted to the innominate bone. The improvement of the posterior coverage of the acetabulum has been suggested to normalize the load transmission on the pelves and to improve the stress environment of SIJs. However, it has been reported that an over-improvement of the posterior coverage limits the range-of-motion of the hip joint (Hamada et al., 2015). The change in the stress environment of the pelvis due to the improvement of the covering therefore seems to be limited.

Finally, this study has a number of limitations. First, the conclusions were derived from a small sample size which was available. In addition, only female patients were investigated. Female pelves have a high sacral slope which means SIJs are easily exposed

to shearing stress. Since the shearing force is applied more to female than to male (Bellamy et al., 1983; Joukar et al., 2018), the load on the SIJs due to hip joint disease and the change in load on the SIJs after surgery may be more significant for females. Secondly, only a subset of anatomical structures has been modeled, including the most relevant osseous, cartilaginous, ligamentous and muscular components. Further refinement of the given models may help gain more insight into the variations in load distribution related to surgery of acetabular dysplasia. Another limitation is related to the choice of the material models (isotropic, homogeneous) and testing conditions (quasi-static). Furthermore, the tissues around the hip joint were composed of deformable cartilage and two major muscles and did not design ligaments nor joint slip. The actual hip joint slides in the joint capsule during exercise, however, the analytical condition of this given simulation was only in standing position, where the bones did not move enough to perform intracapsular movement in the hip joint, so only compressive force transmission occurred. Therefore, this model seemed to reproduce the stress environment in the pelves during standing.

4.5 Conclusions

Finite element analysis based on CT datasets of patients with acetabular dysplasia undergoing surgery was performed to assess stress distribution in double-leg stance in a preoperative and postoperative condition. Comparing the pre- and postoperative findings, the preoperative innominate bones were rotated inward, called in-flare. Improving the posterior coverage of the acetabulum relieved this rotation and the innominate bones were deformed laterally to anteriorly. This reduced the equivalent stress, compressive stress and ligament loading at the SIJs, suggesting that insufficient acetabular morphology may worsen the SIJ stress environment.

Chapter 5

Numerical and experimental validation of effectiveness of pelvic belts as a treatment for sacroiliac joint dysfunction

5.1 Introduction

Sacroiliac joint (SIJ) dysfunction is considered to account for approximately 15% to 30% of symptoms in patients with low back pain (Bernard and Kirkaldy-Willis, 1987; Schwarzer et al., 1995; Forst et al., 2006). The SIJs are located between the sacrum and the ilium and serves as a shock absorber that receives and aids in dissipating the impact of the trunk and the lower limbs (Lovejoy, 2007; Vleeming et al., 2012). Unexpected force or repeated impact is believed to cause joint misalignment and instability and provoke pain arising from the SIJs (Murakami, 2018a; Murakami et al., 2018b). Typical conservative (non-surgical) treatment strategies to relieve the painful SIJs include pelvic belts (Mens et al., 2006; Hammer et al., 2015), injection of local anesthetics into the joint (Murakami et al., 2007; Lee et al., 2010) and physical therapy (Kirkaldy-Willis and Cassidy, 1985; Katada, 2019). Pelvic belts and SIJ fixations are used to improve joint stability by minimizing the extent of joint motion (Wise and Dall, 2008; Smith et al., 2013). Pelvic belts have not been comprehensively investigated in the context of SIJ dysfunction. A study in healthy young women indicated that pelvic belts help reduce SIJ laxity (Damen et al., 2002). Moreover, mathematical analysis indicates that compression force exerted on the anterior superior iliac spine (ASIS) increased SIJ compression and reduced muscle activity (Pel et al., 2008). These reports imply that if the SIJs are fixed with pelvic belts, stability would be enhanced, however, the effectiveness based on the type and tightening method of the pelvic belts remain poorly understood. It has been reported that pelvic belts with a textured sacral pad may enhance the sensory performance of the hip joint and improve motor control (Delshad et al., 2020). Compressive pelvic belts may also be beneficial in the treatment of SIJ dysfunction.

This study aimed to analyze the effect of pelvic rubber belts or padded pelvic belts on stress distribution within the pelves and clarify the effectiveness of such treatments that bilaterally compress the posterior superior iliac spine (PSIS). The pressure distribution was assessed in the pelvic region when pelvic belts were applied. Finite

element analysis of the pelvic model with soft tissues was conducted. It was hypothesized that padded pelvic belts would more effectively compress the SIJs and thus reduce tension of the surrounding ligaments.

5.2 Methods

5.2.1 Finite element model of pelves with surrounding soft tissues

A finite element model of a pelvis with surrounding soft tissues (Fig. 5.1), was created based on the total human model for safety (THUMS Version 4.02 AM50 pedestrian model, 175 cm, 77 kg, Toyota Central R&D Labs, Inc. & Toyota Motor Corporation) using SpaceClaim 2021R1 (Cybernet Systems Co., Ltd., Tokyo, Japan). This model comprises three types of tissues: bones, cartilages and soft tissues (including skin, fat, muscle, etc.). Bones were modeled for the 3rd, 4th and 5th lumbar vertebrae, the sacrum, the both innominate bones and the proximal ends of the both femurs. Cartilage tissues, L3 - 4 disc to L5 - S1 disc, the SIJ cartilages and the hip joint cartilages, were created based on the shape of the pelvic bone models. Soft tissues were defined between the body surface and the pelvic models. A total of 210 spring elements were added in

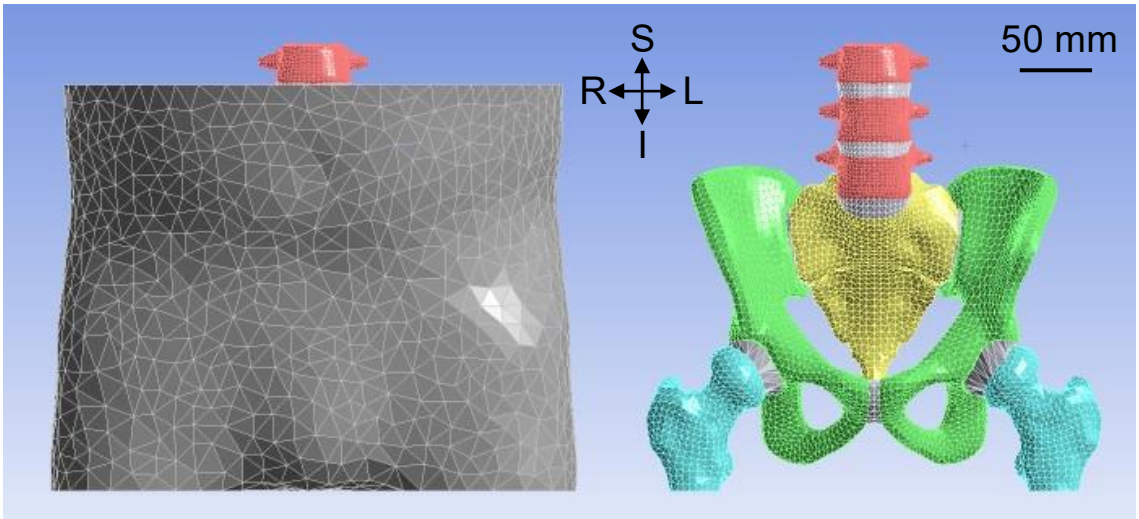

Fig. 5.1 Finite element model of the pelvis including soft tissue, displayed on whole model (left) and hidden the soft tissue (Right) with anterior views. The scale bar: 100 mm. S: superior, L: left (Toyohara et al., 2022a).

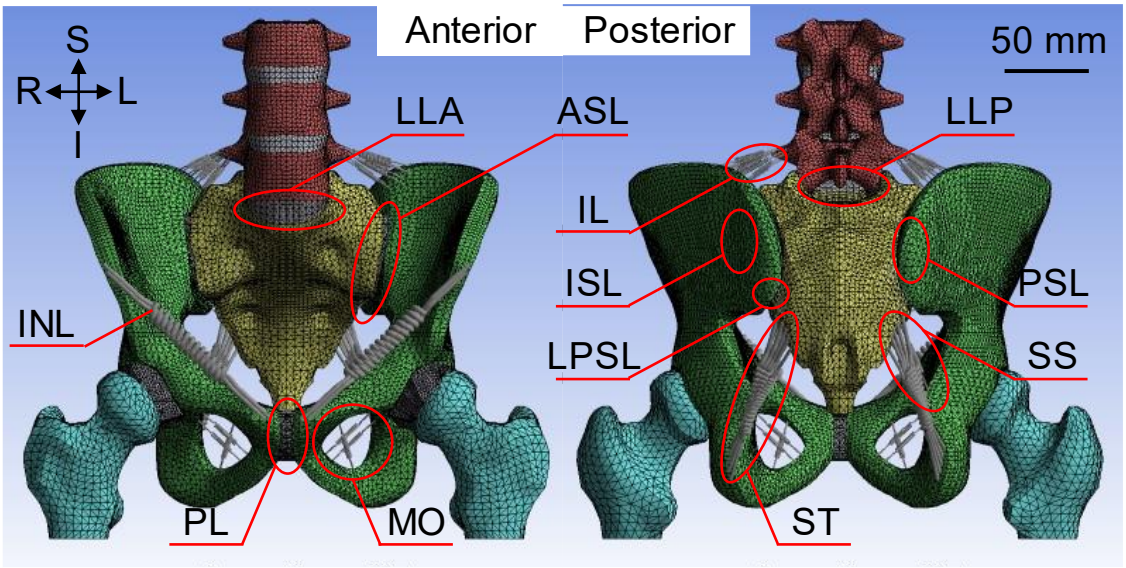

Fig. 5.2 The positions and names of the pelvic ligaments modelled in this study, in a meshed pelvis model with anterior (left) and posterior (right) views. The ligaments are the anterior longitudinal ligament (LLA), anterior sacroiliac ligament (ASL), iliolumbar ligament (IL), inguinal ligament (INL), long posterior sacroiliac ligament (LPSL), obturator membrane (MO), posterior longitudinal ligament (LLP), posterior sacroiliac ligament (PSL),pubic ligament (PL), interosseous sacroiliac ligament (ISL), sacrospinous ligament (SS) and sacrotuberous ligament (ST). The scale bar: 60 mm. S: superior, L: left, R: right (Toyohara et al., 2022a).

place of the ligaments around the pelvis (Toyohara et al., 2020) and 12 types of ligaments were modeled (Fig. 5.2). The ligaments were defined as tension only and could not sustain the bones in the case of compressive load. ANSYS 2021R1 (Cybernet Systems Co., Ltd., Tokyo, Japan) was used for the analysis.

5.2.2 Material properties

Bones were defined as elastic bodies, cartilage as elastic or hyper-elastic bodies and soft tissues as hyper-elastic bodies, respectively. For simplicity, all the tissues were defined as uniformly isotropic materials. The results obtained by Wirtz et al. (2000), Majumder et al. (2007), Sichting et al. (2014) and Ramezani et al. (2014) were used for

Table 5.1 Material properties for the finite element model. C_{10}, C_{01} and C_{11} mean the parameter of Mooney-Rivlin models for hyper-elastic bodies. Material properties for cartilage were used for the cartilage model except for SIJs and symphysis cartilages (modified from Toyohara et al., 2022a).

Material	Young's Modulus[MPa]	Poisson's ratio	C10 [MPa]	C01 [MPa]	C11 [MPa]
Cortical bone (Wirtz et al., 2000)	11,000	0.2	-	-	-
Cartilage (elastic body) (Sichting et al., 2014)	150	0.2	-	-	-
SIJ cartilage (hyper-elastic body) (by personal communication)	-	-	4.1	0.41	0
Symphysis cartilage (hyper-elastic body) (by personal communication)	-	-	0.1	0.45	0.6
Soft tissue (hyper-elastic body) (Majumder et al., 2007)	-	-	0.0855	0.02138	0
Ligament (Ramezani et al., 2019)	350	-	-	-	-

the material properties (Table 5.1). The following strain energy density function, W, was introduced, which is used for a hyper-elastic body, using the Mooney-Rivlin model of a complete non-compressional body. C_{10}, C_{01} and C_{11} are material constants. I_1 and I_2 are the first and second invariants of the distortion, respectively.

$$W = C_{10}(I_1 - 3) + C_{01}(I_2 - 3) + C_{11}(I_1 - 3)(I_2 - 3) \quad (5\text{-}1)$$

5.2.3 Mesh generation

A mesh was created using tetrahedral elements each consisting of 10 nodes (Fig. 5.2). Consequently, the total number of elements and nodes were 264,938 and 442,001, respectively. The average element quality was 0.751, indicating good mesh quality.

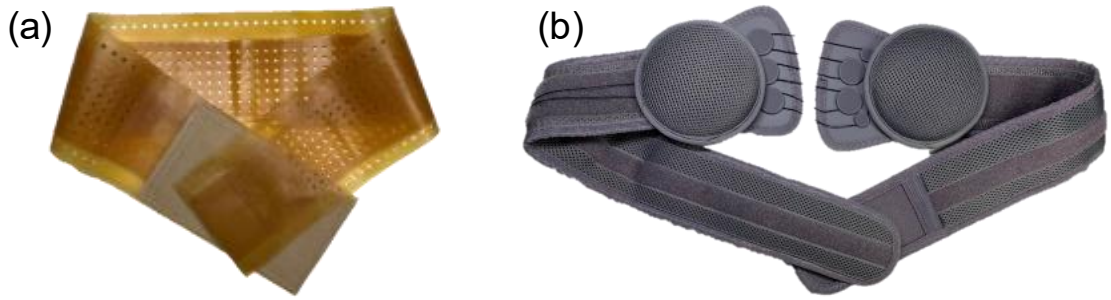

Fig. 5.3 Sample of the (a) pelvic rubber belt and (b) padded pelvic belt used in this study (modified from Toyohara et al., 2022a).

5.2.4 Loading and boundary conditions

A pelvic rubber belt (Balance Control Band, Hakkosha Co., Ltd., Tokyo, Japan) (Fig. 5.3(a)) and a padded belt on the lumbar region (Smartspine SI Support, Ottobock SE & Co. KgaA, Duderstadt, Germany) (Fig. 5.3(b)) was investigated. The pelvic rubber belt was tightened forward (termed “front belt”) and backward (termed “back belt”). For the padded belt (termed “padded belt”), two pads were placed around the lateral sides of the PSIS bilaterally. The pressure distribution was measured under the three conditions. A body pressure distribution measuring device (FSA, Takano Co., Ltd., Nagano, Japan) was used to measure the distribution of the tightening pressure of the pelvic belts. A healthy participant (a 23-year-old man, 182 cm body height, 70 kg body weight) volunteered for this study. Pressure sensors were placed on the body and the pelvic belts were wrapped around the device (Figs. 5.4 and 5.5). Before conducting the measurement, both ASISs were palpated to position the pressure sensors. After wrapping the pelvic belt, the participant stood on both legs and 22 frames were measured for 6.8 s in a sufficiently stable state. The average value of 20 frames, excluding the maximum and minimum values, was used for further analysis.

The soft tissue of the pelvic model was divided into 32 areas in the circumferential direction and 11 areas in the vertical direction at approximately 500 mm^2 and the obtained

pressure was applied to the surface of the soft tissue based on the position of the ASISs (Fig. 5.6(a)).

Four conditions were analyzed, including three types of pelvic belts and the control condition without a pelvic belt attached. To simulate the double-leg stance, a vertical upward surface load of 300 N and a vertical downward surface load of 600 N were applied to the lower ends of both femurs and base of the sacrum, respectively (Fig. 5.6(b)). The anterior aspect of the second sacral spine (Lee et al., 2010) and both entire femora were fixed in space to reproduce sacral motion and reduce the computational load by limiting unnecessary movement of the femur, respectively. Because the soft tissues were not displaced in the vertical direction by tightening of the belt, vertical displacement of the cross-sections of the soft tissues was suppressed. The contact on each surface was defined as follows: the contact surfaces of bone and soft tissue were not separated; the contact

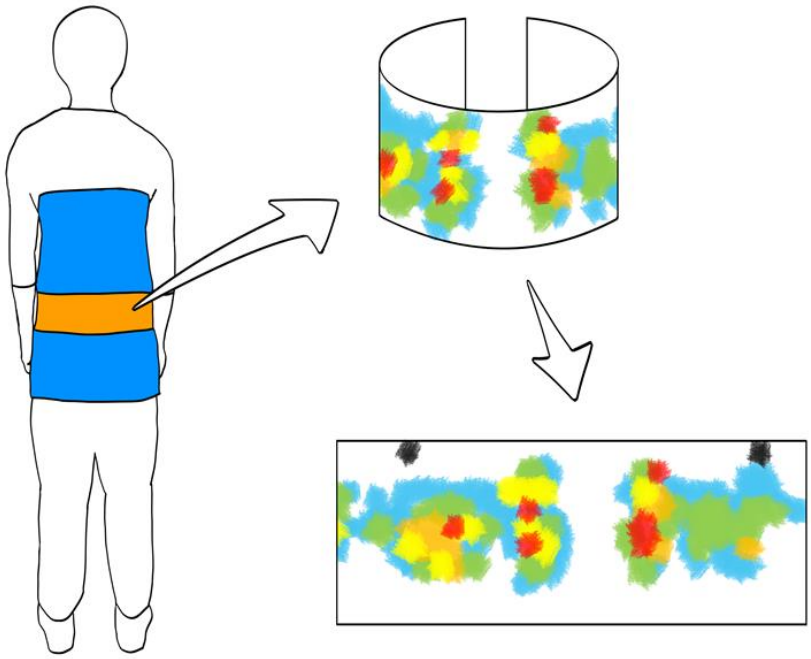

Fig. 5.4 Scheme of pressure measurement in this study. (Left) A pressure measuring device was placed on a body and the pelvic belts were wrapped on the device. Blue: a pressure measuring device. Orange: pelvic belt. (Right top) Pressure distribution on the pelvic belts and (right bottom) straightly opened results (Toyohara et al., 2022a).

surfaces of the SIJ cartilage and bone were rough; and the other contact surfaces were bonded. A lack of separation contact means that the contact surfaces can not be detached and can slide frictionlessly. Rough contact was defined as contact surfaces with detached contact but no ability to slide.

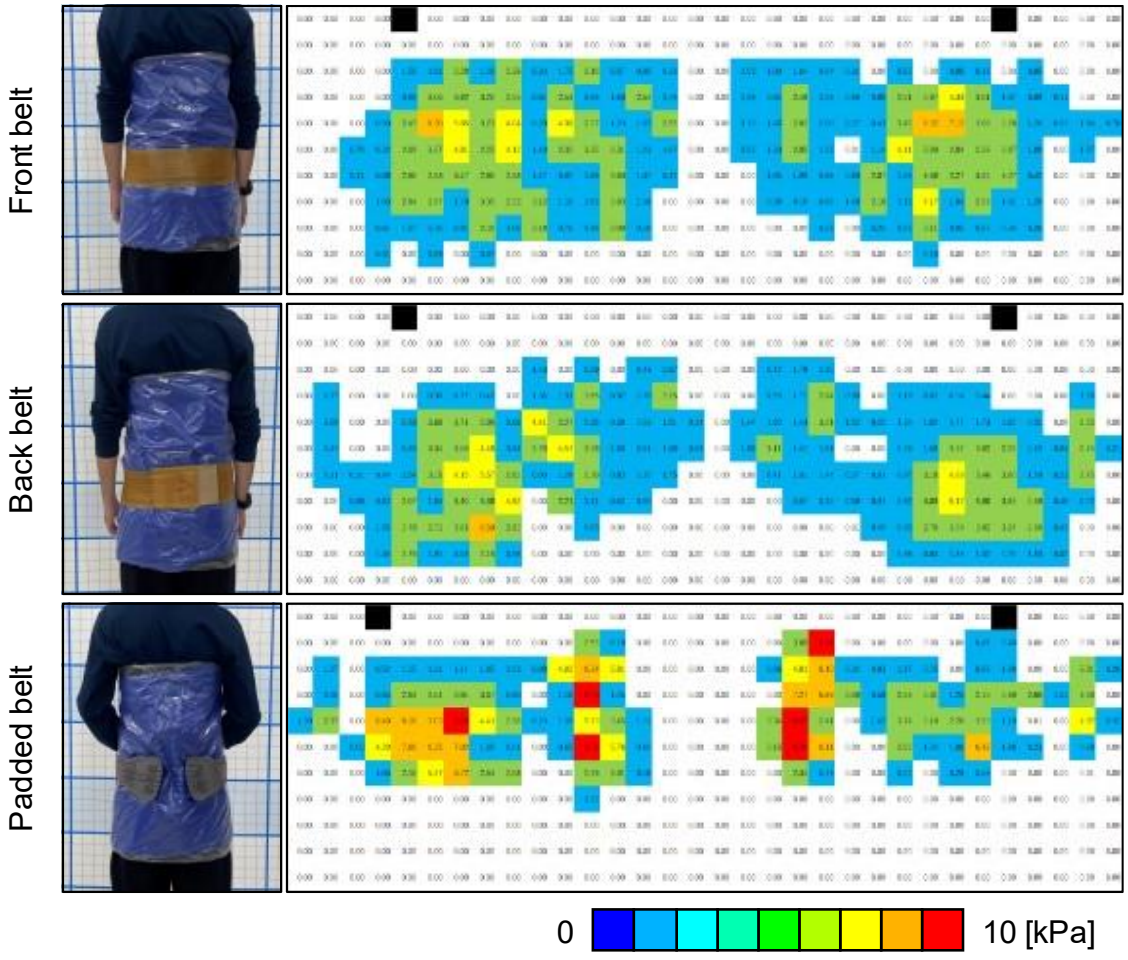

Fig. 5.5 Pelvic belt types and related pressure measurements in-vivo in a setup on the volunteer (left row), and pressure distribution on the pelvic belts (right row). Black areas indicate the anterior superior iliac spines as reference marks (Toyohara et al., 2022a).

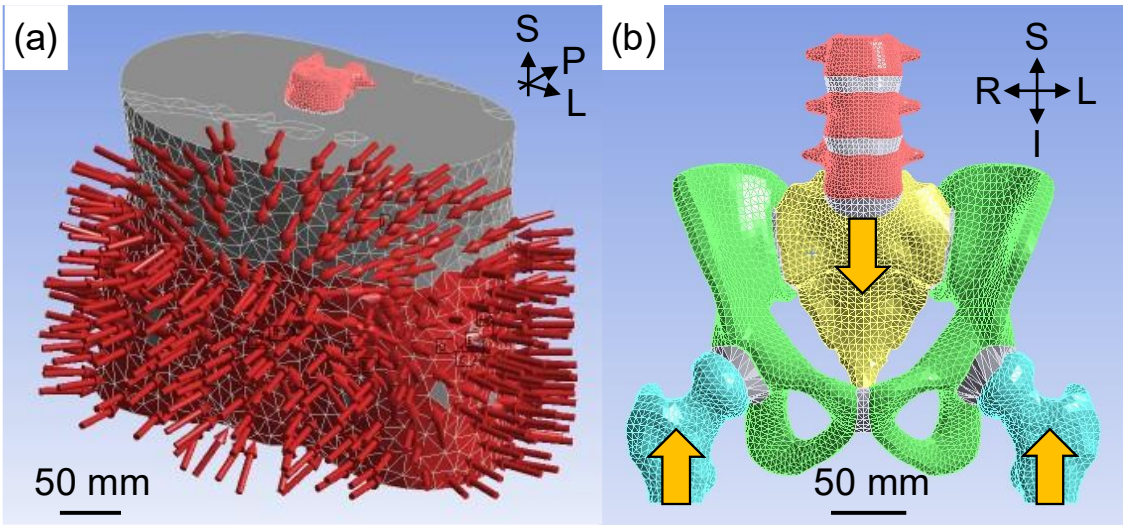

Fig. 5.6 (a) The red arrows indicate the places and directions the pressures are applied (trimetric view), and (b) the orange arrows indicate where the loads are applied (anterior view). The scale bar: 60 mm. S: superior, L: left, A: anterior (Toyohara et al., 2022a).

5.2.5 Analytical parameters

The minimum principal strain of the soft tissues and the pelvis, horizontal displacement of the innominate bone, the minimum principal stress of the SIJs, the displacement of the SIJs and the ligament loading force were investigated. The ligament loading force is the sum of the maximum elastic forces of the spring elements, representing each ligament.

5.2.6 Model validation

Model validation was performed with literature values (Hammer and Klima, 2019). The maximum and mean SIJ displacements, mean strain of the sacrotuberous and sacrospinous ligaments, and ligament load rate in the control condition were used for validation.

5.3 Results

5.3.1 Horizontal displacement of innominate bones

When both types of pelvic belts were applied, the innominate bones rotated outward relative to the control (Figs. 5.7, 5.8). In the control group, the iliac crest moved inward, whereas in the pelvic belt group, the iliac crest was scarcely displaced. The extent of the inward displacement with pelvic belts decreased by 2.99 μm to 8.11 μm (- 2% to 52% compared to the control). The front belt (right: 8.11 μm, - 1%; left: 5.30 μm, 15%) and padded belt (right: 6.85 μm, 15%; left: 6.37 μm, - 2%) had similar changes and the back belt (right: 6.73 μm, 16%; left: 2.99 μm, 52%) exhibited low change. Focusing on the displacement of the ischial limb, the control was displaced outward and the pelvic belt models were displaced inward.

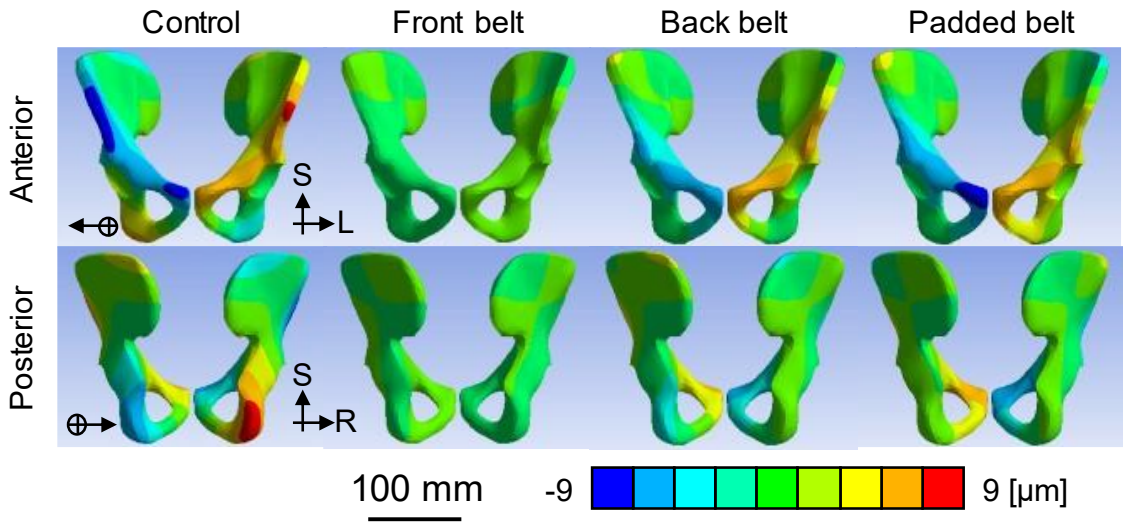

Fig. 5.7 Horizontal displacement of the innominate bones shown from an anterior (1st line) and posterior (2nd line) view. The positive directions are the directions that the arrows point to, to right on the models. The scale bar: 100 mm. S: superior, L: left, R: right (Toyohara et al., 2022a).

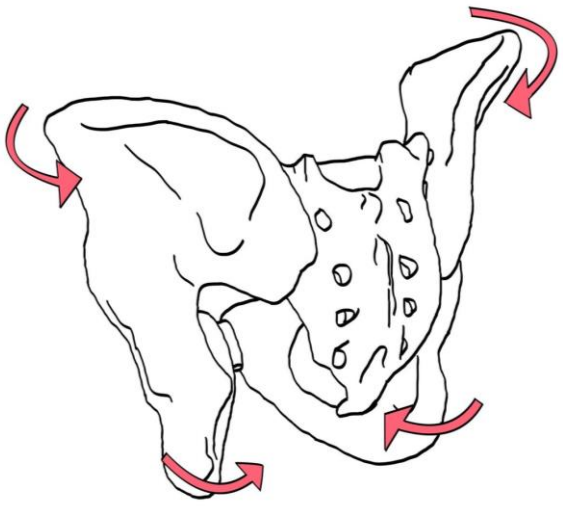

Fig. 5.8 Scheme of pelvic deformation. The innominate bone was rotated outward by using pelvic belts (Toyohara et al., 2022a).

5.3.2 Minimum principal stress on sacroiliac joints

The minimum principal stress indicates the maximum compressive stress with a negative value. In Fig. 5.9, red represents the high-compression area. The anterior and superior parts of the SIJs were in a high-compressive stress state. When the pelvic belt was applied, the compressive stress region increased in the inferior parts. The mean minimum principal stress increased up to 5% with the attached padded belt compared with the control (Fig. 5.10).

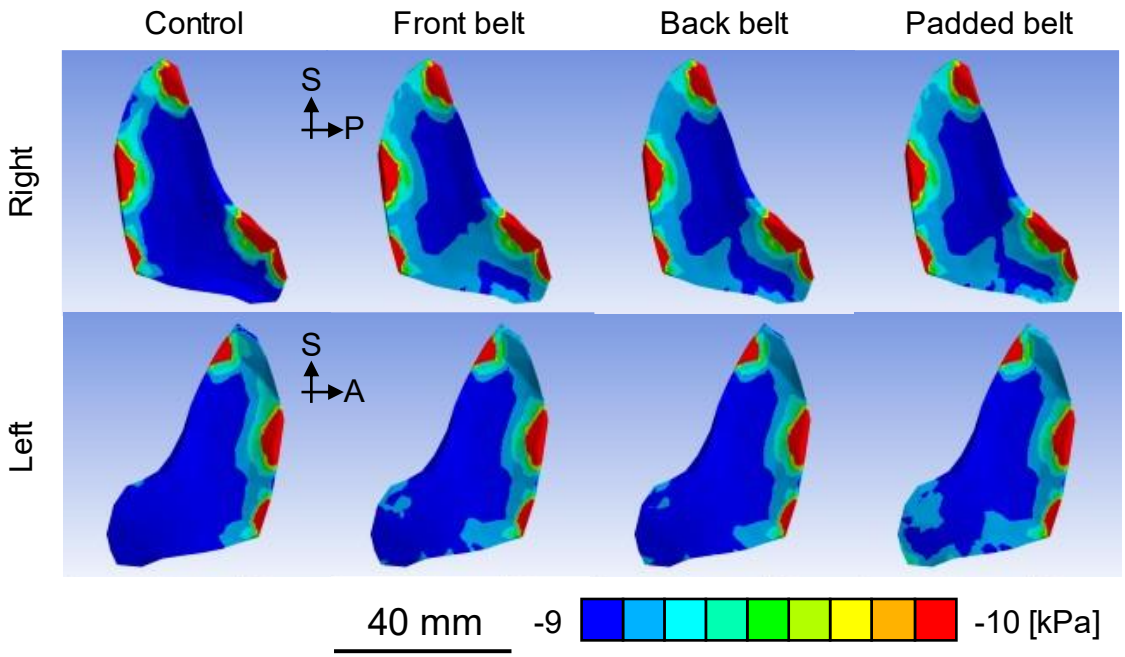

Fig. 5.9 Minimum principal stress distribution of right (1st line) and left (2nd line) sacroiliac joint cartilage shown from left and right, respectively. The red area shows the tensile area, and the tensile area decreased by pelvic belts. The scale bar: 40 mm. S: superior, A: anterior, P: posterior (Toyohara et al., 2022a).

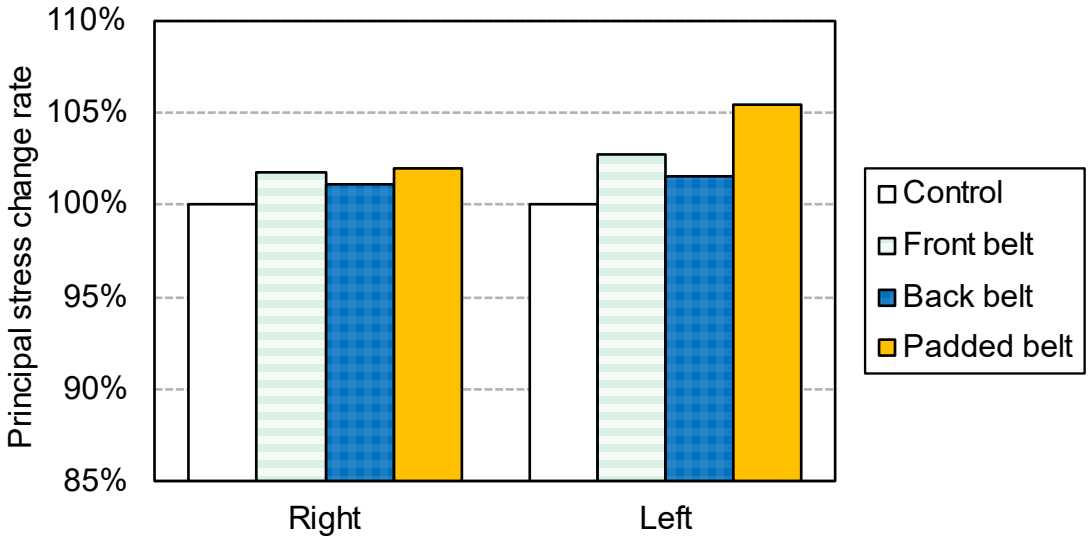

Fig. 5.10 The comparison of mean minimum principal stress rates for the control condition. Right and left mean right and left sacroiliac joints, respectively (Toyohara et al., 2022a).

5.3.3 Displacement of sacroiliac joints

When the pelvic belt was applied in the numerical model, the mean total displacement of the SIJs decreased by 5% to 11% compared with the control condition (Figs. 5.11, 5.12). In particular, it decreased in the front belt (right: - 10%, left: - 9%) and the padded belt (right: - 11%, left: - 8%). The decrease in the back belt was lower than that in the others (right: - 8%, left: - 5%).

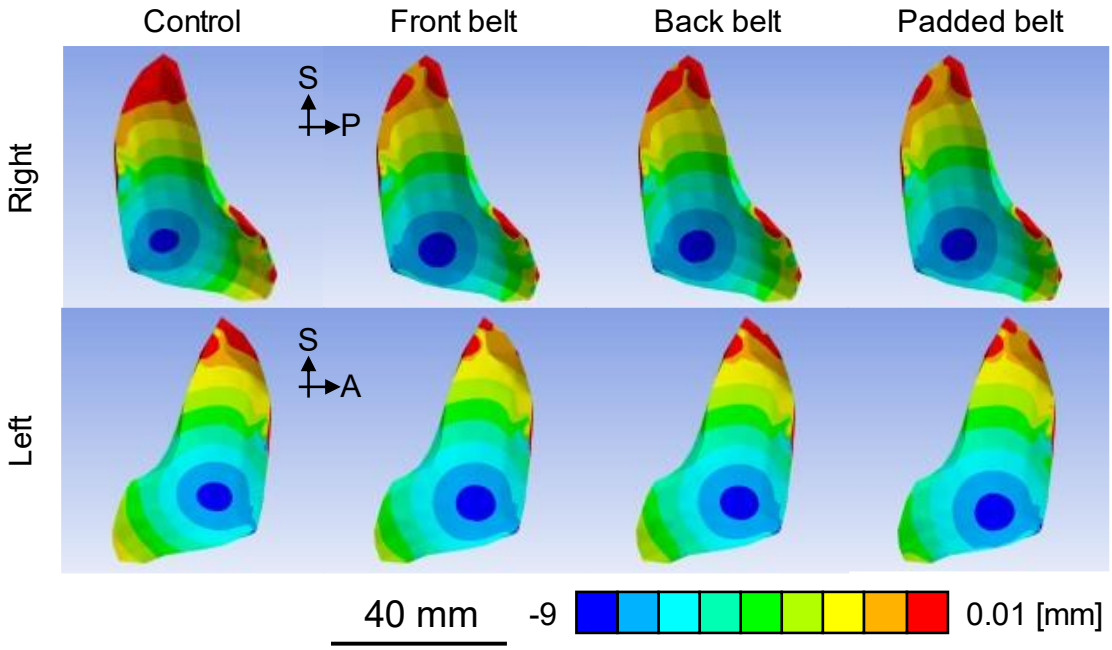

Fig. 5.11 Resultant displacement distribution of right (1st line) and left (2nd line) sacroiliac joint cartilage shown from left and right, respectively. The very low displacement area (blue area) increased with pelvic belts. The scale bar: 40 mm (Toyohara et al., 2022a).

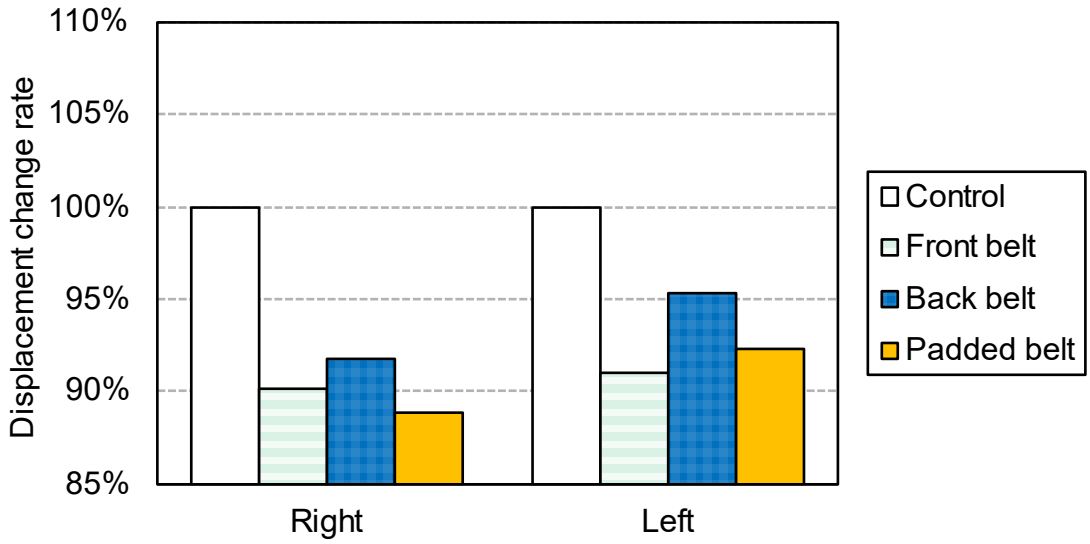

Fig. 5.12 The comparison of mean resultant displacement rates for the control. Right and left mean right and left sacroiliac joints, respectively (Toyohara et al., 2022a).

5.3.4 Loads on pelvic ligaments

Pelvic belt application decreased the ligament loading force on the interosseous sacroiliac ligament (ISL; right: - 6%, left: - 6%), posterior sacroiliac ligament (PSL; right: - 4%, left: - 10%), sacrospinous ligament (SS; right: - 3%, left: - 8%) and sacrotuberous ligament (ST; right: - 7%, left: - 12%). In contrast, the anterior sacroiliac ligament (ASL; right: 7%, left: - 6%) exhibited opposing trends on the left vs. right side, increasing on the right side and decreasing on the left side (Fig. 5.13).

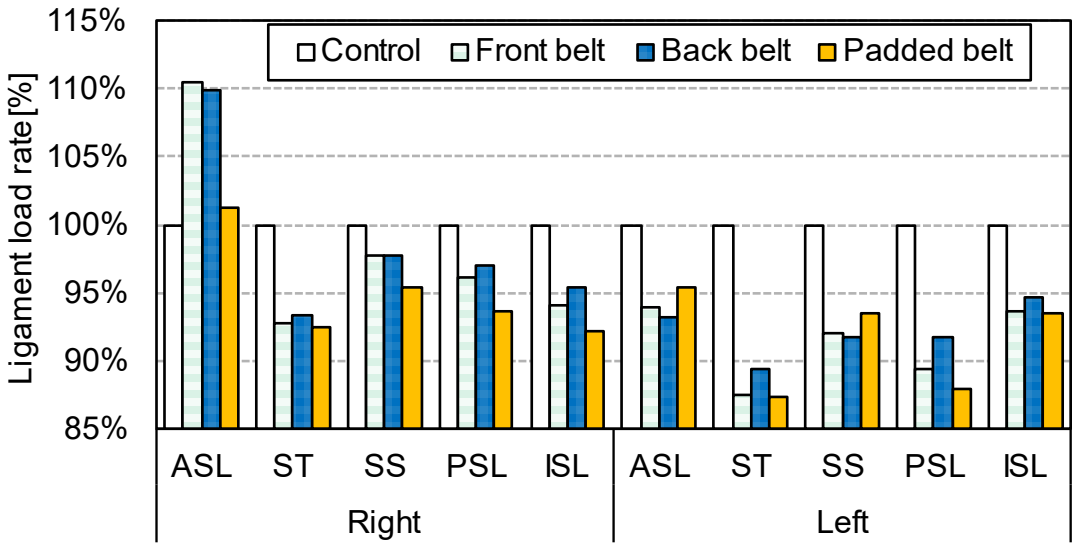

Fig. 5.13 A comparison of ligament loading rates on anterior sacroiliac joint (ASL), sacrotuberous ligament (ST), sacrospinous ligament (SS), posterior sacroiliac ligament (PSL) and interosseous sacroiliac ligament (ISL) for the control. The left and right graphs are the results on the right and left sides of ligaments, respectively (Toyohara et al., 2022a).

5.3.5 Minimum principal strain on soft tissues and pelves

The minimum principal strain indicates the maximum compressive strain. In the soft tissue, all pelvic belts in this study were compressed mainly at the anterolateral and posterior parts under ASIS levels (Fig. 5.14). In the pelvis, the anterolateral parts were also deformed, however, the posterior sides were compressed over the ASIS levels.

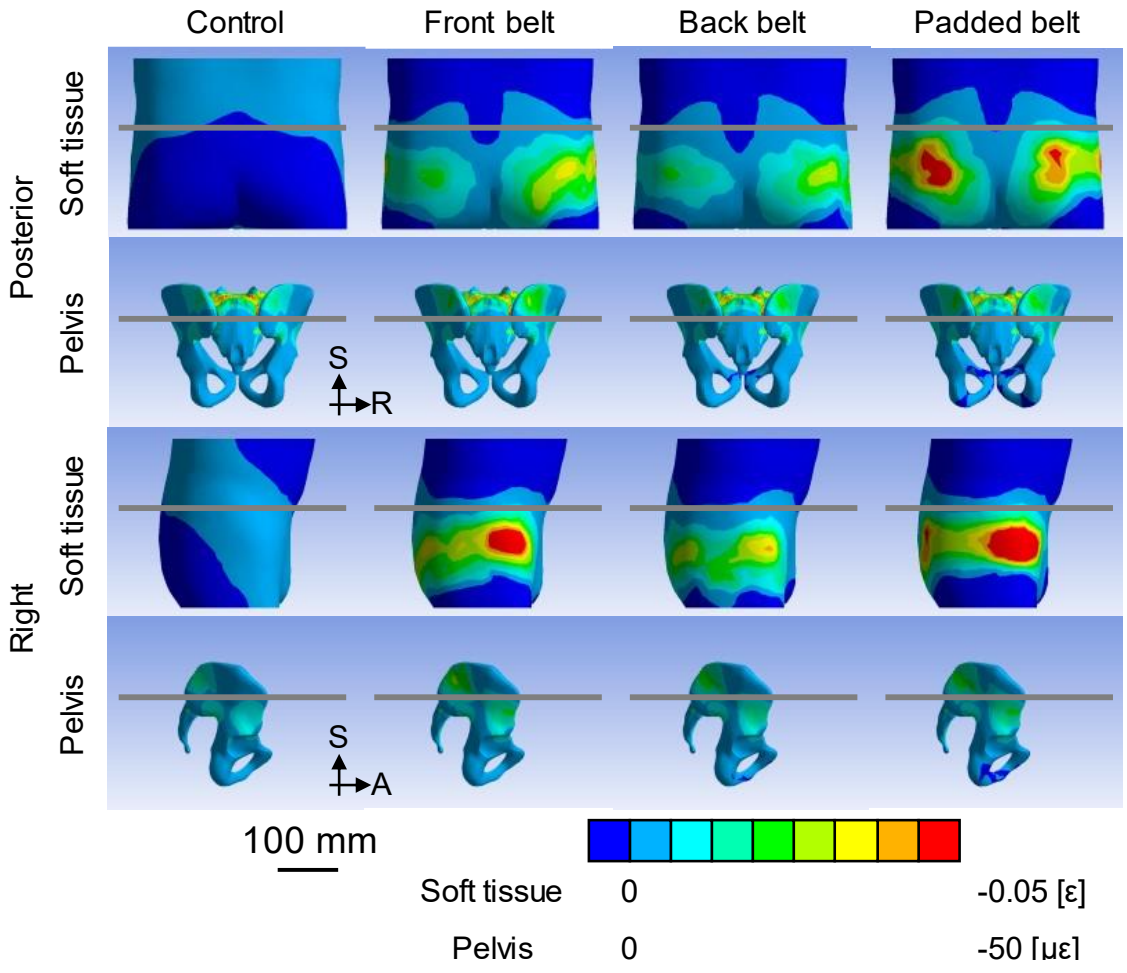

Fig. 5.14 Minimum principal strain distribution of soft tissue (1st and 3rd lines) and pelvis (2nd and 4th lines). The top and bottom two lines are shown from posterior and right views, respectively. The gray lines indicate the level of the anterior superior iliac spines. The scale bar: 100 mm. S: superior, R: right, A: anterior (Toyohara et al., 2022a).

5.3.6 Comparison with previous studies

The range of the SIJ motion was set for maximum displacements, which is 0.47 mm in healthy individuals (Kibsgård et al., 2012), 0.3 mm in cadavers (Hammer et al., 2019c), and 0.6 mm in FEM (Toyohara et al., 2020) and for mean displacements, which is 3.0 μm on cadavers (Varga et al., 2008). In this study, the maximum and mean displacements of the SIJ cartilage in the control were 0.17 mm and 7.33 μm, respectively. The reported mean strains of ST and SS were 0.08% and 0.04% (Buford et al., 2010) and 0.048% and 0.072% (Sichting et al., 2014) and in this study were 0.015% and 0.021%, respectively. The ligament load rates were 2% and 4% for ASL, 11% and 7% for ST, 8% and 5% for SS, 29% and 8% for PSL and 39% and 71% for ISL to the total unilateral ligament load in the literature (Toyohara et al., 2020) and in this study, respectively. The results of this study were compared to those of the contemporary literature and yielded values similar to those of previous studies (Table 5.2).

Table 5.2 Summary of comparison.

Validation data		Literature	This study
Maximum displacement of the sacrum relative to the innominate bone		0.47 mm (healthy) 0.3 mm (cadaver) 0.6 mm (FEM)	0.17 mm
Mean displacement of the sacrum relative to the innominate bone		3.0 μm (cadaver)	7.33 μm
Mean strain of sacrotuberous ligaments		0.08% 0.048%	0.015%
Mean strain of sacrospinous ligaments		0.04% 0.072%	0.021%
Ligaments load rates	Anterior sacroiliac ligaments	2%	4%
	Sacrotuberous ligaments	11%	7%
	Sacrospinous ligaments	8%	5%
	Posterior sacroiliac ligaments	29%	8%
	Interosseous sacroiliac ligaments	39%	71%

5.4 Discussion

In this study, effectiveness of a rubber belt and a padded belt were investigated, showing similar load transfer mechanisms. Because the soft tissue is relatively thin in the anterior lateral parts of the lumbar region, the strain distribution on the pelvis matched the pressure point. Although the posterior pressure points were below the ASIS level, the pelvic area above the ASIS level was deformed. Regardless of the location of the pelvic belt, the upper part of the PSIS was compressed. The strain distribution in the pelvis with the padded belt was similar to that in the front and back belts, although the padded belt locally compressed the posterior region. This study suggests that the padded belt exerts the same pressure on the pelvis as the rubber belt, which may depend on the location of the pad. Statically, pressure on the buttocks reaches the upper part of the PSIS and compresses the posterior soft tissue, which is not considered to directly affect the pelvis. It may, however, support muscles and contribute to strengthening of the force closer (Vleeming and Schuenke, 2019).

Pelvic belts are considered an established treatment for SIJ dysfunction. Bertuit et al. (2018) reported the effectiveness of pelvic belts in patients during pregnancy, where a visual analogue scale (VAS) at the SIJ was reduced by 20 mm in the group with a pelvic belt compared to the group without. Few studies, however, have investigated the mechanisms underlying treatment with pelvic belts in detail. In this study, the difference in the effect between the rubber belt and padded pelvic belt was investigated using a finite element analysis.

When the pelvic belt was applied, the displacement diagrams of the innominate bone showed that the anterior part of the bone moved outward and the ischial limb was displaced inward, which indicated a relatively outward rotation of the innominate bone, called out-flare. The SIJs were considered to be in a compressed state because the compressive force increased and the compressive stress area widened. Vleeming et al. reported that form and force closure improve SIJ stability and the compressive force

supports the force closure (Vleeming and Schuenke, 2019). Therefore, the pelvic belt reduced displacement of the SIJs and enhanced stability.

Ligament loading was reduced on the ST, SS, PSL and ISL. Sichting et al. (2014) have also reported that the mean strain values for the ST and SS decreased, which is consistent with the results of this study. The ST and SS are considered to limit the nutation motion (Kapandji, 1974; Hammer et al., 2019a), and pelvic belts seemed to weaken the nutation with subsequent ST and SS strains. The reduction in the loads of the PSL and ISL was caused by a decrease in SIJ displacement. The opposite loading trends of the ASL may have resulted from slight asymmetry of the pelvic belts or minute differences in the pressure exerted.

Klima et al. (2018) reported that the pelvic belt decreased the angles of nutation and increased the counter-nutation motion of the sacrum using human post-mortem tissues. Sichting et al. (2014) showed that the pelvic belt enhanced the inward rotation of the innominate bone on the coronal plane based on the measurement of the pelvis and SIJ deformation based on a finite element analysis. These results differ from the outward rotation of the innominate bone on the transverse plane observed in this study. Sichting et al. (2014) placed the pelvic belt at a high position around the ASISs, which may be the reason that the results were different. This indicates that the height at which the pelvic belt is positioned may alter its therapeutic effects and treatment mechanisms. Depending on the position of the pelvic belts, patients with SIJ dysfunction reported increased pain relief despite using the same pelvic belts (Soisson et al., 2015). Different patients and/or pathologies may require pelvic belts with different treatment mechanisms to reduce pain. In this study, all pelvic belts yielded similar effects on pelvic kinematics. Only the back belt exhibited a smaller decrease in displacement at the ASISs and SIJs than the others. The difference in the tightening pressure in each belt could have affected the results.

There are few limitations to this study. First, for simplification, the soft tissue was uniform in the model used in this study and the role of the muscles was not considered. Although the soft tissue of the lumbopelvic region is mainly composed of skin, fat and

muscle, these components were modeled as one soft tissue in this study. The material properties of each tissue are different and muscle properties can change during standing and walking. In this actual measurement, the pressure distribution was different when the muscle worked and the simulation should include the muscle conditions. Since these considerations are complicated and this study was conducted in a rest condition without any motion, a simple soft tissue setup was adopted. Second, the tension of the pelvic belt was not specifically controlled although the pelvic belts were worn as tightly as possible to minimize the tension difference in each belt. Third, the pressure distribution measurement system of the pelvic belt did not precisely follow the body shape. The device used in this study was mainly developed to measure body pressure distribution with the participant in the lying position. Because of its mat shape, it became columnar when wrapped around the body and could not be tracked in the exact position. In addition, this could affect the wearing condition of the pelvic belt, since it is necessary to attach the belt while maintaining the shape of the device. For future research, it is important to develop a measuring instrument that can track the shape of the lumbar region without interfering with the pelvic belt.

5.5 Conclusions

The stress distribution within the pelvis when the pelvic belts were attached was evaluated using finite element analysis. The deformation of the innominate bone and the stresses on the SIJ were shown. Two types of pelvic belts caused the innominate bones to rotate outward, called out-flare, thus enhancing the compression force on the SIJ and decreasing SIJ mobility.

Chapter 6

Conclusions and prospects

6.1 Conclusions

Sacroiliac joints (SIJs) can become incompatible due to unexpected forces or repeated impacts, which causes SIJ dysfunction in association with pain. This disease is considered to account for approximately 15% - 30% of the symptoms in patients with low back pain. SIJs have a small range of motion and are often considered a non-movable joint. Therefore, SIJs are not considered as a cause of pain and medical doctors may overlook this disease. SIJ dysfunction is not a well-known disease, however many people may potentially suffer from it. Biomechanics on SIJs in physiology and pathology are poorly studied to date. Physiological functions of SIJs have not been well explained and current surgical treatments to fix the joints may lead to loss of the functions. This study aimed to clarify mechanical functions of SIJs on physiological and pathological pelves and the effect of SIJ morphologies to mechanical environment in the pelves. This study also aimed to visualize stress environment caused by pelvic belts, which is a basic treatment for SIJ dysfunction, to clarify the treatment mechanism.

Chapter 2 demonstrated motions and functions of SIJs during walking. SIJs are considered to be a shock-absorbing system, however, the stress environment has not been well studied. This chapter reproduced in-vivo walking conditions in a kinematic model combining a finite element model of a pelvis, that reproduces the detailed SIJ structure and ligament arrangement, with 3D walking analysis data. Functions of SIJs were investigated in a virtual pelvis without SIJ structures by changing the material properties of SIJs from cartilages to bones. As a result, in models with bilateral SIJs, the displacement differed greatly between the sacrum and the both hip bones on SIJs as the boundary. In models without SIJs, the displacement of the pelvis and loads of pelvic ligaments decreased and the equivalent stress of SIJs increased compared to the model with SIJs. The walking loads cause distortion of the entire pelvis and stress concentration at SIJs were seen due to the morphology of the pelvic ring. However, SIJs helped dissipate

the resulting stresses and the surrounding ligaments were likewise involved in load transmission.

Chapter 3 investigated relations between the SIJs surface morphology and joint motion resistance. SIJ surface models were creased based on CT data of healthy joints and the surface morphologies were characterized. This analysis visualized bony surfaces at the anterior sides and center points may contact each other. In addition, the original friction resistance test equipment was developed and motion resistance was investigated. Differences in resistance due to joint movement directions and combination positions were clarified although it varied from person to person. It was suggested that joint conditions may affect the mobility of SIJs.

Chapter 4 analyzed mechanical environment on SIJs caused by pelvic morphology, using acetabular dysplasia pelves as a pathological example. Acetabular dysplasia is a pelvic morphological abnormality at hip joints, which should affect the stress environment of SIJs. Pelvic finite elemet models were created based on CT data and analyzed to visualize stress distribution on standing. In addition, the abnormal pathological pelves were compared with the postoperative pelves as a physiological condition. The preoperative models were relatively inflare, the sacral nutation movement, SIJ cartilage equivalent stress and the load on the surrounding ligaments decreased with increasing posterior acetabular coverage, i.e., the lack of posterior acetabular covergage increases stress on SIJs. This suggested that the bony structure of acetabulum might play an important role to transmit loading from femurs effectively. Inappropriate pelvic morphologies can worsen stress environment on SIJs, which may contribute to pain development.

Chapter 5 visualized load transfer within the pelvis caused by pelvic belts which are one of treatment options for SIJ dysfunction. This therapy is frequently used in clinic, however, few studies have investigated the mechanism of its effects. This study measured lumbar pressure distribution wearing pelvic belts and reproduced stress environment of pelves affected by pelvic arthoses using a finite element model. With the application of

pelvic belts, the innominate bone rotated outward, which was termed an out-flare. This caused SIJs to compress and cause reduction in sacrotuberous, sacrospinous, interosseous and posterior sacroiliac ligament loading. In addition, this analysis demonstrated that the pressure areas on the skin by pelvic belts and on the bony tissues of the pelvis did not match. This result proposed that an analytical investigation should be important to realize an effective stress environment on the SIJs by pelvic belts.

From the above, these studies successfully showed that the SIJ plays an important role in relieving stress concentration in the pelvic structure. It was clearly suggested that the stress environment may be sensitively affected by the morphologies of SIJs and pelves and that the pelvic belts may change the pressure environment on SIJs.

6.2 Prospects

The studies presented in this dissertation have advanced our understanding of fundamental biomechanics of SIJs. Chapters 2 and 4 analyzed stress environment on physiological and pathological pelves, respectively. Chapter 3 investigated the relationship between SIJ surface morphology and joint motion resistance. Chapter 5 elucidated mechanism of pelvic belt treatments. These findings and additional experiments may develop new treatment strategies that relieve mechanical stimuli by controlling load transmission systems on SIJs.

Chapter 2 demonstrated SIJ movement in physiological pelves and clarified SIJ functions by comparison of a model without SIJ structure virtually. It was not, however, an analysis in pathological pelves, such as SIJ dysfunction. Although medical imaging tests can not provide strong findings (Murakami, 2017), SIJ degeneration may occur (Asada et al., 2019). Since SIJs are assumed not to be able to function well in this disease, pelvic structures or SIJ alignments should be changed. In addition, as shown in Chapter 4, stress environment of SIJs may alter in pathological pelves with pain not derived from SIJs. It has also been reported that immobilization of SIJs inhibits efficient gait (Sanaka et al., 2020), indicating that patients with SIJ dysfunction may walk differently from healthy people. Therefore, SIJs may have high sensitivity to mechanical environments. The current FE model did not consider friction resistances attributed to SIJ surface morphology shown in Chapter 3. Further numerical analysis with surface morphology information and/or actual pelvic data of SIJ dysfunction may reveal mechanical functions of SIJs and contribute to effective treatments for SIJ dysfunction.

Chapter 3 showed shear resistance on nutation positions on physiological SIJs increased or decreased, compared with other positions. Ito et al. (2020) reported that in patients with SIJ dysfunction, the sacra rotated 2.1 degrees downwards, indicating SIJs may keep nutation positions in pathological pelves. This implies that sacra should be rotated to counter-nutation in order to keep constant motion resistance or that load

transmission in the direction of low motion resistance should be controlled. Chapter 4, however, suggests that the morphologies of pathological pelves can affect stress environment on SIJs. In addition, SIJ dysfunction-affected joints showed higher mineralization values than that on healthy joints (Poilliot et al., 2021), implying that the joints may be loaded mechanically and pathology due to SIJ dysfunction. Nishi et al. (2018) reported that the SIJ high-degeneration group aged over 60 years showed lower concavities at the middle and the lower parts and sharp angles at the posterior edge than the low-degeneration group. Therefore, it is highly possible that not only joint positions but also joint surfaces change in pathological pelves. The relations in patients with SIJ dysfunction should be analyzed to utilize the findings on motion resistance due to SIJ surface morphologies for treatments.

In addition, this study investigated the relationship between SIJ surface morphology and joint motion resistance from the perspective on shear resistance, however, considering the joint structure, synovial fluid resistance should be focused on. Fluid properties of articular synovial fluid are mainly explained by squeeze effect and wedge effect. These effects are considered not to be dominant factors because the gaps between the sacrum and ilium are approximately 3 mm (Demir et al., 2007; Kalenderer et al., 2017; Ito et al., 2020) and the range of motion is too small. As shown in Chapter 3, SIJ surfaces have fine small irregularities and gap heights vary from place to place. The morphologies may interfere synovial fluid flow, which can affect fluid resistance and joint motion.

Pelvic belts may be the best treatments on the existing methods to control the load transmission mechanism on SIJs with minimal invasiveness. With application of pelvic belts, this study demonstrated that innominate bones rotated outward, while Sichting et al. (2014) showed enhanced inward rotation. This indicates that pelvic stress environment can easily change depending on types and/or usage of pelvic belts. Pelvic belt treatments have the highest potential to induce expected loads and to control the load-transmitting mechanisms of SIJs among existing treatment methods. As shown in Chapter 5, however, the pressure on skin is not directly linked to load on the pelvis, which requires additional

simulation with various force application and further understanding of underlying mechanical properties. In addition, Delshad et al. (2020) indicated that a pelvic belt with a textured pad enhances effectiveness of pelvic orthoses by additional sensory stimulation, which means that it is necessary to consider not only mechanical analysis but also biological reactions.

Therefore, it is conceivable that treatment techniques considering biomechanics of SIJs are highly required.

Acknowledgements

This study has been conducted in Laboratory of Micro-biomechanics, Division of Human Mechanical Systems and Design, Graduate School of Engineering, Hokkaido University.

This dissertation would not have been possible without the support of many people.

I would like to express my deep gratitude to Prof. Toshiro Ohashi, my supervisor. He gave me not only insightful proposals regarding my research but also lots of advice on mindset as a researcher. He always provided me tolerant and supportive comments and feedback. I am particularly grateful for his kind support.

I would also like to express my great appreciation to Dr. Daisuke Kurosawa at JCHO Sendai Hospital. He instructed a lot of clinical information and introduced me to medical society. Without his long-term and big support, I could not perform my research works.

Prof. Niels Hammer, Medical University of Graz in Austria, is our collaborator and one of the examiners of the thesis evaluation committee. He also provided me anatomical knowledge and insightful comments. During my stay in Medical University of Graz, he instructed me dissection. I would like to offer my special thanks to Niels-sensei.

Greatly thanks to Prof. Shin-Ichi Izumi, Mr. Keita Honda and Mr. Yusuke Sekiguchi at Tohoku University for sharing gait analysis data in chapter 2.

I would like to express my appreciation to Prof. Ayumi Kaneuji at Kanazawa Medical University. He taught me clinical knowledge of hip joints. I would also like to express my gratitude to Prof. Noriyuki Takano at Kanazawa Institute of Technology for model creation. They also provided me valuable advice in chapter 4.

For measurement of pelvic belt compression in chapter 5, I would like to thank Mr. Kouki Kuwano and Mr. Yuta Kawasaki at Hokkaido Research Organization. They kindly helped me to perform our experiment.

I would like to show my gratitude to Dr. Eiichi Murakami at JCHO Sendai Hospital for in-depth discussion.

I would like to thank Mr. Koji Sanaka at Biological Mechanics Laboratory. He taught me how to collaborate with medical doctors and how to study on medical fields. In addition, he instructed basics of experimental technique.

I appreciate a lot with Mrs. Konno, a secretary in our laboratory. She always helped me very kindly. I would like to express my special acknowledge to all lab members. In particular, Mr. Yugo Sakakibara, Mr. Masaya Sakurai, Mr. Takahiro Hiramukai, Mr. Ikki Ogihara and Mr. Kaito Yamada have conducted research collaborated with me.

Finally, I would like to express the deepest appreciation to my family for giving me the opportunity to go on to the doctoral course and for their continued support. In addition, I would like to express the deepest appreciation to my girlfriend, Ms. Saki Omachi, for her dedicated and enormous support.

This study was supported by JST SPRING Grant Number JPMJSP2119 and JSPS KAKENHI Grant Number JP22J11867. I would also like to express my gratitude for their financial support.

References

Anatomy, Back, Sacral Vertebrae. https://www.ncbi.nlm.nih.gov/books/NBK551653/ [accessed 27 December 2022]

Anatomy, Joints. https://www.ncbi.nlm.nih.gov/books/NBK507893/ [accessed 9 January 2023]

Anatomy of the Human Body. https://www.bartleby.com/107/ [accessed 14 December 2022]

Asada, M., Tokunaga, D., Arai, Y., Oda, R., Fujiwara, H., Yamada, K. and Kubo, T. (2019) Degeneration of the sacroiliac joint in hip osteoarthritis patients: a three-dimensional image analysis. *Journal of the Belgian Society of Radiology*, **103**, 36.

Asakura, T. (2015) Manual intervention and discussion for right sacroiliac joint dysfunction. *Journal of Global Standard Manual Medicine*, **1**, 1-7 (in Japanese).

Bellamy, N., Park, W. and Rooney, P.J. (1983) What do we know about the sacroiliac joint? *Seminars in Arthritis and Rheumatism*, **12**, 282-313.

Bernard, T.N. and Kirkaldy-Willis, W.H. (1987) Recognizing specific characteristics of nonspecific low back pain. *Clinical Orthopaedics and Related Research*, **217**, 266-280.

Bertuit, J., van Lint, C.E., Rooze, M. and Feipel, V. (2018) Pregnancy and pelvic girdle pain: analysis of pelvic belt on pain. *Journal of Clinical Nursing*, **27**, e129-e137.

BioDigital Human. https://human.biodigital.com/ [accessed 20 December 2022]

BoneAndSpine. https://boneandspine.com/ [accessed 19 December 2022]

Borowsky, C.D. and Fagen, G. (2008) Sources of sacroiliac region pain: insights gained from a study comparing standard intra-articular injection with a technique combining intra-and peri-articular. *Archives of Physical Medicine and Rehabilitation*, **89**, 2048-2056.

Bowen, V. and Cassidy, J.D. (1981) Macroscopic and microscopic anatomy of the sacroiliac joint from embryonic life until the eighth decade. *Spine*, **6**, 620-628.

Bruna-Rosso, C., Arnoux, P.J., Bianco, R.J., Godio-Raboutet, Y., Fradet, L. and Aubin, C.É. (2015) Finite element analysis of Sacroiliac joint fixation under compression loads. *International Journal of Spine Surgery*, **10**, 16.

Buford, W.L., Moulton, D.L., Gugala, Z. and Lindsey, R.W. (2010) The sacroiliac spine - computer simulation of motion and modeling of the ligaments. *32nd Annual International Conference of the IEEE EMBS*, 5117-5120.

Canale, S.T., Beaty, J.H. and Azar, F.M. (2003) Campbell's operative orthopaedics. *Elsevier Japan*.

Casaroli, G., Galbusera, F., Chande, R., Lindsey, D., Mesiwala, A., Yerby, S. and Brayda-Bruno, M. (2019) Evaluation of iliac screw, S2 alar-iliac screw and laterally placed triangular titanium implants for sacropelvic fixation in combination with posterior lumbar instrumentation: a finite element study. *European Spine Journal*, **28**, 1724-1732.

Clohisy, J.C., Schutz, A.L., st. John, L., Schoenecker, P.L. and Wright, R.W. (2009) Periacetabular osteotomy: A systematic literature review. *Clinical Orthopaedics and Related Research*, **467**, 2041-2052.

CloudCompare. https://www.danielgm.net/cc/ [accessed 27 November 2022]

Cohen, S.P. (2005) Sacroiliac joint pain: a comprehensive review of anatomy, diagnosis and treatment. *Anesthesia and Analgesia*, **101**, 1440-1453.

Dall, B.E., Eden, S.V., Cho, W., Karkenny, A., Brooks, D.M., Hayward, G.M., Moldavsky, M., Yandamuri, S. and Bucklen, B.S. (2019) Biomechanical analysis of motion following sacroiliac joint fusion using lateral sacroiliac screws with or without lumbosacral instrumented fusion. *Clinical Biomechanics*, **68**, 182-189.

Damen, L., Spoor, C.W., Snijders, C.J. and Stam, H.J. (2002) Does a pelvic belt influence sacroiliac joint laxity? *Clinical Biomechanics*, **17**, 495-498.

Delshad, B., Zarean, E., Yeowell, G. and Sadeghi-Demneh, E. (2020) The immediate effects of pelvic compression belt with a textured sacral pad on the sacroiliac function

in pregnant women with lumbopelvic pain: a cross-over study. *Musculoskeletal Science and Practice*, **48**, 102170.

Demir, M., Mavi, A., Gümüsburun, E., Bayram, M. and Gürsoy, S. (2007) Anatomical variations with joint space measurements on CT. *Kobe Journal of Medical Sciences*, **53**, 209-217.

Dreyfuss, P., Dreyer, S.J., Cole, A. and Mayo, K. (2004) Sacroiliac joint pain. *The Journal of the American Academy of Orthopaedic Surgeons*, **12**, 255-265.

Duhon, B.S., Bitan, F., Lockstadt, H., Kovalsky, D., Cher, D., Hillen, T. and on behalf of the SIFI Study Group. (2015) Triangular titanium implants for minimally invasive sacroiliac joint fusion: 2-year follow-up from a prospective multicenter trial. *International Journal of Spine Surgery*, **10**, 13.

Egund, N., Olsson, T.H., Schmid, H. and Selvik, G. (1978) Movements in the sacroiliac joints demonstrated with roentgen stereophotogrammetry. *Acta Radiologica*, **19**, 833-846.

Endo, Y., Kurosawa, D., Murakami, E., Sasaki, K., Takahashi, T. and Kumai, T. (2020) Effect of extracorporeal shock waves on pain originating from the ligamentous enthesis around the sacroiliac joint. *Orthopedic Surgery*, **71**, 1263-1266 (in Japanese).

Forst, S., Wheeler, M., Fortin, J. and Vilensky, J. (2006) The sacroiliac joint: anatomy, physiology and clinical significance. *Pain Physician*, **9**, 61-67.

Fujii, M., Nakashima, Y., Sato, T., Akiyama, M. and Iwamoto, Y. (2011) Pelvic deformity influences acetabular version and coverage in hip dysplasia. *Clinical Orthopaedics and Related Research*, **469**, 1735-1742.

Hamada, H., Takao, M., Nakahara, I., Sakai, T., Nishii, T. and Sugano, N. (2015) Hip range‐of‐motion (ROM) is less than normal after rotational acetabular osteotomy for developmental dysplasia of the hip: a simulated ROM analysis. *Journal of Orthopaedic Research*, **34**, 217-223.

Hammer, N., Steinke, H., Slowik, V., Josten, C., Stadler, J., Böhme, J. and Spanel-Borowski, K. (2009) The sacrotuberous and the sacrospinous ligament - a virtual reconstruction. *Annals of Anatomy*, **191**, 417-425.

Hammer, N., Steinke, H., Böhme, J., Stadler, J., Josten, C. and Spanel-Borowski, K. (2010) Description of the iliolumbar ligament for computer-assisted reconstruction. *Annals of Anatomy*, **192**, 162-167.

Hammer, N., Möbius, R., Schleifenbaum, S., Hammer, K.H., Klima, S., Lange, J.S., Soisson, O., Winkler, D., Milani, T.L. and Eldabe, S. (2015) Pelvic belt effects on health outcomes and functional parameters of patients with sacroiliac joint pain. *PLOS ONE*, **10**, e0136375.

Hammer, N. and Klima, S. (2019) In-silico pelvis and sacroiliac joint motion—a review on published research using numerical analyses. *Clinical Biomechanics*, **61**, 95-104.

Hammer, N., Höch, A., Klima, S., le Joncour, J.B., Rouquette, C. and Ramezani, M. (2019a) Effects of cutting the sacrospinous and sacrotuberous ligaments. *Clinical Anatomy*, **32**, 231-237.

Hammer, N., Ondruschka, B. and Fuchs, V. (2019b) Sacroiliac joint ligaments and sacroiliac pain: a case-control study on micro- and ultrastructural findings on morphologic alterations. *Pain physician*, **22**, E615-E625.

Hammer, N., Scholze, M., Kibsgård, T., Klima, S., Schleifenbaum, S., Seidel, T., Werner, M. and Grunert, R. (2019c) Physiological in vitro sacroiliac joint motion: a study on three-dimensional posterior pelvic ring kinematics. *Journal of Anatomy*, **234**, 346-358.

Hasegawa, Y., Iwase, T., Kitamura, S., Kawasaki, M. and Yamaguchi, J. (2014) Eccentric rotational acetabular osteotomy for acetabular dysplasia and osteoarthritis: Follow-up at a mean duration of twenty years. *Journal of Bone and Joint Surgery*, **96**, 1975-1982.

Hayashi, K. (2000) Biomechanics. *Corona publishing Co., Ltd.*

Heyman, C.H. and Herndon, C.H. (1950) Legg-perthes disease: a method for the measurement of the roentgenographic result. *The Journal of Bone and Joint Surgery*, **32**, 767-778.

Honda, K., Sekiguchi, Y., Muraki, T. and Izumi, S.I. (2019) The differences in sagittal plane whole-body angular momentum during gait between patients with hemiparesis and healthy people. *Journal of Biomechanics*, **86**, 204-209.

iFuse: the triangle-shaped implant designed specifically for the SI joint. https://si-bone.com/providers/solutions/ifuse [accessed 5 December 2022]

Ishiguro, K. and Ishiguro, T. (2017) Sacroiliac joint exercise assistance device in lateral decubitus position (Patent).

Ito, K., Morito, T. and Gamada, K. (2020) The association between sacral morphology and sacroiliac joint conformity demonstrated on CT-based bone models. *Clinical Anatomy*, **33**, 880-886.

Iwai, S., Kabata, T., Maeda, T., Kajino, Y., Watanabe, S., Kuroda, K., Fujita, K., Hasegawa, K. and Tsuchiya, H. (2014) Three-dimensional kinetic simulation before and after rotational acetabular osteotomy. *Journal of Orthopaedic Science*, **19**, 443-450.

Jacob, H. and Kissling, R.O. (1995) The mobility of the sacroiliac joints in healthy volunteers between 20 and 50 years of age. *Clinical Biomechanics*, **10**, 352-361.

Jacobsen, S., Sonne-Holm, S., Søballe, K., Gebuhr, P. and Lund, B. (2005) Hip dysplasia and osteoarthrosis: a survey of 4151 subjects from the osteoarthrosis substudy of the Copenhagen city heart study. *Acta Orthopaedica*, **76**, 149-158.

Jingushi, S., Ohfuji, S., Sofue, M., Horita, Y., Itoman, M., Matsumoto, T., Hamada, Y., Shindo, H., Takatori, Y., Yamada, H., Yasunaga, Y., Ito, H., Mori, S., Owan, I., Fujii, G., Ohashi, H., Iwamoto, Y., Miyanishi, K., Iga, T., Takahira, N., Sugimori, T., Sugiyama, H., Okano, K., Karita, K., Ando, K., Hamaki, T., Hirayama, T., Iwata, K., Nakasone, S., Matsuura, M. and Mawatari, T. (2010) Multiinstitutional

epidemiological study regarding osteoarthritis of the hip in Japan. *Journal of Orthopaedic Science*, **15**, 626-631.

Jingushi, S., Ohfuji, S., Sofue, M., Horita, Y., Itoman, M., Matsumoto, T., Hamada, Y., Shindo, H., Takatori, Y., Yamada, H., Yasunaga, Y., Ito, H., Mori, S., Owan, I., Fujii, G., Ohashi, H., Iwamoto, Y., Miyanishi, K., Iga, T., Takahira, N., Sugimori, T., Sugiyama, H., Okano, K., Karita, K., Ando, K., Hamaki, T., Hirayama, T., Iwata, K., Nakasone, S., Matsuura, M. and Mawatari, T. (2011) Osteoarthritis hip joints in Japan: involvement of acetabular dysplasia. *Journal of Orthopaedic Science*, **16**, 156-164.

Joukar, A., Shah, A., Kiapour, A., Vosoughi, A.S., Duhon, B., Agarwal, A.K., Elgafy, H., Ebraheim, N. and Goel, V.K. (2018) Sex specific sacroiliac joint biomechanics during standing upright. *Spine*, **43**, E1053-E1060.

Joukar, A., Chande, R.D., Carpenter, R.D., Lindsey, D.P., Erbulut, D.U., Yerby, S.A., Duhon, B. and Goel, V.K. (2019) Effects on hip stress following sacroiliac joint fixation: a finite element study. *JOR Spine*, **2**, e1067.

Kalenderer, Ö., Turgut, A., Bacaksiz, T., Bilgin, E., Kumbaraci, M. and Akkan, H.A. (2017) Evaluation of symphysis pubis and sacroiliac joint distances in skeletally immature patients: a computerized tomography study of 1020 individuals. *Acta Orthopaedica et Traumatologica Turcica*, **51**, 150-154.

Kampen, W.U. and Tillmann, B. (1998) Age-related changes in the articular cartilage of human sacroiliac joint. *Anatomy and Embryology*, **198**, 505-513.

Kaneuji, A., Sugimori, T., Ichiseki, T., Fukui, K., Takahashi, E. and Matsumoto, T. (2015) Rotational acetabular osteotomy for osteoarthritis with acetabular dysplasia: conversion rate to total hip arthroplasty within twenty years and osteoarthritis. *The Journal of Bone and Joint Surgery*, **97**, 726-732.

Kaneuji, A., Hara, T., Takahashi, E., Fukui, K., Ichiseki, T. and Kawahara, N. (2021) A novel minimally invasive spherical periacetabular osteotomy: pelvic ring

preservation and patient-specific osteotomy by preoperative 3-dimensional templating. *The Journal of Bone and Joint Surgery*, **103**, 1724-1733.

Kapandji, I. (1974) The physiology of the joints vol.3 the trunk and the vertebral column. *Churchill Livingstone.*

Katada, S. (2019) Principles of manual treatment for sacroiliac joint dysfunction. *Springer.*

Kibsgård, T.J., Røise, O., Stuge, B. and Röhrl, S.M. (2012) Precision and accuracy measurement of radiostereometric analysis applied to movement of the sacroiliac joint. *Clinical Orthopaedics and Related Research*, **470**, 3187-3194.

Kirkaldy-Willis, W.H. and Cassidy, J.D. (1985) Spinal manipulation in the treatment of low-back pain. *Canadian Family Physician*, **31**, 535-540.

Klima, S., Grunert, R., Ondruschka, B., Scholze, M., Seidel, T., Werner, M. and Hammer, N. (2018) Pelvic orthosis effects on posterior pelvis kinematics an in-vitro biomechanical study. *Scientific Reports*, **8**, 15980.

Kozaki, T., Hashizume, H., Nishiyama, D., Iwasaki, H., Tsutsui, S., Takami, M., Yukawa, Y., Minamide, A., Taniguchi, T., Nagata, K., Fukui, D., Tamai, H., Taiji, R., Murata, S., Oka, H. and Yamada, H. (2021) Adjacent segment disease on hip joint as a complication of spinal fusion surgery including sacroiliac joint fixation. *European Spine Journal*, **30**, 1314-1319.

Krishnamoorthy, V., Beck, E., Kunze, K., Cancienne, J., Krivicich, L., Suppauksorn, S., Ayeni, O. and Nho, S. (2019) Radiographic prevalence of sacroiliac joint abnormalities and clinical outcomes in patients with femoroacetabular impingement syndrome. *Arthroscopy: The Journal of Arthroscopic & Related Surgery*, **35**, 2598-2605.e1.

Kurosawa, D., Murakami, E., Ozawa, H., Koga, H., Isu, T., Chiba, Y., Abe, E., Unoki, E., Musha, Y., Ito, K., Katoh, S. and Yamaguchi, T. (2017) A diagnostic scoring system for sacroiliac joint pain originating from the posterior ligament. *Pain Medicine*, **18**, 228-238.

Lee, C.H., Hsu, C.C. and Huang, P.Y. (2017) Biomechanical study of different fixation techniques for the treatment of sacroiliac joint injuries using finite element analyses and biomechanical tests. *Computers in Biology and Medicine*, **87**, 250-257.

Lee, J., Lee, S. and Song, S. (2010) Clinical effectiveness of botulinum toxin A compared to a mixture of steroid and local anesthetics as a treatment for sacroiliac joint pain. *Pain Medicine*, **11**, 692-700.

Liliang, P., Lu, K., Weng, H., Liang, C., Spine, Y.T.- and 2009, undefined. (2009) The therapeutic efficacy of sacroiliac joint blocks with triamcinolone acetonide in the treatment of sacroiliac joint dysfunction without spondyloarthropathy. *Spine*, **34**, 896-900.

Liliang, P., Liang, C., Lu, K., Weng, H., Medicine, F.S.-P. and 2014, undefined. (2014) Modified fluoroscopy-guided sacroiliac joint injection: a technical report. *Pain Medicine*, **15**, 1477-1480.

Lovejoy, C.O. (2007) Evolution of the human lumbopelvic region and its relationship to some clinical deficits of the spine and pelvis. In: *Movement, stability and lumbopelvic pain: integration of research and therapy* (eds Vleeming, A., Mooney, V. and Stoeckart, R.), 141-158. *Churchill Livingstone*.

Majumder, S., Roychowdhury, A. and Pal, S. (2007) Simulation of hip fracture in sideways fall using a 3D finite element model of pelvis-femur-soft tissue complex with simplified representation of whole body. *Medical Engineering and Physics*, **29**, 1167-1178.

Massie, W.K. and Howorth, M.B. (1950) Congenital dislocation of the hip: part I. method of grading results. *The Journal of Bone & Joint Surgery*, **32**, 519-531.

Matsumura, G. (2013) Illustration Anatomy. *Chugaiigaku Co., Ltd.*

Mennell, J.M. (1694) Joint pain: diagnosis and treatment using manipulative techniques. *Little Brown and Company.*

Mens, J.M.A., Damen, L., Snijders, C.J. and Stam, H.J. (2006) The mechanical effect of a pelvic belt in patients with pregnancy-related pelvic pain. *Clinical Biomechanics*, **21**, 122-127.

Merry, C.V. (2010) Mind - primary cause of human evolution. *Trafford Publishing.*

Miller, L.E., Carlton Reckling, W. and Block, J.E. (2013) Analysis of postmarket complaints database for the iFuse SI joint fusion system®: a minimally invasive treatment for degenerative sacroiliitis and sacroiliac joint disruption. *Medical Devices: Evidence and Research*, **6**, 77-84.

Miller, J.A.A., Schultz, A.B. and Andersson, G.B.J. (1987) Load - displacement behavior of sacroiliac joints. *Journal of Orthopaedic Research*, **5**, 92-101.

Mizuno, T. (2022) Effects of diffusion pressure wave therapy on sacroiliac joint disorders. *The 13th Research Meeting of the Japanese Sacroiliac Joint Research Group*, 6 (in Japanese).

Morgan, P.M., Anderson, A.W. and Swiontkowski, M.F. (2013) Symptomatic sacroiliac joint disease and radiographic evidence of femoroacetabular impingement. *HIP International*, **23**, 212-217.

Murakami, T. (2006) Introduction to bioengineering. *Corona Publishing Co., Ltd.*

Murakami, E., Kanno, H., Aizawa, T., Okuno, H. and Noguchi, K. (2007a) Sacroiliac joint arthrodesis for clonic joint pain. *The Journal of Japanese Society of Lumbar Spine Disorders*, **13**,197-203 (in Japanese).

Murakami, E., Tanaka, Y., Aizawa, T., Ishizuka, M. and Kokubun, S. (2007b) Effect of periarticular and intraarticular lidocaine injections for sacroiliac joint pain: prospective comparative study. *Journal of Orthopaedic Science*, **12**, 274-280.

Murakami, E. (2017) Diagnosis and treatment of sacroiliac joint disorder. *Clinical Orthopaedic Surgery*, **52**, 529-536.

Murakami, E. (2018a) Sacroiliac joint disorder: accurately diagnosing low back pain. *Springer.*

Murakami, E., Kurosawa, D. and Aizawa, T. (2018b) Treatment strategy for sacroiliac joint-related pain at or around the posterior superior iliac spine. *Clinical Neurology and Neurosurgery*, **165**, 43-46.

Murakami, E., Kurosawa, D. and Aizawa, T. (2018c) Sacroiliac joint arthrodesis for chronic sacroiliac joint pain: an anterior approach and clinical outcomes with a minimum 5-year follow-up. *Journal of Neurosurgery: Spine*, **29**, 279-285.

Nishi, K., Tsurumoto, T., Okamoto, K., Ogami-Takamura, K., Hasegawa, T., Moriuchi, T., Sakamoto, J., Oyamada, J., Higashi, T., Manabe, Y. and Saiki, K. (2018) Three-dimensional morphological analysis of the human sacroiliac joint: influences on the degenerative changes of the auricular surfaces. *Journal of Anatomy*, **232**, 238-249.

North American Spine Society. https://www.spine.org/coverage [accessed 9 January 2023]

Okuzu, Y., Goto, K., Shimizu, Y., Kawai, T., Kuroda, Y. and Matsuda, S. (2021) Sacroiliac joint degeneration is common in patients with end-stage hip osteoarthritis secondary to unilateral developmental dysplasia of the hip: factors associated with its severity and laterality. *Journal of Orthopaedic Science*, **26**, 135-140.

Pel, J.J.M., Spoor, C.W., Goossens, R.H.M. and Pool-Goudzwaard, A.L. (2008) Biomechanical model study of pelvic belt influence on muscle and ligament forces. *Journal of Biomechanics*, **41**, 1878-1884.

Poilliot, A., Doyle, T., Tomlinson, J., Zhang, M., Zwirner, J. and Hammer, N. (2019a) Quantification of fat in the posterior sacroiliac joint region: fat volume is sex and age dependant. *Scientific Reports*, **9**, 14935.

Poilliot, A.J., Zwirner, J., Doyle, T.D. and Hammer, N. (2019b) A systematic review of the normal sacroiliac joint anatomy and adjacent tissues for pain physicians. *Pain Physician*, **22**, E247-E274.

Poilliot, A., Li, K.C., Müller-Gerbl, M., Toranelli, M., Zhang, M., Zwirner, J. and Hammer, N. (2020) Subchondral bone strength of the sacroiliac joint-a combined approach using computed tomography osteoabsorptiometry (CT-OAM) imaging and

biomechanical validation. *Journal of the Mechanical Behavior of Biomedical Materials*, **111**, 103978.

Poilliot, A., Doyle, T., Kurosawa, D., Toranelli, M., Zhang, M., Zwirner, J., Müller-Gerbl, M. and Hammer, N. (2021) Computed tomography osteoabsorptiometry-based investigation on subchondral bone plate alterations in sacroiliac joint dysfunction. *Scientific Reports*, **11**, 8652.

Ramezani, M., Klima, S., de La Herverie, P.L.C., Campo, J., le Joncour, J.B., Rouquette, C., Scholze, M. and Hammer, N. (2019) In silico pelvis and sacroiliac joint motion: refining a model of the human osteoligamentous pelvis for assessing physiological load deformation using an inverted validation approach. *BioMed Research International*, **2019**, 3973170.

Reijman, M., Hazes, J.M.W., Pols, H.A.P., Koes, B.W. and Bierma-Zeinstra, S.M.A. (2005) Acetabular dysplasia predicts incident osteoarthritis of the hip: the Rotterdam study. *Arthritis & Rheumatism*, **52**, 787-793.

Sanaka, K., Kurosawa, D., Murakami, E., Yoshida, S. and Ozawa, H. (2020) Analysis of gait change after sacroiliac joint fixation by biped walking android model. *Clinical Orthopedic Surgery*, **71**, 401-409 (in Japanese).

Sanaka, K., Hashimoto, K., Kurosawa, D., Murakami, E., Ozawa, H., Takahashi, K., Onoki, T. and Aizawa, T. (2022) The psoas major muscle is essential for bipedal walking – an analysis using a novel upright bipedal-walking android model. *Gait & Posture*, **94**, 15-18.

Schünke, M., Schulte, E., Schumacher, U., Voll, M. and Wesker, K. (2017) Prometheus allgemeine anatomie und bewegungssystem (Eds. Sakai, T. and Matsumura, G.). *Igaku-shoin Ltd.*

Schwarzer, A., Aprill, C. and Bogduk, N. (1995) The sacroiliac joint in chronic low back pain. *Spine*, **20**, 31-37.

Sharp, I.K. (1961) Acetabular dysplasia. *The Journal of Bone and Joint Surgery. British volume*, **43B**, 268-272.

Sichting, F., Rossol, J., Soisson, O., Klima, S., Milani, T. and Hammer, N. (2014) Pelvic belt effects on sacroiliac joint ligaments: a computational approach to understand therapeutic effects of pelvic belts. *Pain Physician*, **17**, 43-51.

Smith, A.G., Capobianco, R., Cher, D., Rudolf, L., Sachs, D., Gundanna, M., Kleiner, J., Mody, M.G. and Shamie, A.N. (2013) Open versus minimally invasive sacroiliac joint fusion: a multi-center comparison of perioperative measures and clinical outcomes. *Annals of Surgical Innovation and Research*, **7**, 14.

Soisson, O., Lube, J., Germano, A., Hammer, K.H., Josten, C., Sichting, F., Winkler, D., Milani, T.L. and Hammer, N. (2015) Pelvic belt effects on pelvic morphometry, muscle activity and body balance in patients with sacroiliac joint dysfunction. *PLOS ONE*, **10**, e0116739.

Stark, J.G., Fuentes, J.A., Fuentes, T.I. and Idemmili, C. (2011) The history of sacroiliac joint arthrodesis: a critical review and introduction of a new technique. *Current Orthopaedic Practice*, **22**, 545-557.

Steinke, H., Hammer, N., Slowik, V., Stadler, J., Josten, C., Böhme, J. and Spanel-Borowski, K. (2010) Novel insights into the sacroiliac joint ligaments. *Spine*, **35**, 257-263.

Sturesson, B., Selvik, G. and Udén, A. (1989) Movements of the sacroiliac joints: a roentgen stereophotogrammetric analysis. *Spine*, **14**, 162-165.

Sturesson, B., Uden, A. and Vleeming, A. (2000) A radiostereometric analysis of the movements of the sacroiliac joints in the reciprocal straddle position. *Spine*, **25**, 364-368.

Suda, T., Ozawa, H., Takahashi, H., Tanaka, S., Nakamura, H. and Mori, S. (2007) Bone biology. *Ishiyaku Publishers Inc.*

Szadek, K.M., Hoogland, P.V.J.M., Zuurmond, W.W.A., De Lange, J.J. and Perez, R.S.G.M. (2010) Possible nociceptive structures in the sacroiliac joint cartilage: an immunohistochemical study. *Clinical Anatomy*, **23**, 192-198.

Takano, N., Shintani, K., Sasaki, H. and Kaneuji, A. (2011) Examination of the stress environment in hip osteoarthritis using a solid model. *Japanese Journal of Clinical Biomechanics*, **32**, 197-202 (in Japanese).

Takayama, A. (1990) Stress analysis and movement in sacroiliac joints. *Journal of Nippon Medical School*, **57**, 476-485 (in Japanese).

Tortora, G.J. and Derrickson, B. (2012) Principles of anatomy and ahysiology (eds Kuwaki, T., Kurosawa, M., Takahashi, K. and Hosoya, Y.). *Maruzen Publishing Co., Ltd.*

Toyohara, R., Kurosawa, D., Hammer, N., Werner, M., Honda, K., Sekiguchi, Y., Izumi, S.I., Murakami, E., Ozawa, H. and Ohashi, T. (2020) Finite element analysis of load transition on sacroiliac joint during bipedal walking. *Scientific Reports*, **10**, 13683.

Toyohara, R., Hiramukai, T., Kurosawa, D., Hammer, N., Ohashi, T. (2022a) Numerical analysis of the effects of padded pelvic belts as a treatment for sacroiliac joint dysfunction. *Bio-Medical Materials and Engineering*, **Pre-press**, 1-14.

Toyohara, R., Kaneuji, A., Takano, N., Kurosawa, D., Hammer, N., Ohashi, T. (2022b) A patient-cohort study of numerical analysis on sacroiliac joint stress distribution in pre- and post-operative hip dysplasia. *Scientific Reports*, **12**, 14500.

Varga, E., Dudas, B. and Tile, M. (2008) Putative proprioceptive function of the pelvic ligaments: biomechanical and histological studies. *Injury*, **39**, 858-864.

Venayre, B., Koyama, Y., Kurosawa, D., Hammer, N., Lingslebe, U., Murakami, E., Ozawa, H. and Ohashi, T. (2021) Quantitative evaluation of the sacroiliac joint fixation in stress reduction on both sacroiliac joint cartilage and ligaments: a finite element analysis. *Clinical Biomechanics*, **85**, 105350.

Visible Body. https://www.visiblebody.com/ [accessed 10 January 2023]

Vleeming, A., Schuenke, M.D., Masi, A.T., Carreiro, J.E., Danneels, L. and Willard, F.H. (2012) The sacroiliac joint: an overview of its anatomy, function and potential clinical implications. *Journal of Anatomy*, **221**, 537-567.

Vleeming, A. and Schuenke, M. (2019) Form and force closure of the sacroiliac joints. *PM and R*, **11**, S24-S31.

Vukasinovic, Z., Spasovski, D., Kralj-Iglic, V., Marinkovic-Eric, J., Seslija, I., Zivkovic, Z. and Spasovski, V. (2012) Impact of triple pelvic osteotomy on contact stress pressure distribution in the hip joint. *International Orthopaedics*, **37**, 95-98.

Weisl, H. (1955) The movements of the sacro-iliac joint. *Acta Anatomica*, **23**, 80-91.

Wiberg, G. (1939) Studies on dysplastic acetabula and congenital subluxation of the hip joint : with special reference to the complication of osteoarthritis. *Acta Chirurgica Scandinavica*, **83**, 7-38.

Wiberg, G. (1953) Shelf operation in congenital dysplasia of the acetabulum and in subluxation and dislocation of the hip. *The Journal of Bone & Joint Surgery*, **35**, 65-80.

Wirtz, D.C., Schiffers, N., Forst, R., Pandorf, T., Weichert, D. and Radermacher, K. (2000) Critical evaluation of known bone material properties to realize anisotropic FE-simulation of the proximal femur. *Journal of Biomechanics*, **33**, 1325-1330.

Wise, C.L. and Dall, B.E. (2008) Minimally invasive sacroiliac arthrodesis: outcomes of a new technique. *Journal of Spinal Disorders and Techniques*, **21**, 579-584.

Yasunaga, Y., Ochi, M., Yamasaki, T., Shoji, T. and Izumi, S. (2016) Rotational acetabular osteotomy for pre- and early osteoarthritis secondary to dysplasia provides durable results at 20 Years. *Clinical Orthopaedics and Related Research*, **474**, 2145-2153.

Yoshida, K. (1999) Structural Medical Science. *Sangakusha Publishing Co., Ltd.*

Publications

[1] Toyohara, R., Kurosawa, D., Hammer, N., Werner, M., Honda, K., Sekiguchi, Y., Izumi, S., Murakami, E., Ozawa, H., Ohashi, T. Finite element analysis of load transition on sacroiliac joint during bipedal walking. *Scientific Reports* **10**, 13683 (2020). (IF: 4.379 as of 2021-2022)

[2] Toyohara, R., Kaneuji, A., Takano, N., Kurosawa, D., Hammer, N., Ohashi, T. A patient-cohort study of numerical analysis on sacroiliac joint stress distribution in pre- and post-operative hip dysplasia. *Scientific Reports* **12**, 14500 (2022). (IF: 4.379 as of 2021-2022)

[3] Toyohara, R., Hiramukai, T., Kurosawa, D., Hammer, N., Ohashi, T. Numerical analysis of the effects of padded pelvic belts as a treatment for sacroiliac joint dysfunction. Bio-Medical Materials and Engineering, Vol. Pre-press, no. Pre-press, pp. 1-14 (2022). (IF: 1.3 as of 2022-2023)

Conferences

[1] Toyohara, R., Kurosawa, D., Hammer, N., Lingslebe, U., Honda, K., Sekiguchi, Y., Izumi, S., Murakami, E., Ozawa, H., and Ohashi, T. “Changes in load on each walking period and sacroiliac joint. What was found by inputting 3D walking data into the finite element model”, *The 10th Research Meeting of the Japanese Sacroiliac Joint Research Group*, Kobe, September 2019.

[2] Toyohara, R., Kurosawa, D., Hammer, N., Werner, M., Honda, K., Sekiguchi, Y., Izumi, S., Murakami, E., Ozawa, H., and Ohashi, T. “Finite element analysis of pelvic stress distribution during normal walking with sacroiliac joint fixation”, *The 33rd JSME Bioengineering Conference*, Jun 2020 (Poster presentation decided (reviewed) 1 year postponed due to the influence of the COVID-19).

[3] Toyohara, R., Kurosawa, D., Hammer, N., Werner, M., Honda, K., Sekiguchi, Y., Izumi, S., Murakami, E., Ozawa, H., and Ohashi, T. “Finite element analysis of pelvic stress distribution during normal walking with sacroiliac joint fixation”, *The 59th Annual Meeting of Hokkaido Branch of Japan Society for Medical and Biological Engineering*, Online, October 2020.

[4] Toyohara, R., Kurosawa, D., Hammer, N., Werner, M., Honda, K., Sekiguchi, Y., Izumi, S., Murakami, E., Ozawa, H., and Ohashi, T. “Finite element analysis of sacroiliac joint motion and restriction received from ligaments”, *The 31st JSME Conference on Frontiers in Bioengineering*, Online, December 2020.

[5] Toyohara, R., Kaneuji, A., Takano, N., Kurosawa, D., Ohashi, T. “Elucidation of the pathogenesis of sacroiliac joint disorders in acetabular dysplasia pelvis: a finite element analysis”, *The 60th Annual Meeting of Hokkaido Branch of Japan Society for Medical and Biological Engineering*, Online, October 2021.

[6] Toyohara, R., Kurosawa, D., Hammer, N., Werner, M., Honda, K., Sekiguchi, Y., Izumi, S., Murakami, E., Ozawa, H., and Ohashi, T. “Function and role of sacroiliac joint during bipedal walking; finite element analysis”, *The 11th Asian-Pacific Conference on Biomechanics*, Kyoto, December 2021.

[7] Toyohara, R., Hiramukai, T., Kurosawa, D., Hammer, N., Ohashi, T. “Investigation of treatment mechanism of pelvic belt for sacroiliac joint dysfunction: a finite element analysis”, *The 34th JSME Bioengineering Conference*, Fukuoka, Jun 2022.

[8] Toyohara, R., Kaneuji, A., Takano, N., Kurosawa, D., Ohashi, T. “Investigation of sacroiliac joint pain in patients with acetabular dysplasia using finite element analysis”, *The 9th World Congress of Biomechanics*, Taipei, July 2022.

[9] Toyohara, R. and Ohashi, T. “Function and role of sacroiliac joint in walking revealed by finite element analysis of pelvis”, *The 30th Annual Meeting of the Japanese Society for the Study of Low Back Pain*, Morioka, Oct 2022.

[10] Toyohara, R., Hiramukai, T., Kurosawa, D., Hammer, N., Ohashi, T. “Elucidation of therapeutic mechanism of pelvic belt for sacroiliac joint dysfunction by finite element analysis”, *The 61st Annual Meeting of Hokkaido Branch of Japan Society for Medical and Biological Engineering*, Online, October 2022.

[11] Toyohara, R. and Ohashi, T. “Effect of articular surface profile of sacroiliac joints on joint motion”, *The 33rd JSME Conference on Frontiers in Bioengineering*, Kobe, December 2022.

Award

[1] Research Encouragement Award at the 59th Annual Meeting of Hokkaido Branch of Japan Society for Medical and Biological Engineering (24th October 2020, online).